TKK Dissertations 110
Espoo 2008

NUMERICAL IMPULSE RESPONSE TESTS TO IDENTIFY DYNAMIC INDUCTION-MACHINE MODELS

Doctoral Dissertation

Anna-Kaisa Repo

Helsinki University of Technology
Faculty of Electronics, Communications and Automation
Department of Electrical Engineering

TKK Dissertations 110
Espoo 2008

NUMERICAL IMPULSE RESPONSE TESTS TO IDENTIFY DYNAMIC INDUCTION-MACHINE MODELS

Doctoral Dissertation

Anna-Kaisa Repo

Dissertation for the degree of Doctor of Science in Technology to be presented with due permission of the Faculty of Electronics, Communications and Automation for public examination and debate in Auditorium S4 at Helsinki University of Technology (Espoo, Finland) on the 4th of April, 2008, at 12 noon.

Helsinki University of Technology
Faculty of Electronics, Communications and Automation
Department of Electrical Engineering

Teknillinen korkeakoulu
Elektroniikan, tietoliikenteen ja automaation tiedekunta
Sähkötekniikan laitos

Distribution:
Helsinki University of Technology
Faculty of Electronics, Communications and Automation
Department of Electrical Engineering
P.O. Box 3000
FI - 02015 TKK
FINLAND
URL: http://sahko.tkk.fi/en/
Tel. +358-9-451 2381
Fax +358-9-451 2991
E-mail: anna-kaisa.repo@tkk.fi

ISBN 978-951-22-9274-5
ISBN 978-951-22-9275-2 (PDF)
ISSN 1795-2239
ISSN 1795-4584 (PDF)
URL: http://lib.tkk.fi/Diss/2008/isbn9789512292752/

TKK-DISS-2447

Picaset Oy
Helsinki 2008

ABSTRACT OF DOCTORAL DISSERTATION	HELSINKI UNIVERSITY OF TECHNOLOGY P.O. BOX 1000, FI-02015 TKK http://www.tkk.fi

Author Anna-Kaisa Repo

Name of the dissertation
Numerical impulse response tests to identify dynamic induction-machine models

Manuscript submitted 7.12.2007	Manuscript revised
Date of the defence 4.4.2008	
☐ Monograph	☒ Article dissertation (summary + original articles)

Faculty Faculty of Electronics, Communications and Automation
Department Department of Electrical Engineering
Field of research Modelling of electrical machines
Opponent(s) Prof. Thomas A. Lipo
Supervisor Prof. Antero Arkkio
Instructor

Abstract

The aim of the study is to identify dynamic models for induction machines using two-dimensional finite-element analyses. Attention is given mainly to cage-induction machines with closed rotor slots and deep rotor bars. However, cage-induction machines with semi-closed rotor slots and slip-ring machines are considered as well.

Two new applications of numerical impulse response tests are presented. The tests are performed within a time-stepping finite-element analysis. First, an impulse excitation is applied to the stator voltage and the response of the stator current is studied. Next, an impulse excitation is applied to the rotor position angle and the response of electromagnetic torque is studied. The results of the impulse tests are used to estimate parameters for small-signal models in the frequency domain. The estimation is performed by fitting the results of an impulse response test to the corresponding analytical small-signal model. The analytical models are based on the theory of electrical machines and their parameters have a physical meaning. Based on the study, it is concluded that the skin effect in rotor bars has a significant influence on the results of the impulse response tests. In order to obtain a good fit, the skin effect has to be taken into account in the structure of the analytical model. In addition, the saturation of iron has a prominent effect. The effects of saturation can be detected as harmonics in the frequency response and in the values of parameter estimates. A model for saturation can be included in the small-signal models. In the case of this more advanced model, the parameter estimates obtain a clear physical interpretation.

The applicability of impulse response tests is based on the assumption of linear time-invariant behaviour of the system. The assumption is studied by several means. Within the tests, the amplitude, length, and initial time of the impulse excitation is varied and the results are compared. It is concluded that, in the case of normal operation points, the assumption can be made. The reasonability of the parameter estimates is evaluated by comparing the values with steady-state circuit parameters. The steady-state parameters are estimated using a time-harmonic finite-element analysis.

When the impulse is applied to the rotor position angle and the torque response is computed, the results predict negative electromagnetic damping within some frequency ranges. This phenomenon is also studied by measurements. It is observed that, within the range of predicted negative damping, self-excited torsional oscillations occur.

Keywords induction machines, parameter estimation, frequency response, finite element analysis

ISBN (printed) 978-951-22-9274-5	ISSN (printed) 1795-2239
ISBN (pdf) 978-951-22-9275-2	ISSN (pdf) 1795-4584
Language English	Number of pages 186

Publisher Helsinki University of Technology, Department of Electrical Engineering

Print distribution Helsinki University of Technology, Department of Electrical Engineering

☒ The dissertation can be read at http://lib.tkk.fi/Diss/2008/isbn9789512292752/

VÄITÖSKIRJAN TIIVISTELMÄ	TEKNILLINEN KORKEAKOULU PL 1000, 02015 TKK http://www.tkk.fi
Tekijä Anna-Kaisa Repo	
Väitöskirjan nimi Numeeriset impulssikokeet dynaamisten epätahtikonemallien identifioinnissa	
Käsikirjoituksen päivämäärä 7.12.2007	Korjatun käsikirjoituksen päivämäärä
Väitöstilaisuuden ajankohta 4.4.2008	
☐ Monografia	☒ Yhdistelmäväitöskirja (yhteenveto + erillisartikkelit)

Tiedekunta	Elektroniikan, tietoliikenteen ja automaation tiedekunta
Laitos	Sähkötekniikan laitos
Tutkimusala	Sähkökoneiden mallinnus
Vastaväittäjä(t)	Prof. Thomas A. Lipo
Työn valvoja	Prof. Antero Arkkio
Työn ohjaaja	

Tiivistelmä

Työn tavoite on identifioida epätahtikoneiden dynaamisia malleja magneettikenttien kaksiulotteisen numeerisen ratkaisun avulla. Erityisesti tutkitaan oikosulkukoneita, joissa on suljetut ja syvät roottoriurat. Myös oikosulkukoneet, joissa on puoliavoimet roottoriurat sekä liukurengaskoneet on huomioitu tutkimuksessa.

Työssä esitetään kaksi uutta sovellusta numeerisille impulssikokeille, joissa sähkökoneen toimintaa simuloidaan aikadiskreetillä elementtimenetelmällä. Ensin tutkitaan staattorivirran vastetta, kun staattorijännitteeseen syötetään impulssimainen heräte. Seuraavaksi tutkitaan sähkömagneettisen vääntömomentin vastetta roottorin asentokulmaan tehtävään herätteeseen. Elementtimenetelmällä tuotettua dataa käytetään analyyttisten sähkökonemallien parametrien estimointiin. Analyyttiset mallit perustuvat sähkökoneiden teoriaan, jolloin niiden parametrit ovat fysikaalisesti järkeviä.

Tutkimuksen perusteella todetaan, että roottorisauvoissa esiintyvä virranahto vaikuttaa huomattavasti impulssikokeiden tuloksiin ja se täytyy ottaa huomioon myös analyyttisessa sähkökonemallissa. Myös kyllästyksellä on merkittävä vaikutus, joka voidaan havaita yliaaltoina impulssikokeiden tuloksissa ja myös estimoitujen parametrien arvoissa. Kyllästys on mallinnettu myös edistyneemmässä analyyttisessä mallissa. Tämän mallin parametreilla on selkeä fysikaalinen tulkinta.

Impulssikokeissa oletetaan, että tutkittavan järjestelmän toiminta voidaan kuvata lineaarisella mallilla valitun toimintapisteen läheisyydessä. Oletusta on tutkittu työssä monin eri tavoin. Impulssiherätteen amplitudia, pituutta ja alkamishetkeä on muutettu ja saatuja simulointituloksia vertailtu. Voidaan todeta, etta lineaarisuusoletus pätee sähkökoneiden yleisissä toimintapisteissä. Estimoitujen parametrien järkevyyttä on arvioitu vertaamalla niitä aikaharmonisella elementtimenetelmällä laskettuihin pysyvää tilaa kuvaaviin parametreihin.

Kun tutkitaan vääntömomentin vastetta roottorin asentokulmaan tehtävälle impulssille, huomataan, että joillakin taajuuksilla koneen sähkömagneettinen vaimennus roottorikulman vääntövärähtelyjen suhteen on negatiivinen. Ilmiötä on tutkittu myös mittauksin. Mittausten perusteella on havaittu, että itseherätteisiä vääntövärähtelyjä esiintyy taajuusalueella, jossa numeerinen impulssikoe ennustaa negatiivisen vaimennuksen.

Asiasanat	epätahtikoneet, parametrien estimointi, taajuusvaste, elementtimenetelmä		
ISBN (painettu)	978-951-22-9274-5	ISSN (painettu)	1795-2239
ISBN (pdf)	978-951-22-9275-2	ISSN (pdf)	1795-4584
Kieli	Englanti	Sivumäärä	186
Julkaisija	Teknillinen korkeakoulu, Sähkötekniikan laitos		
Painetun väitöskirjan jakelu	Teknillinen korkeakoulu, Sähkötekniikan laitos		
☒ Luettavissa verkossa osoitteessa http://lib.tkk.fi/Diss/2008/isbn9789512292752/			

Acknowledgement

This research work was carried out within the Team of Electromechanics at the Department of Electrical Engineering of Helsinki University of Technology. During the work, the facilities, expertise, equipment, and computing capacity provided by the department were in extensive use. The measurements were performed in the department's machine hall. In the measurements related to torsional oscillations, equipment provided by VTT were also utilised.

The greatest support in all the stages of the work was given by Professor Antero Arkkio. Professor Marko Hinkkanen and Mikaela Ranta shared their expertise in control of electric drives. This co-operation gave theoretical grounds and motivation for the research. Paavo Rasilo had a significant contribution in the computations and analyses related to the torque models. The demanding measurements of torsional oscillations were performed by Dr. Seppo Aatola from VTT Technical Research Center of Finland.

This work received financial support from several sources. The long-term funding was provided by The Graduate School of Electrical Engineering. A part of the research was conducted within a project 'Numerical and experimental identification of electrical machine models' funded by the Finnish Funding Agency for Technology and Innovation (TEKES), ABB, Kone and High Speed Tech Ltd. The additional support from Finnish Foundation for Technology Promotion (TES) improved my standard of living.

The colleagues from the Teams of Electromechanics and Electric Drives provided their support and company both inside and outside the department's walls. Andrej Burakov shared an office with me for almost four years and his help was always available. Marika Schröder organised and took care of numerous deeds and details of research, teaching, and travelling. The invaluable help I received at the end of year 2007 will not be forgotten. Ari Haavisto and Jarmo Perho shared their long-term know-how in various parts of a researcher's work spanning from setting up laboratory exercises to drilling iron. Professor Jorma Luomi, Anouar Belahcen, Erkki Lantto, Emeritus Professor Tapani Jokinen and Asko Niemenmaa carried out the first pre-examination of the manuscript within a very short notice. The interest received from TEKES and the representatives of Finnish industry gave motivation for the work.

My sisters, Eveliina and Päivikki, made it possible for me to complete this work within these four years. I was privileged to stay at work as long as needed but also enjoy my hobbies without worrying about the laundry or an empty fridge. My brother Pekka gave me the idea of applying the differential evolution in this work. With my friends Diana and Tanja, I spent exciting, hilarious and relaxing weekends and holidays. There will be more to come.

Thank you all.

It is a lucky coincidence to have met a person with whom one can share both professional and personal interests. The greatest debt I owe to my colleague and friend Jenni Pippuri.

Anna-Kaisa Repo

List of publications

The dissertation consists of an overview and the following publications:

P1. Repo A.-K., Arkkio A. Parameter estimation of induction machines using the numerical impulse method. *Proceedings – SPEEDAM International Symposium on Power Electronics, Electrical Drives, Automation and Motion*, Taormina, Italy, May 2006, No. WA1-19136, 6 p.

P2. Repo A.-K., Arkkio A. Numerical impulse response test to estimate circuit-model parameters for induction machines. *IEE Proceedings – Electric Power Applications*, Vol. 153, No. 6, November 2006, pp. 883–890.

P3. Repo A.-K., Niemenmaa A., Arkkio A. Estimating circuit models for a deep-bar induction motor using time harmonic finite element analysis. *Proceedings – International Conference in Electrical Machines*, Crete, Greece, September 2006, No. 614, 6 p.

P4. Repo A.-K., Arkkio A. Numerical impulse response test to identify parametric models for closed-slot deep-bar induction motors. *IET Electric Power Applications*, Vol. 1, No. 3, May 2007, pp. 307–315.

P5. Repo A.-K., Hinkkanen M., Arkkio A. Parameter estimation for induction motors to study the effects of voltage, frequency and slip. *Proceedings – EPE European Conference on Power Electronics*, Aalborg, Denmark, September 2007, 10 p.

P6. Hinkkanen M., Repo A.-K., Cederholm M., Luomi J. Small-signal modelling for saturated induction machines with closed or skewed rotor slots. *Proceedings – IEEE-IAS Industry Applications Society Annual Meeting,* New Orleans, Louisiana, USA, September 2007, 7 p.

P7. Hinkkanen M., Repo A.-K., Cederholm M., Luomi, J. Small-signal model for saturated deep-bar induction machines. *Proceedings – EPE European Conference on Power Electronics*, Aalborg, Denmark, September 2007, 10 p.

P8. Repo A.-K., Rasilo P., Arkkio A. Dynamic electromagnetic torque model and parameter estimation for a deep-bar induction machine. *IET Electric Power Applications*, in press.

P9. Repo A.-K., Rasilo P., Niemenmaa A., Arkkio A. Identification of electromagnetic torque model for induction machines with numerical magnetic field solution. *IEEE Transactions on Magnetics*, in press.

List of symbols and abbreviations

Symbols

Vector quantities are represented in **bold**, scalar quantities are in *italic* and complex-valued quantities are underlined. The steady-state quantities are denoted by subscript 0.

a_{rel}	relative amplitude, [-]
$\boldsymbol{e}$	electromotive force, [V]
f_{s}	supply (stator) frequency, [Hz]
f	frequency, [Hz]
f_{d}	duration frequency of an impulse or perturbation frequency, [Hz]
I	cost function, [-]
$\boldsymbol{i}$	a current vector, [A]
$\underline{i}_{\mathrm{s}}$	stator current, [A]
$\underline{i}_{\mathrm{r}}$	total rotor current, [A]
$\underline{i}_{\mathrm{r1}}$	rotor current of the first rotor branch, [A]
$\underline{i}_{\mathrm{r2}}$	rotor current of the second rotor branch, [A]
i_{sx}, i_{sy}	direct-axis and quadrature-axis stator current components in synchronous reference frame, [A]
i_{rx}, i_{ry}	direct-axis and quadrature-axis total rotor current components in synchronous reference frame, [A]
i_{r1x}, i_{r1y}	direct-axis and quadrature-axis rotor current components of the first rotor branch in synchronous reference frame, [A]
i_{r2x}, i_{r2y}	direct-axis and quadrature-axis rotor current components of the second rotor branch (synchronous reference frame), [A]
$\boldsymbol{L}^{\mathrm{dyn}}$	dynamic inductance matrix, [H]
L_{c},	mutual rotor leakage inductance, [H]
L_{ct}, $L_{\sigma\mathrm{rt}}$	incremental rotor leakage inductance, [H]
L_{m}, L_{m0}	magnetising inductance of a circuit model, [H]
L_{mt}	incremental magnetising inductance, [H]
L_{s}, L_{r}	stator and rotor self inductances of a circuit model, [H]
L_{t}	incremental coupling inductance, [H]
$L_{\sigma\mathrm{s}}$, $L_{\sigma\mathrm{r}}$	stator and rotor leakage inductances of a circuit model, [H]
$L_{\sigma\mathrm{r1}}$, $L_{\sigma\mathrm{r2}}$	rotor leakage inductance of the first and second rotor branch, [H]

p	number of pole pairs, [-]
R	a coil resistance, [Ω]
R_s	stator resistance, [Ω]
R_c	end-ring rotor resistance, [Ω]
R_{r1}, R_{r2}	resistances of the first and second rotor branches, [Ω]
s	slip, [-]
t	time, [s]
t_d	duration time of a perturbation, [s]
t_1	initial time, [s]
T_d	damping torque, [Nm/rad]
T_e	electromagnetic torque, [Nm]
T_L	load torque, [Nm]
T_s	synchronising torque, [Nm/rad]
$\boldsymbol{u}$	a voltage vector, [V]
$\underline{u}_s$	stator voltage, [V]
$\underline{u}_r$	rotor voltage, [V]
u_{sx}, u_{sy}	direct-axis and quadrature-axis stator voltage components in the synchronous reference frame, [V]
u_{rx}, u_{ry}	direct-axis and quadrature-axis total rotor voltage components in the synchronous reference frame, [V]
$\boldsymbol{X}$	regressor matrix, [-]
$\boldsymbol{Y}$	output vector, [-]
$\hat{\boldsymbol{Y}}$	estimated output vector, [-]
Δ	a small-signal perturbation of a variable, [-]
$\boldsymbol{\theta}$	parameter vector, [-]
θ_r	rotor position angle in electrical radians, [rad]
μ_r	relative permeability, [-]
λ	power factor, [-]
τ_p	pole pitch, [-]
φ	angle with respect to the steady-state stator voltage vector, [rad]
φ_r	phase angle of the impulse excitation for the rotor position angle, [rad]

$\underline{\psi}_s$	stator flux linkage, [Wb]
$\underline{\psi}_r$	total rotor flux linkage, [Wb]
$\underline{\psi}_{r1}$	rotor flux linkage of the first rotor branch, [Wb]
$\underline{\psi}_{r2}$	rotor flux linkage of the second rotor branch, [Wb]
ψ_{sx}, ψ_{sy}	direct-axis and quadrature-axis stator flux linkage components, [Wb]
ψ_{rx}, ψ_{ry}	direct-axis and quadrature-axis rotor flux linkage components, [Wb]
ψ_{r1x}, ψ_{r1y}	direct-axis and quadrature-axis rotor flux linkage components of the first rotor branch in synchronous reference frame, [Wb]
ψ_{r2x}, ψ_{r2y}	direct-axis and quadrature-axis rotor flux linkage components of the second branch in synchronous reference frame, [Wb]
ω_k	angular frequency of a general reference frame, [rad/s]
ω_s	angular frequency of stator quantities, [rad/s]

Abbreviations

DE	differential evolution
DFT	discrete Fourier transform
FE, FEA	finite element, finite-element analysis
FFT	fast Fourier transform
FRF	frequency response function
PRBS	pseudo-random binary sequence
SSFR	standstill frequency response
dc	direct current
mimo	multiple input multiple output
rms	root mean square
siso	single input single output
2D (3D)	two-dimensional (three-dimensional)

Definitions

Impulse

Within this work, a pulse-like excitation signal.

Frequency response function (FRF)

The ratio of output and input variables in frequency domain. Within this work, analytical expressions for FRFs are derived using Laplace transformation. The functions are defined from $t = 0$ on and the FRFs are obtained by replacing Laplace variable s with $j\omega$, where ω is the excitation frequency.

Numerical frequency response function (FRF)

A data vector resulting from a numerical impulse response test. Depending on the test, it can be the ratio of the stator current and stator voltage, or the ratio of the electromagnetic torque and rotor position angle. These are all small-signal quantities or perturbations.

Complex-valued admittance

The small-signal model that defines the space-vector of stator current perturbation with respect to the space-vector of stator voltage perturbation. It can be expressed as a single input - single output frequency response or transfer function. All the small-signal models are functions of frequency.

Mimo admittance

The small-signal model that defines the perturbations of stator current components (real and imaginary parts separately) with respect to the perturbations of stator voltage components. The model takes into account the saturation by structure and it contains steady-state current components. It is expressed as a multiple input - multiple output transfer function.

Torque model

The small-signal model that represents the perturbations of electromagnetic torque with respect to the perturbations of rotor position angle. Complex-valued currents, voltages and flux linkages are assumed as well as in the case of complex-valued admittance.

Steady-state or circuit model

The steady-state models depict the rms values and phase angles of voltages and currents, and the electromagnetic torque at a certain operation point.

Within this dissertation, a double-cage model for the rotor is mainly used. Therefore, if it is not mentioned otherwise, all the small-signal and circuit models are assumed to have the double-cage structure.

1 Introduction

1.1 Background

Electrical machines operate as a part of a comprehensive power system chain. Within the chain, electrical machines, power electronic devices, control units, and mechanics interact with each other via complicated relations. While the systems become more extensive, the need to predict and simulate the behaviour of the chain under different operation modes increases as well.

Recently, a significant increase in the computing capacity has taken place. Today, the operation of electrical machines can be modelled accurately using numerical magnetic field computations. Many complicated physical phenomena, such as saturation of iron and eddy currents in rotor bars, can be taken into account realistically. In order to study the interaction between the machine and, for example, the control devices, a numerical model of the electrical machine can be coupled to a circuit simulator. However, the simulation times are long and therefore the combined model is not suitable for on-line applications. In addition, applying the model requires expertise in finite-element analysis (FEA). Besides, system models containing several numerical models of electrical machines are still today too demanding to simulate.

For many applications, simpler analytical models for electrical machines are sufficient. At steady-state operation, rms values of currents, voltages and electromagnetic torque can be predicted accurately enough by an equivalent circuit. In the case of many common transients, a space-vector or two-axis model consisting of a few differential equations can provide sufficient information about the machine behaviour. Dynamic or small-signal models depict the behaviour of the machine in the neighbourhood of an operation point under small perturbations. These models are needed in the design and implementation of control algorithms. The most usual applications of small-signal models are a different kind of stability analyses. Besides depending of the structure and order, the performance of the analytical models also depends on how closely the parameters correspond to the operation point.

Within this work, mainly small-signal models are discussed. The primary contribution is the development of methods to estimate parameters of analytical small-signal models using time-stepping FEA. However, the steady-state circuit models are also an important part and they are used to evaluate the performance of the small-signal models obtained. The reasonability of the steady-state models is fairly simple to evaluate by comparing their performance with the corresponding operation points obtained by other means such as computations and measurements. Within this work, the steady-state parameters are also utilised to assist the estimation of small-signal parameters. For example, some model parameters or their ratio are fixed to those obtained from steady-state computations. This makes the estimation of small-signal parameters not only faster but also more successful.

1.2 Aim of the work

The main objective of this work is to estimate electrical parameters for induction machines using numerical magnetic field computations. One purpose is to use as short a finite-element

simulation as possible to obtain a sufficient amount of information for the estimation. This means that the dynamics of the machine has to be excited simultaneously within a wide frequency range. For this purpose, an impulse excitation appears as an attractive alternative. Thus, an aim of the work is to study the applicability, advantages and restrictions of the numerical impulse response test. The fundamental question to be answered is: What kind of information can be obtained by applying the numerical impulse response test?

1.3 Contribution

The most important scientific contributions of the study are listed below:

- This study presents two new applications of numerical impulse response tests. Firstly, the impulse excitation is applied to the stator voltage and the response of stator current is studied. Secondly, the impulse is applied to rotor position angle and the response of electromagnetic torque is studied. Both obtained numerical frequency response functions (FRF) can be used to estimate circuit-model parameters.
- In this work, time-discretised FEA is used for parameter estimation of induction machines. It is not used only to imitate measurements but its advantages compared to measurements are also utilised. For example, simplified FE models have been used to distinguish between the effects of saturation and skin effect.
- Previously, a time-harmonic FEA has been applied to estimate steady-state circuit parameters for the traditional T-equivalent circuit. Within this work, the method is developed further to estimate parameters of circuit models with multiple rotor circuits. The performance of circuit models with different rotor structures has been evaluated and an optimal structure has been sought.
- The time-harmonic FEA is also used to estimate circuit parameters in a wide operation range with different types of induction machines. The effects of slip, flux level, and supply frequency on the parameter estimates are studied extensively, and useful information for the design and control of high-performance electric drives is obtained.
- By performing impulse tests with two perpendicular impulses, the parameters of small-signal models that include the skin effect of rotor bars and saturation as a function of magnetising flux and rotor current can be estimated. When using the mimo admittance, both the large-signal and incremental parameters can be estimated simultaneously.
- It has also been noticed that the average of the FRFs obtained from the impulse tests with perpendicular impulses cancels the saturation-induced harmonics within the frequency range of –200…200 Hz. The average FRF corresponds well to the one obtained by using harmonic excitation. The complex-valued admittance can be fitted well to the average FRF.
- When the numerical angle impulse test is applied, a dynamic model for the electromagnetic torque can be obtained. The parameters of the model are estimated using the

data computed at the actual operation point. By using the angle impulse test, the frequency ranges of negative damping can be detected. The measurements performed verify the computation results.

1.4 Structure of the work

The dissertation consists of the following parts:

- Chapter 1 presents an introduction and the aim of the work. The scientific contribution and the publications are listed.
- Chapter 2 presents the literature study performed. It concerns several fields of research related to this study. These are, for example, parameter estimation by different methods, more advanced analytical models for induction machines, and torsional dynamics.
- In Chapter 3, the basic procedure for performing numerical impulse response tests is presented. Estimation of steady-state parameters is described briefly. A general view of the analytical small-signal models used is shown and the curve-fitting technique is also described.
- Since within this work, the numerical impulse response tests are used especially for parameter estimation, the estimation results for several cases are presented in Chapter 4. The estimation results are shown for cage-induction machines since the study has mainly focused on them.
- The results are discussed and summarised in Chapter 5.

The publications included in this dissertation are reprinted in the end-part of the dissertation. Chapters 3 and 4 are based on these publications. However, some results that are not included in the publications are presented in Chapter 3.

Publication P1

The idea of the numerical voltage impulse test is presented. An excitation impulse with a low-dc component is applied to the stator line-to-line voltage. The impulse test is performed once. In addition, a steady-state computation starting from the same initial field as the impulse test is performed. In order to extract the small-signal dynamics, the results of the steady-state computation are subtracted from the results of the impulse test. From the ratio of the voltage impulse and the stator current response, the numerical FRF is obtained. Three different types of induction machines are studied: An 850-kW cage-induction machine with semi-open rotor slots, a 1.7-MW slip-ring machine, and a 300-kW solid-rotor machine with a thin copper layer on the rotor surface.

Small-signal parameters for a T-equivalent circuit are estimated using the impulse test. The analytical model can be referred to as single-cage complex-valued admittance. The parameters obtained are compared with the steady-state parameters estimated using the time-harmonic FEA and impedance method. It is found that the values of inductances obtained from the impulse response test are smaller than the corresponding steady-state values. This refers to the fact that the impulse test can take into account the incremental permeability defined by the

magnetisation curve, whereas the time-harmonic FEA implements only the effective permeability. It is found that, for all the three machines, the fitting is successful. However, it is noted that, in the case of the cage-induction machine, the fitting results are slightly worse than with the two other machines. This is assumed to be related to the skin effect in rotor bars, which is not modelled properly by using only one constant-valued rotor resistance.

The paper has been written by Anna-Kaisa Repo. Professor Antero Arkkio has contributed by means of comments, suggestions and his expertise in finite-element analysis.

Publication P2

The voltage impulse test is applied to estimate the parameters of a 37-kW deep-bar induction machine. Two different impulse types are tried. The applicability of the impulse test is studied by comparing the FRF obtained from the impulse tests with the one obtained using harmonic excitation. The results show a fairly good agreement when using the impulse type similar to the one presented in P1. The effect of the impulse amplitude on the shape of the FRF is also studied. It is noted that the size of the amplitude has only a small effect when it is at the most 20% of the supply voltage.

It is noted that the small-signal model with only one rotor branch cannot be fitted to the numerical FRF over a wide frequency range. Therefore, the parameters are estimated piecewise, using one narrow frequency range at a time. It can be concluded that, in the case of the studied machine, the skin effect significantly affects the shape of the FRF. The parameter estimates are compared with the steady-state parameters obtained from the time-harmonic FEA. As in P1, the estimated inductances given by the two methods differ from each other. This difference is related to the different definitions of permeability between the two FEAs. The value of the estimated rotor resistance varies substantially within the piecewise estimation. It is concluded that, to be able to model a wider frequency range with constant parameters, the order of the small-signal model has to be increased.

The paper has been written by Anna-Kaisa Repo. Professor Antero Arkkio has contributed by means of comments, suggestions and his expertise in finite-element analysis.

Publication P3

Parameter estimation of the 37-kW deep-bar induction machine using time-harmonic FEA is studied. Within the method, the rotor slots are divided into several sub-conductors and the parameters of the corresponding circuit model consisting of one to seven rotor branches are estimated. The slip is varied within a wide range between no-load and standstill conditions. The variation of circuit parameters as a function of slip is studied for circuit models with different numbers of rotor branches. The performance of different circuit models is evaluated using the torque-versus-speed curves.

The parameters are estimated at a constant supply frequency of 50 Hz and varying slip. The torque-versus-speed curves are calculated from the circuit model with each set of parameter estimates. The obtained curves are compared with the one computed, using the time-harmonic FEA. It is noted that, in the case of a T-equivalent circuit, the torque-versus-speed curves vary

significantly, depending on the operation point where the parameters are estimated. However, when using a three-cage model, the values of rotor parameters vary less and the torque-versus-speed curves are close to each other. The effect of saturation on the parameters is also studied by estimating the parameters at different supply voltages. A torque-versus-speed curve is also measured. The time-harmonic FEA and the measurements show a good agreement.

The paper has been written by Anna-Kaisa Repo. Professor Antero Arkkio has developed the finite-element code and also contributed by means of comments and suggestions. Asko Niemenmaa contributed by means of comments.

Publication P4

The work continues from the results obtained in P2. The skin effect in the rotor bars and saturation are studied more closely. The skin effect is included by using a double-cage small-signal model. The model can be referred to as complex-valued admittance. The iron bridges of the closed rotor slots are saturated by the fundamental flux. The effects of saturation can be detected as harmonics in the numerical FRF. The phases of the harmonics depend on the direction of impulse. This phenomenon can be detected when impulse tests are performed using unidirectional impulses aligned to a certain angle with respect to the fundamental voltage vector.

The effect of harmonics is most visible around the frequencies of 100 Hz and –200 Hz. It is noted that, with two perpendicular impulses, these harmonics are at opposite phases. The theoretical derivation confirms the observation. Thus it is concluded that the interference of saturation harmonics can be cancelled by taking the average of the results of two impulse tests. The resulting FRF can be used to estimate the parameters of the small-signal model, and the fit obtained is very good. The average FRF also corresponds well to the FRF obtained using harmonic excitation, where the saturation harmonics are automatically neglected by considering the response only at the excitation frequency.

The paper has been written by Anna-Kaisa Repo. Professor Antero Arkkio has contributed by means of comments, suggestions and theoretical considerations.

Publication P5

A comprehensive parameter estimation using both the time-harmonic FEA and voltage impulse test is performed for two different types of cage-induction machines. The first one is an 80-kW copper-cage machine designed for frequency-converter supply. The other one is the 37-kW machine studied in P1, P3 and P4, designed for a direct on-line supply. For the 80-kW machine, an optimal efficiency at every supply frequency and at several flux levels is looked for by means of time-stepping computations. The constant-torque and field-weakening regions are covered. The steady-state parameters for the T-equivalent circuit are estimated at these points using the time-harmonic FEA. Small-signal parameters of a double-cage model are also estimated at some operation points of continuous use. For comparison, the steady-state parameters of the 37-kW machine are also presented at several flux levels and slips. The small-signal parameters are estimated at rated and half load, and at full and decreased flux. It

is concluded that the estimation of small-signal parameters is in general successful. However, in the case of 80-kW machine at the supply frequencies higher than the base frequency, reasonable estimates for magnetising inductance cannot be found. Despite of this, the obtained fits are still good.

The paper has been written by Anna-Kaisa Repo. Marko Hinkkanen has contributed by means of comments and his expertise in the field of electric drives. Professor Antero Arkkio has contributed by computing a part of the results and commenting on the work.

Publication P6

A small-signal model for induction machines with closed or skewed rotor slots is presented. The model takes into account the saturation by assuming a magnetising inductance and rotor leakage inductance dependent on both the magnetising and rotor currents. The model can be referred to as a *single-cage mimo admittance model*. The numerical voltage impulse test is applied to parameter estimation of a 2.2-kW cage-induction machine. Since the saturation is included in the analytical model, the harmonics caused by anisotropy are also modelled. In contrast to the model used in P3, both the steady-state and incremental magnetising inductances can be obtained from the impulse test. The steady-state parameters are close to the ones obtained using time-harmonic FEA. When the terms related to the saturation are neglected, the small-signal model corresponds to the one used in P3. When the parameters are estimated using the average FRF discussed in P3, it is found that the estimate for the magnetising inductance is between the estimated steady-state and incremental values.

The paper has been prepared in a close co-operation between the authors. It has been written by Dr. Marko Hinkkanen, except for parts describing the numerical impulse response test written by Anna-Kaisa Repo and the results section written by Mikaela Ranta (née Cederholm). Anna-Kaisa Repo has performed the FE computations and assisted in implementing the fitting algorithms. The fitting is performed by Mikaela Ranta. Professor Jorma Luomi has contributed by commenting on the work and the text.

Publication P7

The small-signal model presented in P6 is extended to include the skin effect in deep rotor bars by adding another rotor branch to the circuit model. The model is referred to as the *mimo admittance model*. In this model, the magnetising inductance and one rotor leakage inductance are allowed to depend on the magnetising flux and total rotor current. The other leakage inductances are assumed to be constant. The parameters of the 37-kW machine are estimated using the voltage impulse test. The frequency range is 0…300 Hz. It is concluded that the model presented is able to take into account both the skin effect and load-dependent saturation effects caused by closed rotor slots. Both the steady-state and small-signal parameters are obtained. The parameter estimates are physically reasonable, and the values of the steady-state parameters are close to the ones obtained by time-harmonic FEA.

The paper has been prepared in a close co-operation between the authors. It has been written by Dr. Marko Hinkkanen, except for the introduction and the parts describing the numerical impulse response test written by Anna-Kaisa Repo. The results section is written by Mikaela

Ranta (née Cederholm). Anna-Kaisa Repo has performed the FE computations. The fitting is performed by Mikaela Ranta. Professor Jorma Luomi has contributed by commenting on the work and the text.

Publication P8

A small-signal model for depicting the electromagnetic torque as a function of rotor position angle is presented. The model is referred to briefly as a *torque model*. An impulse excitation is applied to the rotor position angle and the response of electromagnetic torque is computed. An 850-kW cage-induction machine is studied. The model takes into account the skin effect in deep rotor bars. The parameters of the model include seven circuit parameters and four steady-state current components. In the estimation, the stator resistance, the ratio between stator and rotor leakage inductances, and the amplitude of total rotor current are fixed to the values given by the time-harmonic FEA. It is noted that the fit for the numerical data is good and the parameter estimates are close to the values obtained from the time-harmonic FEA.

The computed FRF predicts negative damping within the frequency range of 43…50 Hz. A similar phenomenon is observed by simulating the impulse test with a 37-kW cage-induction machine. The observation is studied also by measurements performed with two 37-kW cage-induction machines. The machines are coupled with a thin shaft and supplied from a synchronous generator. It is noted that at the supply frequencies for which the negative damping is predicted, self-excited torsional oscillations occur. The oscillations can be detected from induced stator-current harmonics as well.

The paper is written by Anna-Kaisa Repo. Paavo Rasilo has participated in developing and testing the analytical models. Professor Antero Arkkio has contributed by valuable comments and considerations, and expertise on measurements. The measurements have been performed in co-operation with Dr. Seppo Aatola from VTT.

Publication P9

Small-signal models for depicting electromagnetic torque are studied for both cage-induction and slip-ring machines. The studied machines have similar stator winding and the same rated power, 1.7 MW. In the case of the cage-induction machine, a double-cage model similar to the one presented in P8 is needed. For the slip-ring machine, the single-cage small-signal model is sufficient. However, since in doubly-fed slip-ring machines the rotor voltage is perturbed proportionally to rotor angle, the related complex-valued coefficient is to be estimated as well. In the estimation, the components of the coefficient are allowed to vary freely. For both machines, the total rotor current is fixed in the estimation. The obtained fits are good and parameter estimates reasonable.

The paper is written by Anna-Kaisa Repo. Paavo Rasilo has performed some of the computations and participated in developing and testing the analytical models. Professor Antero Arkkio has contributed by making valuable comments and considerations. Asko Niemenmaa has contributed by commenting on the work.

2 Literature study

The main objective of this work is to compress the essential information given by FEA to a form of analytical model. This subject has been a matter of interest during the last two decades. Within this chapter, advanced analytical models including the skin effect of rotor bars and saturation are also reviewed. In order to categorise the dissertation, the most recent parameter estimation techniques for induction machines are discussed as well. The frequency-response methods are particularly considered. The angle impulse test is used to model the behaviour of the machine under low-amplitude torsional oscillations. The literature on torsional dynamics dates back to the beginning of last century together with the development of the theory of rotating electrical machines. The related publications are reviewed comprehensively.

2.1 Numerical impulse response tests

In mechanics, experimental impulse testing is applied to detect natural modes and frequencies of structures. In the field of electrical machines, the numerical impulse response test was first applied to model forces acting between the stator and rotor. Tenhunen (2003) and Holopainen (2004) used impulse response tests to replace time-consuming computations performed using the forced whirling frequency method (Arkkio et al., 2000) to model the forces acting between the stator and an eccentric rotor. The rotor was displaced from the central position for a short period of time and the induced forces were computed. The results of time-stepping computations were transformed to the frequency domain. From the ratio of force and displacement, the numerical frequency response function (FRF) of the force was obtained. The numerical FRF was used to estimate the parameters of a low-order parametric model. Burakov (2007) extended the study to concern electrical machines with parallel branches in the stator winding. In this case, more complex analytical models were needed to fit the numerical data.

2.2 Parameter estimation by measurements

2.2.1 Parameter estimation

Typically, parameter estimation is based on a curve-fitting procedure, while the data for the estimation is provided by measurements (Nelles, 2001). The objective is to minimise the difference between the real output vector $\boldsymbol{Y}$ and estimated output vector $\hat{\boldsymbol{Y}}$ in a least squares sense, defined as

$$\boldsymbol{I} = \sum_{k=1}^{n} \left(Y(k) - \hat{Y}(k) \right)^2 . \tag{1}$$

The desired parameter estimates are those that minimise the value of the cost function $\boldsymbol{I}$. Often, it is possible to formulate the model in linear form

$$\boldsymbol{Y} = \boldsymbol{X}\boldsymbol{\theta} , \tag{2}$$

where $\boldsymbol{X}$ is the regressor matrix and $\boldsymbol{\theta}$ is the parameter vector to be estimated. The linear form can be solved as a linear least-squares problem using the pseudo inverse formula

$$\boldsymbol{\theta} = \left(\boldsymbol{X}^{\mathrm{T}} \boldsymbol{X} \right)^{-1} \boldsymbol{X}^{\mathrm{T}} \boldsymbol{Y} . \tag{3}$$

An important advantage of using linear regression is that it requires only one iteration step. It is therefore suitable for on-line estimation. However, numerical properties of the regression matrix may cause some difficulties. If $\boldsymbol{X}^{\mathrm{T}}\boldsymbol{X}$ is ill-conditioned, the matrix inversion can be unreliable. Therefore, (3) is often replaced by Gaussian elimination, for example in Matlab®. The linear regression is a global optimisation method since (3) has an unequivocal solution. A common modification for the basic method is a recursive least squares method. Each data sample is weighted by a factor that is decreased according to how old the sample is. The method is used for on-line estimation.

Linear regression has been a widely applied method of estimating the circuit parameters of induction machines. One of the first studies was presented by Velez-Reyes (1989). The state-space model of the induction machine is first transformed into a transfer function, the coefficients of which are functions of electrical parameters and speed,

$$\frac{\underline{i}_{\mathrm{s}}}{\underline{u}_{\mathrm{s}}} = \frac{b_1 s + b_0}{s^2 + a_1 s + a_0}, \tag{4}$$

where

$$\begin{aligned} a_1 &= \frac{R_{\mathrm{s}}L_{\mathrm{r}} + R_{\mathrm{r}}L_{\mathrm{s}}}{L_{\mathrm{s}}L_{\mathrm{r}} - L_{\mathrm{m}}^2} - \mathrm{j}\omega_{\mathrm{r}} \\ a_0 &= \frac{L_{\mathrm{r}}R_{\mathrm{s}}}{L_{\mathrm{s}}L_{\mathrm{r}} - L_{\mathrm{m}}^2}\left(\frac{R_{\mathrm{r}}}{L_{\mathrm{r}}} - \mathrm{j}\omega_{\mathrm{r}}\right) \\ b_1 &= \frac{L_{\mathrm{r}}}{L_{\mathrm{s}}L_{\mathrm{r}} - L_{\mathrm{m}}^2} \\ b_0 &= \frac{L_{\mathrm{r}}}{L_{\mathrm{s}}L_{\mathrm{r}} - L_{\mathrm{m}}^2}\left(\frac{R_{\mathrm{r}}}{L_{\mathrm{r}}} - \mathrm{j}\omega_{\mathrm{r}}\right) \end{aligned} . \tag{5}$$

The transfer function can be transformed to a second-order differential equation that can be formulated to correspond to (2). In this case, the vector $\boldsymbol{Y}$ consists of the second derivatives of stator current, and the matrix $\boldsymbol{X}$ is constituted from the stator voltages and currents and their first derivatives. The parameter vector $\boldsymbol{\theta}$ consists of four parameters that are functions of circuit parameters and speed. The derivatives are obtained by filtering. The parameter estimation is performed using the recursive least squares method. Recently, the linear formulation has been applied, for example, by Cirrincione et al. (2003a, 2005). In the estimation procedure, the so-called *K*-parameters, which are functions of the electrical parameters, are first estimated. From those, the steady-state parameters of (5) are calculated.

Using the linear model is simple and straightforward but it has drawbacks. Firstly, the derivatives of current and voltage have to be obtained from the measurements. High-level signal-processing equipment is required. Ribeiro et al. (1999) have formulated a discrete-time model where the derivatives are treated as discrete-time filters. At high sampling rates, the discrete-time model corresponds to a continuous-time model. The measurements of derivatives are obtained from digital state-variable filtering. Several operation conditions and model modifications have been studied. It is suggested, for example, that, in order to obtain the best esti-

mates, the stator resistance should be estimated first in a separate process. In (Ribeiro et al., 2000), similar studies have been performed for PWM supply. Fang et al. (2004) have implemented a slightly different model in an on-line estimator. The second-order derivatives are depicted by second-order filters but the model is modified so that it is only of the first order. The performance has been verified by measurements.

Another drawback is related to the linear dependency of the parameters. The parameter vector $\boldsymbol{\theta}$ of a T-equivalent circuit model (5) consists of four terms that are functions of five circuit parameters. Therefore, all the five circuit parameters cannot be solved unequivocally. A rule defining the dependency between the parameters can be included in the estimation by using a constrained regression. The problem of linear dependency between the parameters is present in all the estimation where only the stator quantities are used (Corcoles et al., 2002). In (Cirrincione, 2003b), a constrained total least squares method was tried and good estimation results were obtained.

If the circuit parameters are to be estimated directly without intermediate parameters, the model cannot be formulated as (2). The minimisation problem has to be treated as a nonlinear least squares fit. Nonlinear functions may have several local minima and, in order to obtain the desired one, reasonable initial values for the parameters have to be chosen. In many recent works on the parameter estimation of induction machines, gradient-based algorithms have been applied.

Proca and Keyhani (2002) used a constrained optimisation to estimate the circuit parameters within a wide operation range. Under a steady-state operation, a 10% step was applied to the supply voltage amplitude. The fitting was performed by comparing the output of the state-space model to the measurements. In this case, however, the initial values for flux linkages were also estimated. From the results of several operation points, circuit parameters were modelled as a function of a current or frequency. The magnetising inductance was found to depend strongly on the direct-axis stator current and the leakage inductance on the stator current amplitude. The rotor resistance varied with rotor frequency, and, for model implementation, an on-line observer for the resistance was developed. The obtained model performed well compared to measurements when performing large-signal transients. The advantage of the method is that it gives good estimates for large-signal parameters at various operation points. However, it is fairly time-consuming.

Alternatives of the gradient-based optimisation methods are stochastic search methods such as simulated annealing, simplex and genetic algorithms (Nelles, 2001). Within the last decade, genetic algorithms and evolutionary programming have become widely applied methods within the structural optimisation of electrical machines (Palko, 1996). They do not require any knowledge of the gradients of the target function nor reasonable initial values to converge to the desired minimum.

Alonge et al. (1998) presented estimation of circuit parameters and rotor inertia for induction machines using genetic algorithms. The estimation data – stator voltage and current, and speed – were produced by a transient test from standstill to a steady-state operation point. The

fitting was performed by simulating the two-axis model and equation of motion, and comparing the model output to the measured quantities. Huang et al. (2001) also applied genetic algorithms when estimating circuit parameters from data provided by a start-up to no-load condition. The estimation was performed by calculating the full-load torque, locked-rotor torque, and breakdown torque from the circuits and comparing the values to those provided by the manufacturer. Orlowska-Kowalska et al. (2006) performed parameter estimation at standstill using genetic algorithms. A step excitation was superimposed on the supply voltage. The phases were controlled by a PWM frequency converter so that no torque was produced.

An evolutionary algorithm called differential evolution (Price et al., 2005) has become a popular optimisation technique. The algorithm is fast and suitable for complicated optimisation problems. Ursem and Vadstrup (2003) compared the performance of several stochastic search algorithms, including the differential evolution in the parameter estimation of cage-induction machines. The circuit parameters and the moment of inertia were estimated for both the space-vector model and a model including saturation. The saturation was modelled by depicting the magnetising inductance as a function of the magnetising current, which gave rise to two additional parameters to be estimated. The estimation data were produced by simulating a start-up with the two models with known parameters. It was observed that the differential evolution found the correct parameters every time and, in addition, it converged the fastest of the several stochastic algorithms tried.

When the estimation data is produced by measurements, such factors as measurement errors and noise originating from different sources have to be considered. If the estimation data is produced by finite-element computations, as in the case of this work, these factors can be omitted. Within this dissertation, most of the analytical models contain more electrical parameters than the basic T-equivalent circuit. In addition, the mimo admittance and torque model contain steady-state current components. Some of those are also estimated. Therefore, the linear formulation (3) cannot be applied. A nonlinear fitting technique is to be used. The models contain some parameters for which it may be difficult to find reasonable initial values. Therefore, some stochastic algorithms have been studied and, from those, the differential evolution is chosen for the estimation.

2.2.2 Double-cage models

Parameters of double-cage circuit models have also been determined by measurements. Corcoles et al. (2002) have applied the Levenberg-Marquardt algorithm to estimate the circuit parameters of a double-cage induction machine from steady-state measurements. In the model, the core-losses are neglected and the stator resistance is assumed to be known. A minimum number of parameters is estimated by eliminating two of the total four leakage inductances. In the first case, the value of one of the leakage inductances is set to zero and the other parameters are estimated. In the second case, two leakage inductances are assumed to be equal. The estimation is performed using a gradient-based method. The results obtained with the two methods are in good agreement with measurements.

Lindenmeyer et al. (2005) have also estimated the steady-state parameters of a double-cage model using a nonlinear estimation technique. The cost function minimises the differences of the measured and estimated stator current amplitudes, power factor, and electromagnetic torque. The nameplate and other standard data provided by the manufacturer are used as constraints for the estimation. The saturation of leakage inductances is modelled using so-called describing functions. Nangsue et al. (1999) have used a genetic algorithm to estimate parameters for a T-equivalent circuit, a simplified, and a double-cage circuit model. These previous studies covering the double-cage models have focused on estimating steady-state parameters.

2.2.3 Signal injection

Holliday et al. (1994) presented an on-line parameter estimation technique that uses high-frequency signal injection for excitation. For the injected signal at frequencies 7.5…13.5 times the fundamental, the observable equivalent circuit can be approximated as the locked-rotor equivalent circuit. The resistances and leakage inductances were measured at several injection frequencies and compared with the ones obtained from locked-rotor tests performed at the corresponding supply frequencies. The results showed a good agreement and it was concluded that the on-line signal injection could be used to obtain the parameters as a function of frequency. The parameter variation with respect to temperature could also be tracked. The tests were performed at several flux levels and it was noticed that the behaviour of the parameters was independent of the magnetising flux. The stator resistance was measured using a dc injection. The amplitudes of the applied signals were 5…7% of the fundamental supply voltage. Those amplitudes are of the same order of magnitude as the ones used in this dissertation.

Sensorless position and velocity estimation using a signal injection became a topic of interest in the 1990s. Jansen and Lorenz (1995) presented a method to detect rotor position by tracking magnetic saliencies produced by the rotor slot openings. In the method, a balanced three-phase signal within frequencies 500…2000 Hz was injected to the PWM supply of an induction motor. The high-frequency stator current response can be modelled by a simplified equivalent circuit that consists only of the stator and rotor leakage inductances. The variation of this high-frequency impedance depends on the rotor position. The frequency of the signal has to be high enough to enable the skin effect of rotor bars to limit the penetration depth close to the rotor surface. On the other hand, at frequencies above 2 kHz the skin effect in the laminations might unnecessarily complicate the estimation. In this case, the saliency caused by saturation has to be attenuated by compensation. The signal amplitudes were very low, 0.1…0.3% of the fundamental supply. The amplitudes of this magnitude do not disturb the normal operation of the machine. However, in order to distinguish such a small response signal from measurements, high-level signal-processing devices and techniques are required.

In (Jansen et al., 1996), the method was applied utilizing the saturation-induced saliencies. Both the semi-closed and closed-slot induction machines were studied by simulations and locked-rotor measurements. The method was found more applicable for open or semi-closed slots since then the saliency is mainly induced by the main flux. In the case of closed slots, it was noticed that the saliency was more dependent on the direction of the rotor current vector,

which complicated the position tracking. This result refers to that the rotor current is an important factor when considering the effects of saturation, particularly, in the case of closed rotor slots.

Holtz (2006) has presented a comparison between the different methods proposed to be used in sensorless speed control. The methods are based either on the on-line estimation of model parameters or tracking saliencies by signal injection. The excitation signals are classified into rotating, alternating and PWM-produced signals.

In one of the most recent studies (Briz et al., 2007), a high-frequency signal injection has been used for temperature monitoring. Instead of estimating the stator resistance with a dc excitation, the so-called stator-transient impedance is measured by using a signal of 200…400 Hz. The stator-transient impedance is proportional to the temperature of stator windings.

Jang et al. (2004) have used FEA to study the effects of frequency and amplitude of high-frequency signal injection in the case of permanent magnet machines. The computation results show a good agreement with the measurements. It is concluded that FEA can be used for finding a suitable excitation signal for the application at hand.

Applying such excitation signals which would contain a wide range of excitation frequencies has not been presented. A reason might be that distinguishing the response from noisy measurement data can be difficult. However, in the case of FE computations this problem does not exist. In the signal injection, the saturation-induced saliency or anisotropy, is detected by an excitation signal. Within this dissertation, the effects of saturation are also detected in the results of impulse response tests. Within the previous work discussed above, the locked-rotor parameters or stator resistance are usually estimated by using a suitable frequency for the signal. In the case of impulse response test, several parameters, including the magnetising inductance, are obtained simultaneously.

2.2.4 Frequency response tests

In the case of synchronous machines, the standstill frequency response test (SSFR) is a standardised method and an alternative for the sudden three-phase short-circuit test to estimate the parameters such as time constants from frequency response data (IEEE Guide, 1996). A similar procedure has been applied to model the frequency response of large induction machines by Willis et al. (1989). The excitation frequencies are supplied one by one to the stator winding with one phase disconnected. The drawback of the method is that it is time-consuming. In addition, the frequency response tests are mainly performed at standstill and zero flux. Therefore, the parameter estimates have to be refined to correspond better to the rated operation point.

Verbeeck et al. (1999) have proposed a modified excitation signal to obtain the corresponding frequency response data. The excitation signal is constructed from individual harmonic components at certain frequencies. The complete signal contains ten components per decade. Since several frequencies are excited simultaneously, the measurement time is decreased significantly. In addition, both the stator and field windings can be excited simultaneously. The technique has been applied to testing of synchronous machines. The advantage of the method

is that the frequency contents are different from, for example, the harmonics produced by the machine itself in normal operation. In this way, distinguishing the response from the measured data is simpler.

If a model with non-physical parameters is accepted, the frequency response data can be depicted by a transfer function. In control engineering, fitting a transfer function for measured frequency-response data is commonly used in the design of compensators for stabilising closed-loop systems. One of the first methods for fitting frequency responses was presented by Levi (1959). In the method, the transfer function is formulated so that it can be solved in a linear least squares sense. The coefficients of the resulting transfer function can be refined iteratively to match better with the frequency response data. The algorithm is readily available, for example, in Matlab. Within this dissertation, this technique has also been applied. The resulting transfer functions are compared with the small-signal models with physical parameters.

2.2.5 Summary on excitation signals

If a system is excited only at one frequency at a time, the corresponding responses can be easier to separate from the data, especially, if it is contaminated by noise. However, it usually is preferred that several frequencies are excited simultaneously. In this case, all the estimation data are obtained faster and the data samples are collected almost at the same time instant. A typical excitation signal used for identification purposes is the chirp signal, a sinusoidal signal the frequency of which varies within the desired frequency range. A widely applied excitation signal is also a pseudorandom binary sequence (PRBS). This signal varies randomly between two values. The sequence is repeated after some period of time.

For on-line estimation, either additional excitation signals are superimposed on the fundamental supply or the harmonics contents of the supply itself is used for excitation. Moraes et al. (2003) have used a single low-amplitude sinusoidal excitation. At low speeds, the excitation frequency is twice the supply frequency and at high speeds around 15…30% of the supply. Holliday et al. (1994) injected signals at frequencies 7.5…13.5 times the fundamental to estimate resistances and leakage inductances. Fang et al. (2005) have used a sum of three sinusoidals at three low frequencies. This type of signal has also been applied by Conte et al. (2003). Lance et al. (2003) have studied the use of PWM signals to identify the impulse response, stator resistance, and speed under different operating conditions. The PWM is modified to act as a low-amplitude PRBS signal. Velez-Reyes et al. (1989) used a 60 Hz square-wave signal. PWM voltage source is used, for example, by Lima et al. (1997) and Ribeiro et al. (2000). In their study, a dc component was added to the modulating voltage for a short period of time to estimate the stator resistance.

Peixoto et al. (2000) studied the parameter estimation at standstill when the average electromagnetic torque has to be zero. This requirement is obtained with a PWM inverter voltage supply choosing the voltage vectors so that for nonzero values of the direct-axis stator voltage, the quadrature-axis voltage is zero and vice versa. Ribeiro et al. (1999) and Cirrincione et al. (2002) had the same objective. The excitations for different phases are synchronised so that

the electromagnetic torque is not produced but the magnetizing current is as close to a normal operating-point value as possible. In order to perform the SSFR test for synchronous machines more time-efficiently, Verbeeck et al. (1999) have proposed a modified excitation signal. It is constructed from sinusoidal signals of interesting frequencies.

Based on the review, it can be concluded that various types of excitation signals have been tried for parameter estimation. However, applying an impulse excitation has not been proposed.

2.3 Parameter estimation by finite elements

Parameter estimation using FEA can be classified into different categories based on how the analysis is performed. In order to obtain steady-state parameters, static magnetic field solutions or time-harmonic field solutions can be applied. These methods are fast but they require modifications and expertise on the FE code applied. An alternative is to simulate the behaviour of the machine by a time-stepping FEA regarding the computation results as idealised measurements. In this case, techniques developed for parameter estimation by measurements can be also applied for processing the computation results.

Chari and Silvester (1971) used a static FEA with first-order elements to calculate the negative-sequence and zero-sequence reactances of a turbo-generator. The calculation results were found to correspond well to the measurements. Chari et al. (1981) studied the steady-state operation of synchronous generators under different loads. They calculated direct and quadrature axis reactances. The direct-axis armature and field reactances were separated by means of linearised analysis. The magnetic field of an operation point was first solved with variable permeabilities in the elements. Then, the permeabilities were fixed and the armature and field windings were excited separately. From the induced flux linkages, the reactances were obtained. Macdonald et al. (1985) deduced that to model the operation of turbo-generators under saturated conditions, cross-coupling reactances are needed as well. Current excitations were applied in the directions of the two axes, and from the flux linkages induced on different axes, the reactances were obtained.

In (Williamson and Begg, 1985), (Williamson et al., 1990) and (Williamson and Robinson, 1991), a mixed model consisting of an equivalent circuit and both time-harmonic and time-stepping FEA is applied in order to reduce the computing requirements. The model is developed for induction machines. The equivalent circuit parameters are derived from minimal field models so that, for the stator, a pole and for the rotor, a slot are modelled. The field solution is performed in two stages. After a nonlinear field solution of the studied operation point, the reluctivities of the elements are fixed. The stator and rotor currents are used as a source of the field one by one and the field induced by every current is solved using a linear field solution. From the field solutions, an impedance matrix is computed. It defines the relation between the applied source currents and induced potential differences in different conductors. When the reference values for potential differences are known, the impedance matrix and current vector can be found iteratively. The parameters of the equivalent circuit can be solved from the impedance matrix. The stator and rotor currents are calculated from the equivalent

circuit obtained and they are used as new sources of the field. Iteration is carried on until the desired correspondence between the known and computed potential differences is achieved.

Arkkio (1987) used the concept of impedance matrix to derive the five parameters of a T-equivalent circuit. In this case as well, the reluctivities given by the nonlinear field solution are fixed. A coupling matrix is defined by supplying current to one stator phase or rotor bar at a time and solving the induced potential differences. The fairly large coupling matrix is compressed to an impedance matrix by using positive phase-sequence components. The parameters of the equivalent circuit can be obtained from the elements of the impedance matrix. In this method, the rotor skew can be taken into account by dividing the cross-section of a machine into several slices, which are rotated with respect to each other.

This method has been used by Seman et al. (2001) in an advanced simulation model that takes into account the skin effect and saturation. The model parameters are calculated at different operation points and they act as an additional input for a two-axis model. Suontausta (1988) has modelled the effects of saturation and skin effect on rotor slot impedance using the time-harmonic FEA. The FE model of the slot impedance was combined with an analytical method applied to determine the circuit parameters and operation-point quantities.

The method has also been applied by Hinkkanen et al. (2006) in a study concerning the effects of saturation in different types of equivalent circuits. The influence of the rotor skew is also considered. Within the work, circuit parameters were estimated, for example, as a function of rotor flux and current. It was concluded that, in the case of closed rotor slots or a skewed rotor, the value of magnetising inductance depends significantly on the rotor current. By including the phenomenon in the machine model, the performance of an induction-motor drive can be improved. The accuracy of the parameter estimates was evaluated by measurements for a 2.2-kW cage-induction machine. The results showed a good agreement.

Ojo et al. (1990) modelled saturation for large-signal applications such as on-line starting by using a modified equivalent circuit. In the model, the magnetising, core, leakage, and end-winding inductances are divided into non-saturable and saturable parts. The saturation is modelled by saturation factors that are functions of operating-point fluxes. The effect of saturation is obtained by multiplying the change in flux by a saturation factor. The saturation factors are both measured and determined using an FEA. The measurements and computation results show a very good agreement.

Lemaire-Semail et al. (1991) used time-harmonic FEA to estimate the steady-state circuit parameters and also the dynamic magnetising inductance to include the saturation. The model was applied to field-oriented vector control and it was noted that this improved the control performance during a step response. In the estimation, the flux level is defined by magnetising current and the element reluctivities are fixed. By linear analysis, the flux linkages of conductors are calculated and transformed to two-axis components. The dynamic magnetising inductance is obtained by repeating the linear analysis at different values of magnetising current and defining the rate of change of flux density from those. The FEA results were found to agree well with measurements.

Yahiaoui et al. (1994) used 2D time-harmonic analysis to study the effect of magnetising and load current, and slip on the circuit parameters. An end-ring resistance and reactance were calculated using a 3D formulation. It was found that the rotor frequency does not affect them significantly. In (Yahiaoui et al., 1995), the variation of parameters with the stator current components was studied. It was concluded that, in the case of closed rotor slots and when the machine is saturated, the circuit parameters are affected by both the direct-axis and quadrature-axis current components.

Dolinar et al. (1997) have used a quasi-three-dimensional time-harmonic FEA to produce data for parameter estimation of the two-axis model. In this method, the rotor is at standstill and, as in (Arkkio, 1987), the rotor skew is taken into account by dividing the rotor core into slices at slightly different position angles. One stator phase is supplied at a time and the other phases are open. In order to include the effects of saturation, several values of the magnetising current are used for excitation. For the two-axis model, the vector sum of the phases is calculated. The inductances are defined from the electromotive force, and the rotor resistance is calculated as a sum of the power losses in individual rotor bars. Finally, the average values of different slices are augmented by the end-region reactance and resistance to obtain the equivalent circuit parameters.

Bae et al. (1997) have used the results of time-harmonic FEA as training data for a neural network model of the cage rotor. After user training, the network can be used independently as a design tool. The electrical parameters of the rotor are computed with FEA for different slot shapes and values of slip. Four dimensions of the rotor slot geometry and the slip are given as inputs to the neural network for which the outputs are the rotor resistance and leakage inductance. The reference value of the bar resistance is calculated from the Joule loss. The leakage inductance is calculated from three different parts: the slot leakage inductance is calculated from the energy stored in the slot, and the bridge leakage inductance and the air-gap leakage inductance are calculated from the vector potential differences.

Bianchi et al. (1999) calculated circuit parameters by imitating the no-load and locked-rotor tests at different flux levels and rotor frequencies. The electromagnetic torque was calculated by using the parameters obtained and the values were compared with those computed directly at each operation point.

Papazacharopoulos et al. (2004) calculated the parameters of an advanced two-axis model for induction machines using FEA. The two-axis model is intended to be used in an inverter supply and iron losses caused by switching harmonics are taken into account. In addition to the traditional iron loss resistance, two resistances representing the stray losses are included in the circuit model. While the basic parameters are derived using a two-dimensional (2D) FEA, the iron losses are calculated using a three-dimensional (3D) model.

Use of the time-stepping FEA for parameter estimation has been studied less. Kanerva (2005, 2006) applied a parameterized induction machine model in the coupled simulation model of FEA and circuit simulator. Parameters extracted from the FE solution are the dynamic inductance $\boldsymbol{L}^{\mathrm{dyn}}$, which includes the effects of saturation, and the electromotive force $\boldsymbol{e}$ including

the saliency and slotting. The dynamic inductance matrix consists of dynamic inductances between the phases. Adding the coil resistance R, the voltage equation becomes

$$\boldsymbol{u} = R\boldsymbol{i} + \boldsymbol{L}^{\mathrm{dyn}} \frac{\mathrm{d}\boldsymbol{i}}{\mathrm{d}t} + \boldsymbol{e}\,, \tag{6}$$

where $\boldsymbol{u}$ is the voltage vector and $\boldsymbol{i}$ the current vector. After each nonlinear field solution, the reluctivities of the elements are fixed. An incremental current is fed to each phase winding one by one and the change in the vector potential is solved from the linearised system. From this solution, the incremental magnetic flux and the components of the dynamic inductance can be defined. The electromotive force is calculated by subtracting the effect of dynamic inductance from the total flux derivative.

For synchronous machines, time-stepping FEA has been used to imitate the traditional tests performed to estimate the transient parameters. For example, Hannalla and Macdonald (1977) simulated a field decrement test and Turner and Macdonald (1982) a flux decay test using time-discretised FEAs. In the latter, the obtained parameters were compared to those determined experimentally. In general, the correlation was good. The quadrature-axis parameters had the largest deviation which was assumed to be related to the simplifications made in the FE computation.

More recently, Chaudhry et al. (1995) have used time-stepping FEA to provide training data for artificial neural networks. The neural network is used to estimate the reactances of a turbo-generator. Amaya et al. (2003) have used time-stepping FEA to simulate the sudden three-phase short-circuit test (IEEE Guide, 1996). The obtained parameters were close to the measured ones. Arjona (2004) has calculated parameters of a turbo-generator from a transient simulated by time-stepping FEA. In the test, a step excitation was superimposed on the field voltage while the machine was operating at no load. Perez et al. (2001) have performed SSFR test by using time-stepping FEA. The transfer functions were fitted to the frequency-response data obtained by using a genetic algorithm.

Within this dissertation, the method presented in (Arkkio, 1987) has been used to estimate steady-state parameters. The method is extended to the parameter estimation for circuit models with multiple rotor branches. Based on the review, it seems that the parameter estimation using time-discretised FEAs has been applied to synchronous machines only. The estimation is performed by imitating the tests typically carried out by measurements. There are no studies describing an estimation procedure designed particularly for FEAs. On the other hand, the estimation methods based on time-harmonic analyses are implemented in the FE code and applying them requires an available source code and expertise in the implementation. A general disadvantage of using FEA is that detailed knowledge of the machine geometry is required.

2.4 Advanced analytical models

2.4.1 Including skin effect in rotor bars

Rotor parameters of a deep-bar or double-cage induction machine vary with the rotor frequency. This variation is caused by the skin effect in the rotor bars. Analytical models with

constant-valued rotor resistance and leakage inductance can be applied only within a narrow operation range. For space-vector or two-axis models, the skin effect is typically taken into account by adding another parallel rotor branch to the basic T-equivalent circuit (Boldea et al., 1988). The advantage of this kind of ladder-circuit models is that the rotor parameters can have a physical interpretation that can be exploited in the estimation. For example, in (Levy et al., 1990) and (Williamson and Gersh, 1996), the geometry of rotor slots is used for the estimation of parameters of different rotor branches.

Figure 1 presents a circuit model of six rotor parameters for space-vectors. If the rotor currents are assumed to flow as denoted in Figure 1, the rotor slot can be interpreted to be divided into two parts, both of which have a resistance and their own leakage inductance. The rotor circuits have a resistive coupling through the end rings and a mutual leakage inductance.

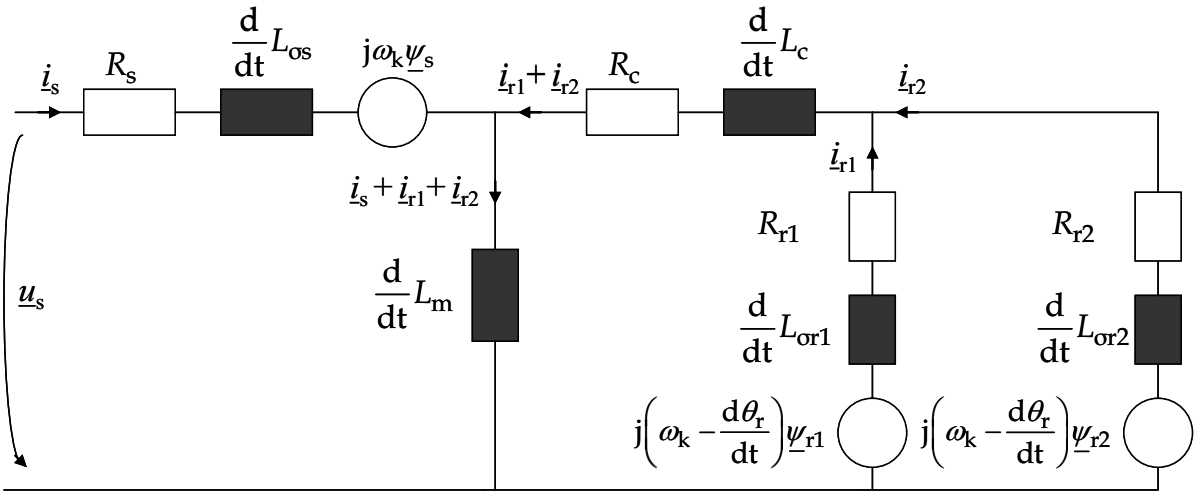

Figure 1. A double-cage equivalent circuit.

R_s is the stator resistance, $L_{\sigma s}$ the stator leakage inductance, and L_m the magnetising inductance. R_c is the rotor resistance associated with common end-rings and L_c the mutual rotor leakage inductance. R_{r1} and $L_{\sigma r1}$ are the resistance and leakage inductance of the first rotor branch and R_{r2} and $L_{\sigma r1}$ the resistance and leakage inductance of the second rotor branch, respectively. The reference frame is rotating at speed ω_k

The corresponding voltage and flux linkage equations are

$$\underline{u}_s = R_s\underline{i}_s + \frac{d\underline{\psi}_s}{dt} + j\omega_k\underline{\psi}_s \tag{7}$$

$$0 = \left(R_{r1}+R_c\right)\underline{i}_{r1} + R_c\underline{i}_{r2} + \frac{d\underline{\psi}_{r1}}{dt} + j\left(\omega_k - \frac{d\theta_r}{dt}\right)\underline{\psi}_{r1} \tag{8}$$

$$0 = R_c\underline{i}_{r1} + \left(R_c+R_{r2}\right)\underline{i}_{r2} + \frac{d\underline{\psi}_{r2}}{dt} + j\left(\omega_k - \frac{d\theta_r}{dt}\right)\underline{\psi}_{r2} \tag{9}$$

$$\underline{\psi}_s = \left(L_m + L_{\sigma s}\right)\underline{i}_s + L_m\left(\underline{i}_{r1}+\underline{i}_{r2}\right) \tag{10}$$

$$\underline{\psi}_{r1} = L_m\underline{i}_s + \left(L_m + L_c + L_{\sigma r1}\right)\underline{i}_{r1} + \left(L_m + L_c\right)\underline{i}_{r2} \tag{11}$$

$$\underline{\psi}_{\mathrm{r2}} = L_{\mathrm{m}}\underline{i}_{\mathrm{s}} + \left(L_{\mathrm{m}} + L_{\mathrm{c}}\right)\underline{i}_{\mathrm{r1}} + \left(L_{\mathrm{m}} + L_{\mathrm{c}} + L_{\sigma\mathrm{r2}}\right)\underline{i}_{\mathrm{r2}}. \tag{12}$$

The equation for electromagnetic torque is

$$T_{\mathrm{e}} = \frac{3}{2} pL_{\mathrm{m}} \operatorname{Im}\left\{\underline{\psi}_{\mathrm{s}}^{*}\underline{i}_{\mathrm{s}}\right\}. \tag{13}$$

$\underline{u}_{\mathrm{s}}$ is the stator voltage, $\underline{i}_{\mathrm{s}}$ the stator current, and $\underline{\psi}_{\mathrm{s}}$ the stator flux linkage. $\underline{i}_{\mathrm{r1}}$ and $\underline{i}_{\mathrm{r2}}$ are the currents and $\underline{\psi}_{\mathrm{r1}}$ and $\underline{\psi}_{\mathrm{r2}}$ the flux linkages of the two rotor branches. T_{e} is the electromagnetic torque. p is the number of pole pairs and θ_{r} the electrical rotor angle.

In (Healey et al., 1995) and (Smith et al., 1996), a slightly different approach is used. The total rotor resistance and leakage inductance are described as a function of frequency by performing locked-rotor tests in a wide range of frequencies. The data are used for estimating the parameters of a multi-cage model when the parameters obtained are those, which give the best fit. In this approach, the strict geometrical interpretation is relaxed.

Often, the effect of six rotor parameters can be combined into a smaller number of parameters. For example, the leakage flux of the upper cage can be assumed to be very small and the respective leakage inductance $L_{\sigma\mathrm{r1}}$ is neglected. Also, the effect of end-ring resistance R_{c} can be combined into the values of the two other rotor resistances. These assumptions have been made by, for example, De Doncker (1992) in a double-cage model for field-oriented control.

Alternative methods of modelling the skin effect aim at the best possible fit for a wide frequency range. In (Sudhoff et al., 2001, 2002, 2003), the frequency-dependent behaviour of the rotor is modelled as a high-order transfer function for which the coefficients are obtained by standstill frequency-response measurements. In (Kwon, 2006), genetic algorithms have been applied to obtain the required data for parameter estimation of the model presented in (Sudhoff et al., 2001, 2002, 2003). In (Retiere et al., 1999) and (Riu et al., 2002, 2003), the rotor side is modelled as a so-called half-order system. In this method, the frequency response data are fitted to a non-integer order transfer function.

Thiringer (1996) has measured transfer functions between different small-signal variables and compared the results with those given by analytical models. For certain shapes of rotor slots, a double-cage model was needed to include the skin effect detected from the measurements. However, the parameters of the double-cage model have not been estimated using the measured data.

Within this dissertation, the double-cage model defined by (7)–(13) is adopted for taking into account the skin effect. The small-signal models are derived from those equations. For the frequency ranges studied, the double-cage model is sufficient. In order to simplify the estimation of small-signal parameters, the small-signal models are simplified by neglecting $L_{\sigma\mathrm{r1}}$. In addition, some of the parameters are fixed in advance.

2.4.2 Including saturation

The inclusion of the effects of saturation into analytical models has been the focus of attention since the beginning of 1980s. Especially the magnetising flux saturation was found to have a

significant influence on the performance of both the large-signal and small-signal models. In the space-vector theory, the air gap of an induction machine is treated as uniform and the value of magnetising inductance as constant with respect to the circumferential angle. However, the permeability of saturable materials decreases when the flux density increases. The reluctivity faced by the flux is not constant but varies with the magnetomotive force and air-gap flux. The air gap appears as non-uniform.

Brown et al. (1983) presented an asymmetrical two-axis model for induction machines. Using the currents as state variables leads to modelling a so-called cross saturation or intersaturation effect. However, the physical existence of the cross-saturation was questioned by Kovacs (1983) and again defended by Vas et al. (1984). Boldea and Nasar (1984, 1988) presented a generalised procedure to include saturation in different machine types. These also covered the induction machines experiencing the skin effect in rotor bars that was modelled by multiple-cage circuits. It was assumed that the effects of magnetising-flux and leakage-flux saturation, and the skin effect can be treated and modelled as separate phenomena.

The models for including magnetising-flux saturation in single-cage and deep-bar or double-cage induction machines are summarized by Vas (1992). The direct-axis quantities are denoted by subscript x and quadrature-axis quantities by subscript y, respectively. Since the magnetising inductance is assumed to depend on the amplitude of magnetising current, the derivative of the direct-axis magnetising-flux linkage ψ_{mx} becomes

$$\begin{aligned}\frac{d\psi_{\mathrm{mx}}}{dt} &= \frac{d\left(L_{\mathrm{m}} i_{\mathrm{mx}}\right)}{dt} = L_{\mathrm{m}} \frac{di_{\mathrm{mx}}}{dt} + i_{\mathrm{mx}} \frac{\partial L_{\mathrm{m}}}{\partial \left|\underline{i}_{\mathrm{m}}\right|} \frac{d\left|\underline{i}_{\mathrm{m}}\right|}{dt} \\ &= \left[L_{\mathrm{m}} + \frac{i_{\mathrm{mx}}^2}{\left|\underline{i}_{\mathrm{m}}\right|^2} \left(\frac{\partial \left|\underline{\psi}_{\mathrm{m}}\right|}{\partial \left|\underline{i}_{\mathrm{m}}\right|} - \frac{\left|\underline{\psi}_{\mathrm{m}}\right|}{\left|\underline{i}_{\mathrm{m}}\right|} \right) \right] \frac{di_{\mathrm{mx}}}{dt} + \frac{i_{\mathrm{mx}} i_{\mathrm{my}}}{\left|\underline{i}_{\mathrm{m}}\right|^2} \left(\frac{\partial \left|\underline{\psi}_{\mathrm{m}}\right|}{\partial \left|\underline{i}_{\mathrm{m}}\right|} - \frac{\left|\underline{\psi}_{\mathrm{m}}\right|}{\left|\underline{i}_{\mathrm{m}}\right|} \right) \frac{di_{\mathrm{my}}}{dt} ,\end{aligned} \tag{14}$$

where L_{m} is the magnetising inductance as a function of the amplitude of magnetising current. $\underline{i}_{\mathrm{m}}$ is the magnetising current vector and i_{mx} and i_{my} are its components, respectively. The effective (steady-state) inductance L_{m0} (Luomi et al., 1986) and tangential (incremental) L_{mt} are defined as

$$\frac{\left|\underline{\psi}_{\mathrm{m}}\right|}{\left|\underline{i}_{\mathrm{m}}\right|} = L_{\mathrm{m0}} \text{ and } \frac{\partial \left|\underline{\psi}_{\mathrm{m}}\right|}{\partial \left|\underline{i}_{\mathrm{m}}\right|} = L_{\mathrm{mt}} , \tag{15}$$

where $\underline{\psi}_{\mathrm{m}}$ is the amplitude of the magnetising flux and $\underline{i}_{\mathrm{m}}$ the amplitude of magnetising current. The derivative of ψ_{mx} can be written

$$\frac{d\psi_{\mathrm{mx}}}{dt} = \left[L_{\mathrm{m}} + \frac{i_{\mathrm{mx}}^2}{\left|\underline{i}_{\mathrm{m}}\right|^2} \left(L_{\mathrm{mt}} - L_{\mathrm{m0}} \right) \right] \frac{di_{\mathrm{mx}}}{dt} + \frac{i_{\mathrm{mx}} i_{\mathrm{my}}}{\left|\underline{i}_{\mathrm{m}}\right|^2} \left(L_{\mathrm{mt}} - L_{\mathrm{m0}} \right) \frac{di_{\mathrm{my}}}{dt} . \tag{16}$$

In the case of space-vector equations, the direct-axis flux depends only on the direct-axis current and $L_{\mathrm{mt}} = L_{\mathrm{m0}}$. In that case, (16) is simplified to

$$\frac{d\psi_{\mathrm{mx}}}{dt} = L_{\mathrm{m}} \frac{di_{\mathrm{mx}}}{dt} . \tag{17}$$

The derivative of quadrature-axis magnetising flux linkage ψ_{my} can be obtained similarly

$$\frac{d\psi_{\mathrm{my}}}{dt} = \frac{i_{\mathrm{mx}} i_{\mathrm{my}}}{\left|\underline{i}_{\mathrm{m}}\right|^2}\left(L_{\mathrm{mt}} - L_{\mathrm{m0}}\right)\frac{di_{\mathrm{mx}}}{dt} + \left[L_{\mathrm{m}} + \frac{i_{\mathrm{my}}^2}{\left|\underline{i}_{\mathrm{m}}\right|^2}\left(L_{\mathrm{mt}} - L_{\mathrm{m0}}\right)\right]\frac{di_{\mathrm{my}}}{dt}. \tag{18}$$

Dolinar et al. (2003) have used this approach to include the effects of magnetising-flux saturation into linearised control of induction machines.

When the currents are used as state variables, the terms related to the cross-saturation originate from the time derivatives. Another usual alternative is to choose stator and rotor flux linkages as state variables. When these are used, the cross-saturation is not visible but the effect of saturation is included in the value of magnetising inductance, which varies with the operation point.

Depending on the application, other sets of state variables may be preferred. Levi (1995) has presented generalised models to include the main flux saturation, and classified the selection of state variables into three categories. Some of the models need the derivative of magnetising inductance and some the derivative of the inverse of magnetising inductance. When the flux linkages are used as state variables, neither one is needed. A similar study is presented for a double-cage model in (Levi, 1996). In (Levi, 1997), the effect of neglecting the cross-saturation term from different models was studied. It was found that in order to obtain accurate results, the cross-saturation is to be included in those models where the derivative of magnetising inductance is needed. However, it was found that omitting the cross-saturation terms did not affect the performance of those models that contain the derivative of the inverse of magnetising inductance.

When the reference frame is aligned with the magnetising current, the cross-saturation terms and the differences of inductances are neglected in (16) and (18). If the direct axis is aligned with the magnetising flux, the flux linkage derivatives become

$$\frac{d\psi_{\mathrm{mx}}}{dt} = L_{\mathrm{mt}}\frac{di_{\mathrm{mx}}}{dt} \text{ and } \frac{d\psi_{\mathrm{my}}}{dt} = L_{\mathrm{m0}}\frac{di_{\mathrm{my}}}{dt}. \tag{19}$$

This idea was utilised by Melkebeek (1983a, 1983b) in a small-signal model for an induction machine. The physical interpretation of the phenomenon was also presented. It was deduced that only the incremental changes that affect the amplitude of the magnetising flux are related to the incremental magnetising inductance. The incremental changes in the phase are related to the steady-state inductance. A similar approach for large-signal simulations has been proposed by He and Lipo (1984). They presented a state-space model where the direct axis is aligned with the magnetising flux and the saturation needs to be modelled in that direction only. The advantage of this approach is that the values of steady-state and incremental magnetising inductance can be obtained from the magnetising curve. Within these works, the saturation of leakage inductances and the influence of rotor current were omitted. In addition, the skin effect in rotor bars was not included in the models.

The idea of the magnetising-flux orientation was applied for a double-cage model by Williamson and Healey (1996). In the model, the magnetising inductance was allowed to depend

on the magnetising current and one rotor leakage inductance was allowed to depend on the total rotor current. The performance of the model was evaluated experimentally with a 7.5-kW cage-induction machine and by simulations for a 3.75-MW machine. It was noticed that incorporating the skin effect improved the model performance significantly compared with a single-cage model. Including saturation improved the model further, especially, by reducing the overshoot in step-response tests.

The effect of saturation on the small-signal parameters of synchronous machines has been studied by Verbeeck et al. (2000). The traditional SSFR test is performed at zero flux. Within the work, SSFR tests were also carried out at different flux levels. It was noticed that especially the value estimated for magnetising inductance depends on the flux level. However, a straightforward comparison of the results was somewhat difficult, since several different measurement set-ups were used in the tests.

Some other methods of including saturation have also been presented. Kerkman (1985) used the magnetising flux and rotor current as state variables. The magnetising current is defined as an odd function of the magnetising flux. Moreira and Lipo (1990) included the effect of the third harmonic caused by permeance variations in the values of inductances. In the model, the stator and rotor self inductances depend on the flux level and rotor position angle. The model was proposed to be implemented in steady-state simulations.

Within this dissertation, the estimation of parameters is performed at the true operating-point flux in which case the effects of saturation are included in the values of parameter estimates. In the case of mimo admittance, saturation is modelled by using both the steady-state and incremental inductances. In addition, the effect of rotor current on the values of inductances is taken into account. When the values of inductances depend on both the magnetising and rotor current, the terms related to cross-saturation appear in any reference frame. However, there is no need for cancelling those since both the steady-state and incremental parameters are obtained from the estimation.

2.5 Torsional oscillations

2.5.1 History of analytical models

The hunting phenomenon of electrical machines had already been recognised by the beginning of the 1900s. The first studies of oscillations concerned synchronous machines, but soon they were extended to other machine types as well. Analytical equations for hunting torque components for synchronous machines were presented by Doherty and Nickle (1928) and, in a more general form, by Park (1929, 1933). A synchronous machine oscillating at low amplitude was characterized by a complex torque coefficient. The imaginary part is referred to as a *damping coefficient* (damping torque) and the real part as a *spring constant* (synchronising torque). The damping torque acts in phase with the rotor angle and the synchronising torque in phase with the speed. The synchronising and damping torque coefficients T_s and T_d are the real and imaginary parts of a complex ratio between torque and angle deviations $\Delta\underline{T}$ and $\Delta\underline{\theta}_r$ defined as

$$\frac{\Delta \underline{T}(\mathrm{j}\omega)}{\Delta \underline{\theta}_{\mathrm{r}}(\mathrm{j}\omega)} = T_{\mathrm{s}}(\omega) + \mathrm{j}\omega T_{\mathrm{d}}(\omega). \tag{20}$$

Nickle and Pierce (1930) and Wagner (1930) studied the effect of stator resistance on the damping torque. They noticed that, above a certain value, which depends on the power angle and synchronous reactance, the damping becomes negative.

Equivalent circuits to model the hunting of different machine types were presented by Kron (1942). In the companion paper by Concordia et al. (1942), the doubly-fed induction machine was studied more closely and an analytical expression and equivalent circuits to predict torque oscillations were derived. By setting the rotor voltage to zero, these expressions also hold for cage-induction machines. The torsional oscillations induce two harmonic components to the stator current. In the stator frame of reference, these components occur at fundamental frequency plus and minus the oscillation frequency. In the corresponding equivalent circuits, the frequency shift is taken into account in the expressions of resistances and rotor voltage. In addition, the steady-state equivalent circuit is needed. All the quantities are expressed as per unit values. Thus, the power corresponds to the torque and the voltage corresponds to the flux. From the steady-state and oscillation-induced voltages and currents, the torque coefficients can be calculated.

The torque coefficients for power selsyns were presented by Concordia (1945). Selsyns are devices that consist of a type of rotary transformer driving an electrical motor. In the study, it was found that, if the stator resistance of the motor becomes very high, the instability disappears. In (Concordia, 1950), the damping torque of synchronous machines at low speeds was studied. Operation at low speeds corresponds to the situation in which the stator resistance is increased. It was found that, at speeds of a couple of percentage points of the rated speed, the damping torque is negative but, at operation points close to standstill, it is again positive. In this case, the effect of damper circuits was neglected. When they were included, it was noticed that the range of negative damping almost disappeared. Concordia also studied the synchronising and damping torques for induction machines using the circuit models (Concordia, 1952). It was found that the negative damping occurs at high slips and low oscillating frequencies or at small, normal operating slips within a range below the fundamental frequency.

Instability and oscillations of induction machines became again a subject of interest in the 1960s along with the growth in variable-frequency drives. Rogers (1965) used linearised analysis to study the speed transients caused by small perturbations in the supply voltage and load torque. Using a root-locus technique it was shown that, at low supply frequencies, a possibility of instabilities exists. Lipo and Krause (1969) performed a stability analysis using linearised equations and the Nyquist criterion for an inverter-fed induction motor. Since energy can flow between the filter of the inverter and the magnetic circuit of the induction machine, instabilities may occur. The effect of circuit and filter parameters on the stability boundaries was studied. Unstable regions occurred at supply frequencies between 5…40 Hz. It was noted, for example, that increasing the magnetising reactance or supply voltage increases the region of instability. The results of linearised analysis were evaluated by simulating the state-

space model when the load torque was switched between the predicted stable and unstable operation points. Within the regions of predicted instabilities, steady oscillations were detected. In the discussion, the reviewers presented measurements performed using an almost similar drive. Sustained oscillations were detected as well. As in the simulations, the oscillations did not increase unboundedly. In addition, the measured amplitudes were small. Related to the work, Nelson et al. (1969) used the linearised equations and root-locus method to study the stability issues in the case of sinusoidal supply. The region of instability occurred between 15…25 Hz under the rated load torque. It was noted that increasing the rotor or stator resistance, i.e. meaning increasing resistive losses, stabilised the machine. Simulations were also performed by a state-space model. The sustained oscillations were detected as well.

Within this dissertation, negative electromagnetic damping for induction machines has been observed. By performing simulations and measurements, it has been noticed that within a frequency range of negative damping, self-excited torsional oscillations occur. These oscillations can be detected from the rotation speed but also from the two harmonic components induced on the stator current. From the results of FEAs performed, it has also been observed that the range of negative damping disappears when the stator resistance is neglected.

2.5.2 Recent work

Damping and synchronising torques of synchronous machines have been studied using linearised models by Shaltout (1992). The presented method applies time responses of torque, rotor angle and speed. The damping component and synchronising component are estimated from the responses by a least squares fit. In addition, the eigenvalue analysis is performed and the effect of load on the parameters has been studied. In (Shaltout and Abu Al-Feilat, 1994), starting of a large cage-induction machine has been modelled. The response of the system has been simulated when a unit step transient to the stator voltage and a sinusoidal and ramped sinusoidal excitation to the torque are applied as excitation signals. Recently, the complex-torque method has received some criticism from Tabesh and Iravani (2005). The discussed drawbacks are the inability to predict all oscillatory modes and their damping, and instability originating from real-valued poles.

Lee and Hsu (1995) have studied torsional oscillations of multiple-winding induction machines with both sinusoidal and PWM supply. They modelled the effects of saturation and hysteresis of the magnetising branch in the analytical model by describing functions. Simulations were performed by a state-space model and eigenvalue analyses were carried out. Oscillations excited by different starting techniques were studied. It was noted that the PWM supply increases the torsional oscillations compared to sinusoidal supply. It was suggested that the severity of the oscillations can be reduced by using soft starting and selecting a suitable displacement angle between the winding sets.

Smith and Ran (1994) used simulations and measurements to study the torsional dynamics of electrical submersible pumps during soft starting. They discussed the effect of negative damping in the case of induction machines and concluded that the starting has to be designed with care in order to reduce the oscillations. The analytical simulation model consisted of supply

system, transformer, soft starter, induction motor and a shaft. The model neglected the saturation and skin effect. It was noted that increasing the load torque or supply voltage increases the range of negative damping.

Ueda et al. (1992) performed a stability analysis with respect to torsional oscillations in the case of a V/f-controlled PWM supplied induction machine. The stability limits were derived analytically using Hurwitz's stability criterion. They deduced that the source of instability was the existence of non-zero stator resistance. Increasing the rotor time constant with respect to the mechanical time constant increases the negative damping.

Some recent studies on torsional dynamics of synchronous and induction machines have been performed by Tabesh and Iravani. In (Tabesh and Iravani, 2004), a frequency-response-based method is presented. The stability regions are identified using the Nyquist criterion for an open-loop transfer function consisting of electrical and mechanical transfer functions. Two indices, system damping and sensitivity to torsional oscillations, are used to describe the torsional behaviour. The small-signal model between the rotor angle and electromagnetic torque is presented for synchronous machines and the performance is compared with simulations. The parameters of the system are taken from the first IEEE Benchmark system for subsynchronous resonance (SSR) (IEEE Committee Report, 1977). The method is suitable for both synchronous and induction machines, and also for systems of machines. In (Tabesh and Iravani 2006), the authors have applied similar means to study the small-signal dynamics of a grid-connected wind farm. The comprehensive model consists of wind-energy capturing mechanism, electrical network with series compensation, system of induction generators and shaft mechanics.

Self-excited oscillations and forced oscillations of a shaft system usually occur within a low-frequency range of 100 Hz. However, the increasing number of power electronic devices has also drawn attention to higher oscillation frequencies. Wang et al. (2001) have modelled torsional oscillations caused by supply voltage harmonics. The performance of the induction machine as a function of frequency has been modelled by performing no-load and locked-rotor tests at several frequencies. The circuit-model parameters are calculated separately for different supply-frequency components and the total performance is obtained as the sum of different components. Based on the data, a neural network model for predicting the harmonics and torsional oscillations has been developed. The study was focused on the effects of the 5th and 7th supply harmonics and the induced torsional oscillation at six times the supply frequency. The proposed neural network model is able to take into account the time-variation also.

Widdle et al. (2006) have studied high-frequency oscillations originating from switching harmonics by measurements. These oscillations range up to 30 kHz and are interesting from the point of view of acoustic noise. The shaft oscillations were measured using accelerometers and the torque response was calculated from the measured voltages and currents. In order to include the effect of switching harmonics, the torque was calculated using an advanced analytical induction machine model presented by Sudhoff et al. (2001). The system model also includes a flexible shaft. The detected oscillations occur at multiples of switching harmonic frequencies.

2.5.3 Reported sources of oscillations

Different sources of torsional excitations have been listed, for example, in (Sheppard, 1988). An impulse excitation containing a wide range of frequencies may originate from a rock crusher, for example. Periodic excitations at low frequencies can be produced by fans, propellers and compressors, and the harmonics of variable-speed drives. In an inverter supply, the fifth and seventh harmonics produce a periodic torque at six times the fundamental frequency.

Shadley et al. (1992) studied self-excited torsional oscillations observed during the starting of induction motors, particularly, in the case of submersible pumps. It was stated that the oscillation may be initiated at the slips where the tangent of the torque-versus-speed curve is positive. They reported a coupling failure for a 75-kW cage-induction-motor driven system. They stated that the oscillation amplitude is higher when the inertia of the load is at least twice as large as the inertia of the rotor. In the measured case, the ratio was more than 40. The system was simulated using multimass and simplified state-space models.

SSR originating from compensated transmission lines is a well-known phenomenon, particularly in the case of synchronous machines. Joswig and Kulig (2001) reported SSR caused by slip-ring machines with faulty rotor windings. The slip-ring motors were connected to synchronous generators. A fault occurred, and several machines were damaged simultaneously. The incident was simulated using a state-space model for the machines and mechanics. It was found that, during the running up of a slip-ring motor, SSR occurred and the shear pins of the shaft were torn off.

Based on the review, a conclusion can be made that the torsional oscillations are a subject of interest. The frequency range of oscillations depends on the natural frequencies and exciting sources. Within this dissertation, the frequency range studied is below a couple of hundred hertz. Thus, high-frequency oscillations are not included in the study. In the previous works, analytical models the parameters of which are obtained, for example, from the locked-rotor and no-load tests, are used to model torsional dynamics. The torsional dynamics has not been studied using FEA and it has not been applied to parameter estimation.

2.6 Conclusions

The parameter estimation of induction machines can be classified based on the purpose and application of the analytical model. Recently, plenty of attention was paid to on-line estimation and real-time tracking of the changes at the operation point. This type of parameter estimation is also applied to sensorless tracking and control of rotor angle and speed. However, improved methods for performing so-called standstill tests are continuously proposed and studied. The purpose of these is to obtain a set of parameters that model the rated operation as realistically as possible. By estimating parameters under different operation conditions, the behaviour of parameters as a function of, for example, magnetising current or rotor frequency, can be determined. These dependencies and variation of parameters can then be implemented in high-accuracy control or simulations of transient phenomena. Especially the development of power electronics and variable-frequency drives has increased the attention directed both to the accuracy of parameter estimates and structure of the analytical models.

In the majority of the previous works, the data for the estimation have been produced by measurements. Estimation by finite elements is usually performed by means of time-harmonic analyses. Then, the parameters sought are mainly intended to depict steady-state operation and such quantities as operation-point torque, for example. The time-discretised methods have been mainly used for simulating transient tests typically performed by measurements. These studies have mainly concentrated on synchronous machines. The purpose of the tests has been to obtain parameters that are able to predict large-signal transients. The corresponding parameters can be referred to as large-signal parameters. However, computing a transient may today still require plenty of time and computing capacity.

To excite the dynamics of a machine, several different types of low-amplitude signals have been tried. The estimated parameters are assumed to predict the dynamic behaviour of the machine. Usually, the parameters are determined by fitting an analytical model to, for example, a frequency response. The resulting parameters are those that give the best fit for the estimation data. Often, a clear indication of whether the parameters are intended to depict large-signal or small-signal dynamics is missing. In the case of small-signal models, the saturation has been modelled by assuming a magnetising inductance dependent on the magnetising current. Such models, in which the effect of load is considered, have not been proposed. Also, the effect of saturation on the leakage inductances has been neglected.

Torsional oscillations have been a subject of interest for a long time, and several analytical models for predicting torsional dynamics have been proposed. Analytical models are favoured since often the simulations are performed for systems consisting of several machines, their control and supply, and mechanical devices. The studies have been focused on synchronous machines, although, for example, the phenomenon of self-excited oscillations of induction machines has also been recognised. However, FEAs have not been applied and the parameters of the analytical machine models are typically those obtained by traditional means. Parameter estimation based on torsional dynamics has not been presented.

The numerical impulse response test has proved to be an efficient tool for modelling electromagnetic forces. It has not been used for other electrical machine or drive applications. The present research was started to look for and study new potential applications for the numerical impulse response tests.

3 Methods

Several different types of induction machines have been studied. The focus has been on a 37-kW deep-bar machine with closed rotor slots. Another machine chosen for a closer inspection is an 850-kW cage-induction machine with semi-closed rotor slots. Rated values of the machines are given in Table I. The shapes of the rotor slots are shown in Figure 2.

TABLE 1 Rated values for the 37-kW and 850-kW cage-induction machines.

Rated power	P_N	[kW]	37	850
Rated stator voltage	U_{sN}	[V]	380 (star)	690 (delta)
Number of pole pairs	p		2	3
Rated stator frequency	f_N	[Hz]	50	50
Rated slip	s_N	[%]	2.00	0.53

(a) b)

Figure 2. Cross sections of the rotor slots, (a) the 37-kW machine, (b) the 850-kW machine.

3.1 Finite-element analyses

This work is founded on computations performed using 2D finite-element analyses. The impulse response tests are performed within the time-stepping FEA. The steady-state parameters are estimated using the time-harmonic FEA.

3.1.1 Time-stepping FEA

The time-discretised FEA takes into account the magnetic saturation, skin effect in rotor bars, and rotation of the rotor. However, it is used to identify much simpler analytical models. In the case of a complete FE model, tracking the effects of different physical phenomena can be complicated. Within this work, simplified FE models have been used for comparison. In order to neglect the effects of saturation, a linearised FE model is used. Linearising means that the relative permeability of saturable materials of the cores and shaft is set to a constant value of 1000. In the case of closed rotor slots, the bridges closing the slots are replaced by air so that the steady-state parameters from the impedance method are approximately equal for the nonlinear and linear machine at the rated operation. The results obtained from the linearised FE model can be compared with the original nonlinear FE model to evaluate the effect of saturation.

In the case of the cage-induction machine, the rotor bars are modelled as thick conductors where an eddy-current formulation is used (Strangas and Theis, 1985). The current density along the cross section varies with the rotor frequency. The influence of skin effect can be studied by replacing the cage rotor by a filamentary phase winding similar to slip-ring ma-

chines. With a zero rotor voltage, the model corresponds fairly well to a cage-induction machine with uniform current density in the cross-sections of bars. If, in addition, the saturation is removed by linearising the materials and the same operation point is computed, the differences between the computation results of the two FE models can be assumed to be mainly related to skin effect.

Within the FE code applied, core losses are calculated in post-processing by statistical means. The information on losses is used in P5, where the variation of parameters as a function of efficiency is studied while the machine is controlled to run in the most energy-efficient way. In all the analytical models applied in this work, the core losses are neglected.

3.1.2 Impedance method

The steady-state circuit parameters are estimated using a time-harmonic FEA. The time-variation of quantities is assumed sinusoidal and the rotation of rotor is taken into account using the slip frequency for rotor quantities. The estimation procedure is discussed in Section 2.3 and presented in detail in (Arkkio, 1987). Within the present work, the circuit parameters of multiple-cage models are estimated using a similar approach. In this case, the rotor bars are divided into several sub-conductors. The details are given in P3. Figure 3 presents a flow diagram of the main stages of the procedure for a single-cage model. The method is referred to as the *impedance method*.

3.2 Impulse tests and harmonic excitation

Two different types of numerical impulse tests have been studied. In the first part of the study, the impulse excitation is applied to the space vector of the stator voltage and the response of the stator current is studied. In the second part, the impulse excitation is applied to the rotor position angle and the response of electromagnetic torque is studied. The FRFs obtained from impulse tests are compared with the FRF values computed frequency by frequency. In this second method, a sinusoidal excitation at a certain frequency is superimposed on the input variable and only the response of the output variable at the corresponding frequency is considered. In the case of the linear time-invariant system, the response differs from zero only at the excitation frequency. In the case of nonlinear or time-variant systems, the input signal may also excite some other frequencies. However, in the procedure they are neglected. This method is referred as the *harmonic excitation* and it is used for evaluating the results of impulse tests.

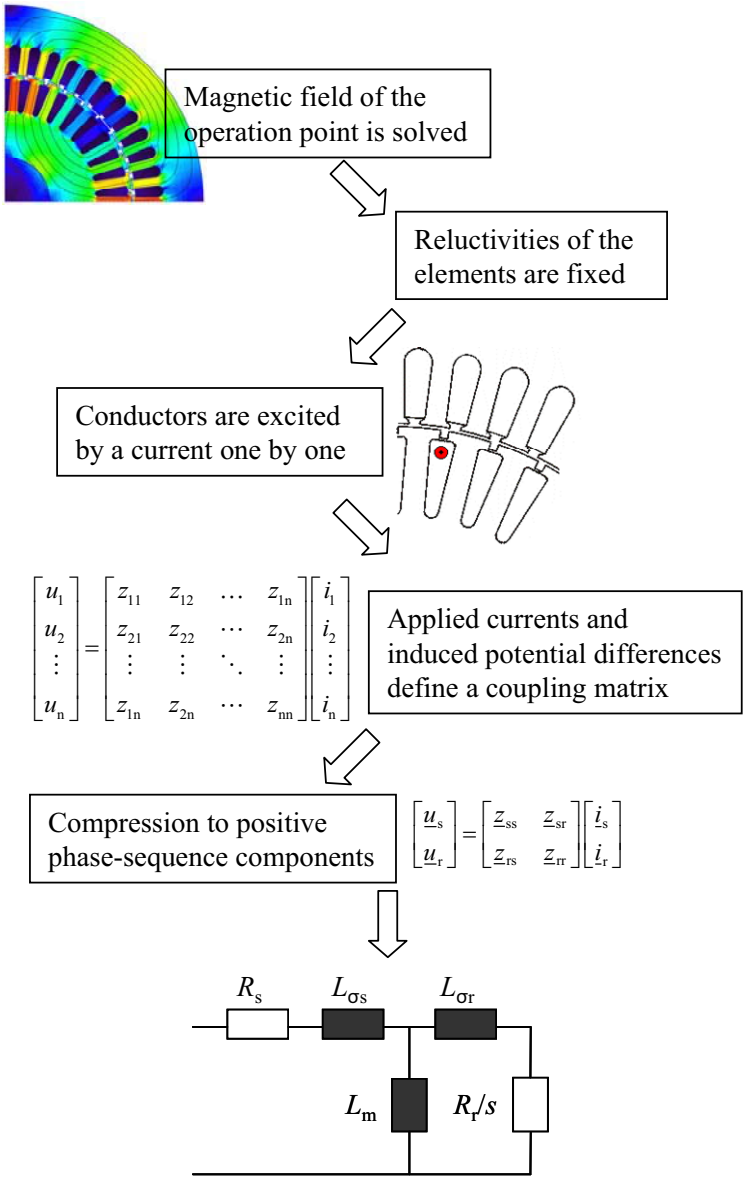

Figure 3. A flow diagram of the parameter estimation performed by means of the time-harmonic FEA.

3.2.1 Voltage impulse test

The voltage impulse is superimposed on the space vector of line-to-line voltage. It is aligned at a certain angle φ with respect to the steady-state voltage vector $\underline{v}$.

$$\underline{v}_s + \Delta\underline{v}_s = \left|\underline{v}_s\right| e^{j\omega_s t} + \left|\Delta\underline{v}_s\left(t\right)\right| e^{j(\omega_s t+\varphi)}. \tag{21}$$

Two different types of voltage impulses have been studied in P4. The time-dependency of a simple impulse is defined as

$$\left|\Delta\underline{v}_s\left(t\right)\right| = \begin{cases} a_{rel}\hat{v}\sin^2\left(2\pi f_d t\right), & t_1 \le t \le t_1 + t_d \\ 0, & \text{otherwise} \end{cases}. \tag{22}$$

The first impulse tests were performed using (22) and setting $\omega_s t + \varphi = 0$ in (21). In P1, an impulse with the amplitude of a low-dc component was applied. The time-dependency of the amplitude is defined by

$$\left|\Delta \underline{v}_\mathrm{s}\left(t\right)\right| = \begin{cases} a_\mathrm{rel}\hat{v}\sin^3\left(4\pi f_\mathrm{d} t\right) + c a_\mathrm{rel}\hat{v}\sin^2\left(2\pi f_\mathrm{d} t\right), & t_1 \le t \le t_1 + t_\mathrm{d} \\ 0, & \text{otherwise} \end{cases} . \tag{23}$$

The relative amplitude a_rel defines the maximum amplitude with respect to the amplitude of supply voltage $\hat{v}$ and has been, within this study, 1…20%. Frequency f_d and duration time t_d define the shape and length of the impulse. c defines the impulse amplitude at dc, and in the computations, this has been 0.15. The length of the impulse defines the frequency contents and, therefore, the application range of the impulse. For example, with a sinusoidal impulse shape, when $t_\mathrm{d} = 5$ ms, the frequency contents obtained are –200…200 Hz in the stationary reference frame. By shortening the impulse to half, the frequency contents can be doubled (Ewins, 2000). Figure 4 presents the impulse shape (22) in frequency domain. The frequency contents of the impulse (23) are shown in P1 and P2.

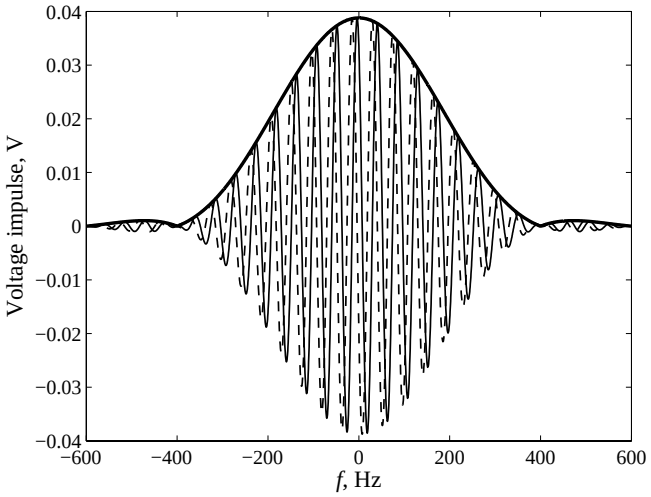

Figure 4. Voltage impulse (22) in frequency domain. The real part is shown with the thin solid line, the imaginary part the dashed line, and amplitude with the thick solid one.

The small-signal dynamics is extracted from the steady-state operation point by performing a steady-state simulation starting from the same initial field. The results of the steady-state computation are then subtracted from the results of the impulse test. The process is also applied for the harmonic excitation.

Since the analytical small-signal models, both complex-valued and mimo admittances, are derived for phase variables, the space vector $\Delta \underline{u}_\mathrm{s}^\mathrm{k}$ is computed from the voltages over the stator phase windings and the space vector $\Delta \underline{i}_\mathrm{s}^\mathrm{k}$ from the phase currents. These are transformed to the frequency domain using FFT, and, from the ratio, the FRF of the stator current is obtained as

$$\frac{\Delta \underline{i}_\mathrm{s}^\mathrm{k}\left(\mathrm{j}\omega\right)}{\Delta \underline{u}_\mathrm{s}^\mathrm{k}\left(\mathrm{j}\omega\right)} = \underline{Y}\left(\mathrm{j}\omega\right). \tag{24}$$

k refers to reference frame rotating at ω_k.

In P4, the direction of the impulse has been studied with impulse (22) by varying φ in (21). Figure 5 shows the FRFs obtained using two perpendicular impulses with $\varphi = 0$ and $\varphi = \pi/2$.

The differences between the two FRFs are mostly visible around 100 Hz and –200 Hz. In P4, it is concluded that they are related to the harmonics induced by saturation. The frequency range used for parameter estimation is –200…200 Hz, and the harmonics may disturb the fitting. However, it has been noticed that, if the average of the two FRFs in Figure 5 is calculated, the saturation-induced harmonics around 100 and –200 Hz are cancelled. Figure 6 presents the average FRF calculated from the FRFs in Figure 5. It is compared with the FRF produced by the harmonic excitation. The correlation is very good.

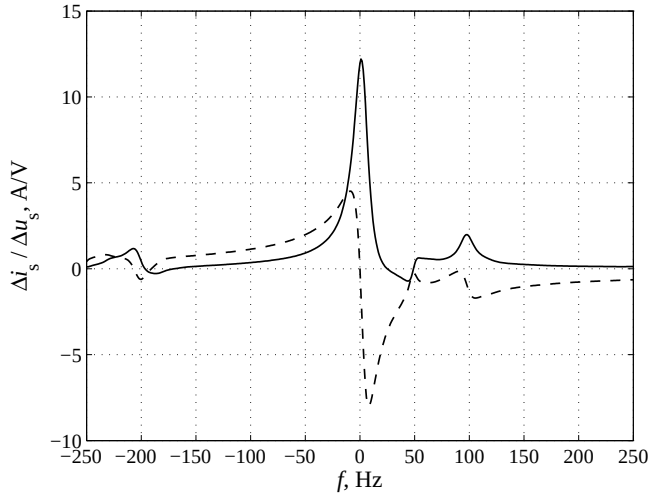

(a)

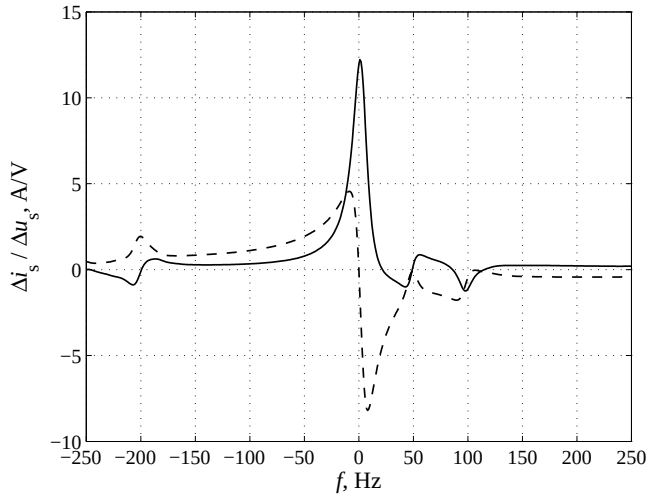

(b)

Figure 5. FRFs obtained using perpendicular impulses. (a) $\varphi = 0$ and (b) $\varphi = \pi/2$. The real part is shown with the solid line, the imaginary part with the dashed line.

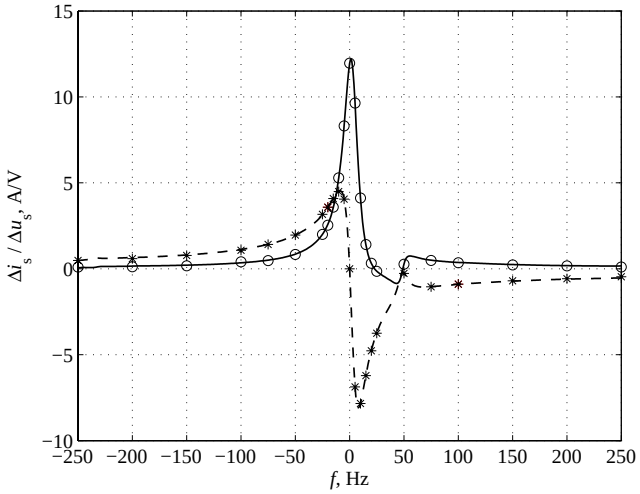

Figure 6. The average of FRFs from Figure 5(a) and (b). The real part is shown with the solid line, the imaginary part with the dashed line. The harmonic excitation (real part with circles, the imaginary part with asterisks).

In the case of the mimo admittance, the saturation effects are included in the model. In order to solve the impedance matrices presented in P6 and P7, the voltage impulses performed in different directions are used as separate, independent inputs and the corresponding stator current responses as separate outputs. In contrast to (24), the data are treated component-wise. Altogether, four numerical FRFs are needed: i_{sx} / u_{sx}, i_{sy} / u_{sy}, i_{sx} / u_{sy}, and i_{sy} / u_{sx}. When the two perpendicular impulses are applied, the frame of reference where the fitting is performed, can be aligned so that impulse at $\varphi = 0$ corresponds to $u_{sy} = 0$ and $\varphi = 2\pi$ and $u_{sx} = 0$.

3.2.2 Angle impulse test

The basic procedure for the angle impulse test is similar to the voltage impulse test. The amplitude of the angle impulse is proportioned to the pole pitch τ_p. The time-dependency of the impulse is defined as

$$\Delta\theta_r(t) = \begin{cases} a_{rel}\tau_p \sin\left(2\pi f_d t + \varphi_r\right), & t_1 \le t \le t_1 + t_d \\ 0, & \text{otherwise} \end{cases}. \tag{25}$$

The phase angle φ_r and the duration time t_d are related to the initial time t_1 and the frequency f_d so that $\Delta\theta_r = 0$ at t_1 and at $t_1 + t_d$. If the position angle is perturbed as explained, the angular speed of the rotor is perturbed by a period of a sinusoid. This means that, at the end of the impulse, the rotor angle returns to the original position in the synchronous reference frame. An angle impulse is presented in Figure 7.

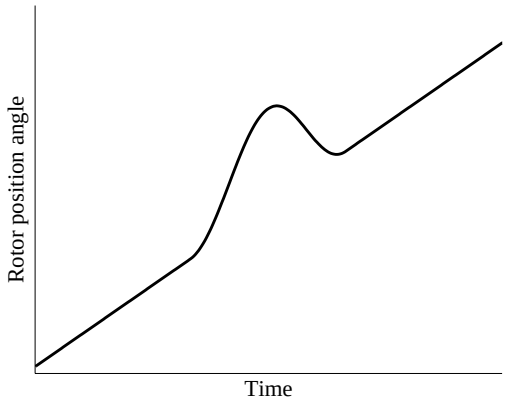

Figure 7. Impulse applied to rotor position angle.

In the case of the angle impulse test, the response of the electromagnetic torque is studied. This means that both signals are real-valued and the FRF can be written as

$$\frac{\Delta T_{\mathrm{e}}(\mathrm{j}\omega)}{\Delta \theta_{\mathrm{r}}(\mathrm{j}\omega)} = G(\mathrm{j}\omega)\,. \tag{26}$$

The corresponding analytical model is referred to as *the torque model*. Figure 8 shows the FRFs obtained for the 850-kW cage-induction machine by using the angle impulse test and harmonic excitation. In this case, $a_{\mathrm{rel}} = 0.01$ and $f_{\mathrm{d}} = 100$ Hz.

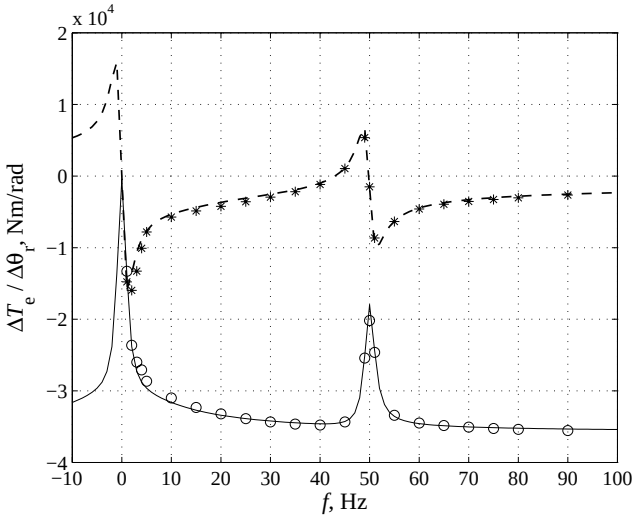

Figure 8. The FRFs obtained from the angle impulse test. The real part is shown with the solid line, the imaginary part with the dashed line. The harmonic excitation (real part is shown with circles, the imaginary part with asterisks).

3.3 Analytical small-signal models

Within the work, several types of induction machines have been considered. The study is focused on a cage-induction machine with deep rotor bars. Because of the skin effect, the values of circuit parameters depend strongly on the frequency. In order to use a small-signal model with constant circuit parameters, an additional rotor branch is needed. The double-cage equivalent circuit and space-vector equations are presented in Section 2.4.1 (Figure 1). In P4,

and P5, the complex-valued admittances are used and in P1 and P2, the complex-valued admittances for a single-cage rotor are applied. In P6 and P7, the mimo admittance is used. Next, a general view on the double-cage small-signal model is presented. Subscripts x and y refer to direct and quadrature-axis variables defined in the synchronous reference frame. In P6 and P7, subscripts d and q are used, respectively.

The small-signal voltage equations derived from (7)–(12) are

$$
\begin{aligned}
\Delta u_{\mathrm{sx}} &= R_{\mathrm{s}}\Delta i_{\mathrm{sx}} + \frac{\mathrm{d}\Delta\psi_{\mathrm{sx}}}{\mathrm{dt}} - \omega_{\mathrm{k}}\Delta\psi_{\mathrm{sy}} \\
\Delta u_{\mathrm{sy}} &= R_{\mathrm{s}}\Delta i_{\mathrm{sy}} + \frac{\mathrm{d}\Delta\psi_{\mathrm{sy}}}{\mathrm{dt}} + \omega_{\mathrm{k}}\Delta\psi_{\mathrm{sx}} \\
0 &= \left(R_{\mathrm{r1}} + R_{\mathrm{c}}\right)\Delta i_{\mathrm{r1x}} + R_{\mathrm{c}}\Delta i_{\mathrm{r2x}} + \frac{\mathrm{d}\Delta\psi_{\mathrm{r1x}}}{\mathrm{dt}} + \left(\omega_{\mathrm{r0}} - \omega_{\mathrm{k}}\right)\Delta\psi_{\mathrm{r1y}} + \psi_{\mathrm{r1y0}}\frac{\mathrm{d}\Delta\theta_{\mathrm{r}}}{\mathrm{dt}} \\
0 &= \left(R_{\mathrm{r1}} + R_{\mathrm{c}}\right)\Delta i_{\mathrm{r1y}} + R_{\mathrm{c}}\Delta i_{\mathrm{r2y}} + \frac{\mathrm{d}\Delta\psi_{\mathrm{r1y}}}{\mathrm{dt}} + \left(\omega_{\mathrm{k}} - \omega_{\mathrm{r0}}\right)\Delta\psi_{\mathrm{r1x}} - \psi_{\mathrm{r1x0}}\frac{\mathrm{d}\Delta\theta_{\mathrm{r}}}{\mathrm{dt}} \\
0 &= \left(R_{\mathrm{r2}} + R_{\mathrm{c}}\right)\Delta i_{\mathrm{r2x}} + R_{\mathrm{c}}\Delta i_{\mathrm{r1x}} + \frac{\mathrm{d}\Delta\psi_{\mathrm{r2x}}}{\mathrm{dt}} + \left(\omega_{\mathrm{r0}} - \omega_{\mathrm{k}}\right)\Delta\psi_{\mathrm{r2y}} + \psi_{\mathrm{r2y0}}\frac{\mathrm{d}\Delta\theta_{\mathrm{r}}}{\mathrm{dt}} \\
0 &= \left(R_{\mathrm{r2}} + R_{\mathrm{c}}\right)\Delta i_{\mathrm{r2y}} + R_{\mathrm{c}}\Delta i_{\mathrm{r1y}} + \frac{\mathrm{d}\Delta\psi_{\mathrm{r2y}}}{\mathrm{dt}} + \left(\omega_{\mathrm{k}} - \omega_{\mathrm{r0}}\right)\Delta\psi_{\mathrm{r2x}} - \psi_{\mathrm{r2x0}}\frac{\mathrm{d}\Delta\theta_{\mathrm{r}}}{\mathrm{dt}}\,.
\end{aligned}
\tag{27}
$$

The small-signal quantities are denoted by Δ. The steady-state quantities are denoted by subscript 0. The saturation is included in the model so that the magnetising and rotor leakage inductances are assumed to depend on the magnetising current and total rotor current. The flux linkage equations are

$$
\begin{aligned}
\Delta\psi_{\mathrm{sx}} &= \left(L_{\mathrm{m0}} + L_{\mathrm{s\sigma}}\right)\Delta i_{\mathrm{sx}} + L_{\mathrm{m0}}\left(\Delta i_{\mathrm{r1x}} + \Delta i_{\mathrm{r2x}}\right) \\
&\quad + \Delta L_{\mathrm{m}}\left(i_{\mathrm{r1x0}} + i_{\mathrm{r2x0}} + i_{\mathrm{sx0}}\right) \\
\Delta\psi_{\mathrm{sy}} &= \left(L_{\mathrm{m0}} + L_{\mathrm{s\sigma}}\right)\Delta i_{\mathrm{sy}} + L_{\mathrm{m0}}\left(\Delta i_{\mathrm{r1y}} + \Delta i_{\mathrm{r2y}}\right) \\
&\quad + \Delta L_{\mathrm{m}}\left(i_{\mathrm{sy0}} + i_{\mathrm{r1y0}} + i_{\mathrm{r2y0}}\right) \\
\Delta\psi_{\mathrm{r1x}} &= L_{\mathrm{m0}}\Delta i_{\mathrm{sx}} + \left(L_{\mathrm{m0}} + L_{\mathrm{c0}} + L_{\mathrm{\sigma r1}}\right)\Delta i_{\mathrm{r1x}} + \left(L_{\mathrm{m0}} + L_{\mathrm{c0}}\right)\Delta i_{\mathrm{r2x}} \\
&\quad + \Delta L_{\mathrm{m}}\left(i_{\mathrm{sx0}} + i_{\mathrm{r1x0}} + i_{\mathrm{r2x0}}\right) \\
&\quad + \Delta L_{\mathrm{c}}\left(i_{\mathrm{r1x0}} + i_{\mathrm{r2x0}}\right) \\
\Delta\psi_{\mathrm{r1y}} &= L_{\mathrm{m0}}\Delta i_{\mathrm{sy}} + \left(L_{\mathrm{m0}} + L_{\mathrm{c0}} + L_{\mathrm{\sigma r1}}\right)\Delta i_{\mathrm{r1y}} + \left(L_{\mathrm{m0}} + L_{\mathrm{c0}}\right)\Delta i_{\mathrm{r2y}} \\
&\quad + \Delta L_{\mathrm{m}}\left(i_{\mathrm{sy0}} + i_{\mathrm{r1y0}} + i_{\mathrm{r2y0}}\right) \\
&\quad + \Delta L_{\mathrm{c}}\left(i_{\mathrm{r1y0}} + i_{\mathrm{r2y0}}\right)
\end{aligned}
\tag{28}
$$

$$
\begin{aligned}
\Delta\psi_{\mathrm{r2x}} &= L_{\mathrm{m0}}\Delta i_{\mathrm{sx}} + \left(L_{\mathrm{m0}} + L_{\mathrm{c0}} + L_{\sigma\mathrm{r2}}\right)\Delta i_{\mathrm{r2x}} + \left(L_{\mathrm{m0}} + L_{\mathrm{c0}}\right)\Delta i_{\mathrm{r1x}} \\
&\quad + \Delta L_{\mathrm{m}}\left(i_{\mathrm{sx0}} + i_{\mathrm{r1x0}} + i_{\mathrm{r2x0}}\right) \\
&\quad + \Delta L_{\mathrm{c}}\left(i_{\mathrm{r1x0}} + i_{\mathrm{r2x0}}\right) \\
\Delta\psi_{\mathrm{r2y}} &= L_{\mathrm{m0}}\Delta i_{\mathrm{sy}} + \left(L_{\mathrm{m0}} + L_{\mathrm{c0}} + L_{\sigma\mathrm{r2}}\right)\Delta i_{\mathrm{r2y}} + \left(L_{\mathrm{m0}} + L_{\mathrm{c0}}\right)\Delta i_{\mathrm{r1y}} \\
&\quad + \Delta L_{\mathrm{m}}\left(i_{\mathrm{sy0}} + i_{\mathrm{r1y0}} + i_{\mathrm{r2y0}}\right) \\
&\quad + \Delta L_{\mathrm{c}}\left(i_{\mathrm{r1y0}} + i_{\mathrm{r2y0}}\right)
\end{aligned}
\quad .
$$

The small-signal electromagnetic torque needed for the torque model is

$$
\Delta T_{\mathrm{e}} = \frac{3}{2} pL_{\mathrm{m}}\left(i_{\mathrm{sb0}}\Delta\psi_{\mathrm{sa}} - i_{\mathrm{sa0}}\Delta\psi_{\mathrm{sb}} + \psi_{\mathrm{sa0}}\Delta i_{\mathrm{sb}} - \psi_{\mathrm{sb0}}\Delta i_{\mathrm{sa}}\right). \tag{29}
$$

In the flux linkage equations (28), the terms in the second and third rows in each equation originate from saturation. The complex-valued admittance is obtained by taking only the first rows into account.

It is assumed that L_{m} and L_{c} are both functions of magnetising and total rotor current. The perturbations of the inductances can be considered as dynamic inductances. They depend on the derivatives of the inductances at the respective operation point.

$$
\begin{aligned}
\Delta L_{\mathrm{m}} &= \left(\frac{\partial L_{\mathrm{m}}}{\partial i_{\mathrm{m}}}\frac{\partial i_{\mathrm{m}}}{\partial i_{\mathrm{mx}}}\right)\Delta i_{\mathrm{mx}} + \left(\frac{\partial L_{\mathrm{m}}}{\partial i_{\mathrm{m}}}\frac{\partial i_{\mathrm{m}}}{\partial i_{\mathrm{my}}}\right)\Delta i_{\mathrm{my}} \\
&\quad + \left(\frac{\partial L_{\mathrm{m}}}{\partial i_{\mathrm{r}}}\frac{\partial i_{\mathrm{r}}}{\partial i_{\mathrm{rx}}}\right)\Delta i_{\mathrm{rx}} + \left(\frac{\partial L_{\mathrm{m}}}{\partial i_{\mathrm{r}}}\frac{\partial i_{\mathrm{r}}}{\partial i_{\mathrm{ry}}}\right)\Delta i_{\mathrm{ry}} \\
\Delta L_{\mathrm{c}} &= \left(\frac{\partial L_{\mathrm{c}}}{\partial i_{\mathrm{r}}}\frac{\partial i_{\mathrm{r}}}{\partial i_{\mathrm{rx}}}\right)\Delta i_{\mathrm{rx}} + \left(\frac{\partial L_{\mathrm{c}}}{\partial i_{\mathrm{r}}}\frac{\partial i_{\mathrm{r}}}{\partial i_{\mathrm{ry}}}\right)\Delta i_{\mathrm{ry}} \\
&\quad + \left(\frac{\partial L_{\mathrm{c}}}{\partial i_{\mathrm{m}}}\frac{\partial i_{\mathrm{m}}}{\partial i_{\mathrm{rx}}}\right)\Delta i_{\mathrm{mx}} + \left(\frac{\partial L_{\mathrm{c}}}{\partial i_{\mathrm{m}}}\frac{\partial i_{\mathrm{m}}}{\partial i_{\mathrm{ry}}}\right)\Delta i_{\mathrm{my}}
\end{aligned}
\quad , \quad .
\tag{30}
$$

After differentiation and defining the steady-state and incremental inductances as

$$
L_{\mathrm{m0}} = \frac{\psi_{\mathrm{m}}}{i_{\mathrm{m}}},\ L_{\mathrm{mt}} = \frac{\partial\psi_{\mathrm{m}}}{\partial i_{\mathrm{m}}},\ L_{\mathrm{c0}} = \frac{\psi_{\sigma\mathrm{r}}}{i_{\mathrm{r}}},\ L_{\mathrm{ct}} = \frac{\partial\psi_{\sigma\mathrm{r}}}{\partial i_{\mathrm{r}}},\ \text{and}\ L_{\mathrm{t}} = \frac{\partial\psi_{\mathrm{m}}}{\partial i_{\mathrm{r}}} = \frac{\partial\psi_{\sigma\mathrm{r}}}{\partial i_{\mathrm{m}}}, \tag{31}
$$

the dynamic inductances can be written, using the stator and rotor currents, as

$$
\begin{aligned}
\Delta L_{\mathrm{m}} &= \frac{i_{\mathrm{mx}}}{i_{\mathrm{m}}^2}\left(L_{\mathrm{mt}} - L_{\mathrm{m0}}\right)\left(\Delta i_{\mathrm{sx}} + \Delta i_{\mathrm{r1x}} + \Delta i_{\mathrm{r2x}}\right) + \frac{i_{\mathrm{my}}}{i_{\mathrm{m}}^2}\left(L_{\mathrm{mt}} - L_{\mathrm{m0}}\right)\left(\Delta i_{\mathrm{sy}} + \Delta i_{\mathrm{r1y}} + \Delta i_{\mathrm{r2y}}\right) \\
&\quad + \frac{i_{\mathrm{rx}}}{i_{\mathrm{r}} i_{\mathrm{m}}} L_{\mathrm{t}}\left(\Delta i_{\mathrm{r1x}} + \Delta i_{\mathrm{r2x}}\right) + \frac{i_{\mathrm{ry}}}{i_{\mathrm{r}} i_{\mathrm{m}}} L_{\mathrm{t}}\left(\Delta i_{\mathrm{r1y}} + \Delta i_{\mathrm{r2y}}\right)
\end{aligned}
\quad , \tag{32}
$$

$$\Delta L_{\mathrm{c}} = \frac{i_{\mathrm{rx}}}{i_{\mathrm{r}}^2}\left(L_{\mathrm{ct}} - L_{\mathrm{c0}}\right)\left(\Delta i_{\mathrm{r1x}} + \Delta i_{\mathrm{r2x}}\right) + \frac{i_{\mathrm{ry}}}{i_{\mathrm{r}}^2}\left(L_{\mathrm{ct}} - L_{\mathrm{c0}}\right)\left(\Delta i_{\mathrm{r1y}} + \Delta i_{\mathrm{r2y}}\right) + \frac{i_{\mathrm{mx}}}{i_{\mathrm{m}} i_{\mathrm{r}}} L_{\mathrm{t}}\left(\Delta i_{\mathrm{sx}} + \Delta i_{\mathrm{r1x}} + \Delta i_{\mathrm{r2x}}\right) + \frac{i_{\mathrm{my}}}{i_{\mathrm{m}} i_{\mathrm{r}}} L_{\mathrm{t}}\left(\Delta i_{\mathrm{sy}} + \Delta i_{\mathrm{r1y}} + \Delta i_{\mathrm{r2y}}\right) \quad . \tag{33}$$

The small-signal model with currents as state variables is obtained by substituting (32) and (33) into the flux linkage equations (28) and substituting those into voltage equations (27). In the Laplace domain, the time derivatives are replaced by Laplace-variable s and in the frequency domain by $\mathrm{j}\omega$.

The complex-valued admittance for fitting the results of voltage impulse tests is obtained by setting the perturbations of the rotor angle to zero. The corresponding transfer function is presented in P4. The torque model for fitting the results of the angle impulse test is obtained by setting the perturbations of the stator voltage to zero. The model is presented in P8. The corresponding complex-valued admittances for a single-cage rotor are presented in P1 and P9. In the case of the mimo admittance, the stator leakage inductance is neglected in order to simplify the model and the fitting. The mimo admittance for a single-cage rotor is presented in P6 and for a double-cage rotor in P7.

In all the models, the angular frequency of the stator is constant and assumed to be known. Core losses are not modelled.

3.4 Curve fitting

The parameters of the complex-valued and mimo admittances, and of the torque model are estimated using the differential evolution algorithm (Price et al., 2005). In this method, an initial set of parameter vectors is constructed from a given range of random floating-point numbers. The best one is called the target vector. Two other randomly selected vectors are subtracted from each other and weighted with a weighting coefficient F. Adding the third randomly selected vector to the weighted difference vector creates a so-called noisy vector. The new parameter vector candidate is constructed by selecting its parameters either from the noisy vector or target vector. The selection is controlled by a measure of probability called crossover constant CR. The new candidate vector is then compared with the previous target vector and the best one is chosen as the next target vector. A generation step is depicted in the flow chart in Figure 9.

A drawback of evolutionary algorithms is that they may require a large number of generations in order to find the global minimum. The number of iterations can be reduced if the evolutionary algorithm is used only to find the neighbourhood of the minimum. The parameter estimates obtained can then be set as initial values for a gradient algorithm that is able to converge to the minimum rapidly. In this work, the Levenberg-Marquardt algorithm has been used for this purpose. It can be used for fitting complex-valued data if the data are separated into real and imaginary parts. However, in the cases studied, the number of iterations needed for the differential evolution has been only 1000…3000. Therefore, using the two estimation techniques in succession has not proved to be of any significant benefit in this work.

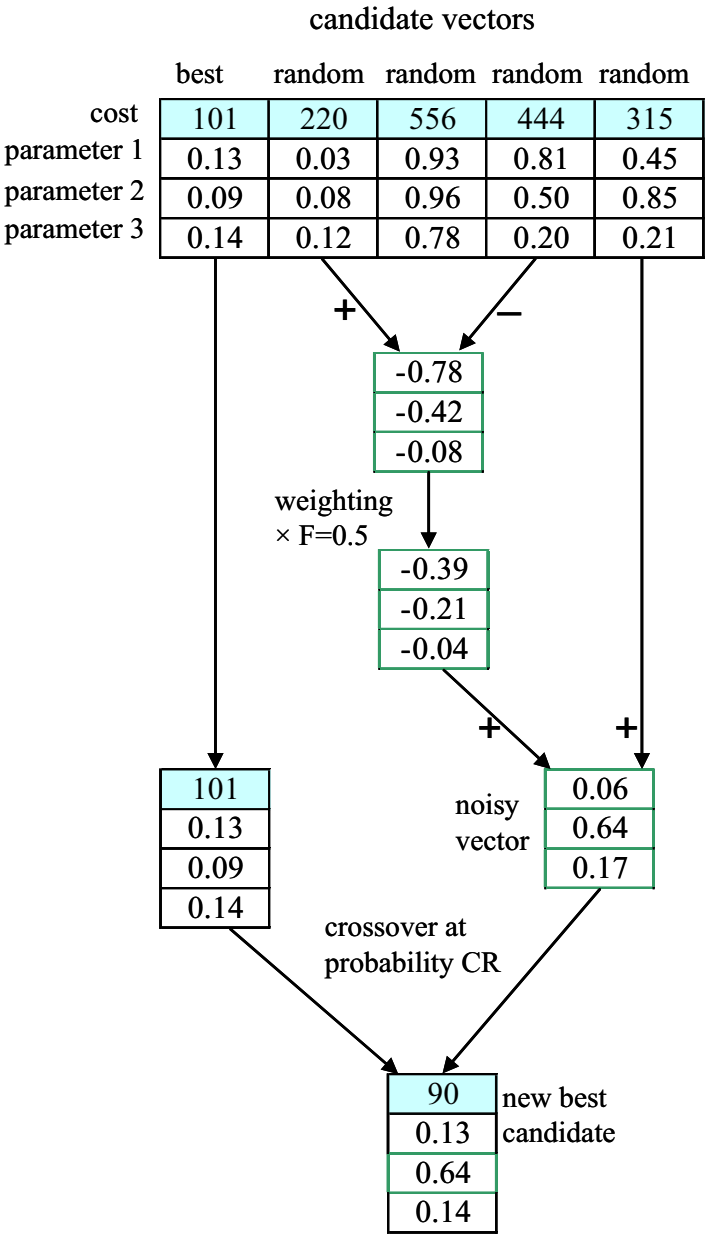

Figure 9. A flow chart of differential evolution.

4 Results

4.1 Estimation results

In this section, estimation results of both steady-state and small-signal model parameters are presented. The emphasis, however, is on the results of impulse tests and small-signal model parameters. The estimation results are shown for the 37-kW and 850-kW cage-induction machines. In addition, the 37-kW machine with linearised material is considered since the effects of saturation have a great importance when interpreting and comparing the results. Three different impulse tests have been applied to obtain the results:

- the voltage impulse test using the impulse (23) with low-dc component, performed once;
- the voltage impulse test using the simple impulse (22), performed twice with perpendicular impulses;
- the angle impulse test.

In the case of all the impulse tests, a steady-state computation is also performed. In order to fit the analytical small-signal models to the numerical data, the small-signal dynamics have to be separated from the frequencies produced by the machine at the fundamental supply. The extraction is performed by subtracting the results of the steady-state computations from the results of the impulse tests. The remaining small-signal data are referred to as the *numerical FRF*s. Three different small-signal models are used for parameter estimation:

- complex-valued admittance: a complex-valued (space-vector) small-signal model for fitting the results of the voltage impulse tests (both voltage impulse tests);
- mimo admittance: a small-signal model including saturation for fitting the results obtained using two perpendicular voltage impulses;
- torque model: a complex-valued small-signal model for fitting the results of angle impulse tests.

The validity of parameters of the steady-state models is evaluated by calculating some important operation-point quantities from the obtained circuit models. The steady-state parameters are obtained both from the impedance method and the voltage impulse test by fitting the mimo admittance. The corresponding operation points are also calculated using small-signal models and parameters in order to show the differences. The accuracy of the complex-valued admittance is evaluated by comparing the output of the model to the computation results of the harmonic excitation. Even though the same FE model is used in all the computations, the methods are independent of each other.

4.1.1 37-kW cage-induction machine

In P4, the complex-valued admittance is studied. The parameters are estimated using the numerical FRFs obtained from two different voltage impulse tests. First, the impulse test is performed once with impulse type (23). Next, the impulse test is performed twice with perpen-

dicular impulses (22) at $\varphi = 0$ and $\varphi = \pi/2$. However, in order to obtain an unequivocal fit, some assumptions concerning the parameters are made. It is assumed that:

- R_s is known (could also be estimated);
- the ratio of leakage inductances is known, $L_{\sigma r2}$ is calculated using that ratio and the current parameters estimates of L_c, R_{r1}, R_{r2} and $L_{\sigma s}$;
- R_c is known (could be neglected);
- $L_{\sigma r1}$ is zero.

The known parameters in the list above are fixed to the values given by the impedance method.

The torque model for fitting the results of angle impulse test is presented in P8. In addition to nine circuit parameters (Figure 1), the model contains altogether six steady-state current components. All of them cannot be estimated. The assumptions concerning the circuit parameters are similar to those used in the case of fitting the results of voltage impulse tests. In addition, the steady-state current components are treated in the following way:

- stator current components are taken from the steady-state time-stepping computation;
- the total rotor current is calculated using the known stator voltage, stator current and estimates of R_s, $L_{\sigma s}$ and L_m obtained from the impedance method;
- the components of $\boldsymbol{i}_{r1}$ are estimated and the components of $\boldsymbol{i}_{r2}$ are calculated from those and the total rotor current.

Table 2 presents the parameter estimates obtained from the impedance method and the three impulse tests.

TABLE 2 Parameter estimates for the 37-kW cage-induction machine (nonlinear FE model).

		Impedance method	Volt. imp (low dc) complex. adm.	Volt. imp (aver.) complex. adm.	Angle imp. torque model
R_s	[mΩ]	83.57*	83.57*	83.57*	83.57*
$L_{\sigma s}$	[mH]	0.784	0.564	0.619	0.436
L_m	[mH]	26.8	12.0	13.7	28.6
L_c	[mH]	1.07	0.624	0.616	0.857
R_c	[mΩ]	15.39	15.39*	15.39*	15.39*
$L_{\sigma r1}$	[mH]	0.0151	0*	0*	0*
R_{r1}	[mΩ]	198	192	278	196
$L_{\sigma r2}$	[mH]	0.859	0.869**	0.948**	0.857**
R_{r2}	[mΩ]	69.42	66.04	72.45	69.74

* fixed in advance, ** calculated

In P6 and P7, the mimo admittance and the mimo admittance for a single-cage rotor are studied. In addition to the circuit parameters, three incremental inductances are to be estimated. Therefore, the stator leakage inductance is set to zero. This assumption has also been made in, for example, (Corcoles et al., 2002). The mimo admittance contains altogether six steady-state current components. In order to find an unequivocal fit, the knowledge of the operation point is utilised more efficiently. R_{r2} and the rotor currents are not estimated but solved from the known values of stator voltage and current, and other parameter estimates. The procedure is explained in detail in P7.

Table 3 presents the parameters obtained using the mimo admittance. They are compared with the parameters obtained by using a complex-valued admittance. The model is otherwise similar to the complex-valued admittance discussed previously but $L_{\sigma s}$ and R_c are neglected, as in the case of the mimo admittance. On the other hand, in contrast to the previous models, R_s is estimated also. In the case of mimo admittance, L_m corresponds to L_{m0} and L_c to L_{c0}, respectively.

TABLE 3 Small-signal parameters obtained from the voltage impulse test for the 37-kW machine ($L_{\sigma s}$ and R_c neglected).

		Volt. imp (two imp.) mimo admittance	Volt. imp (aver. of two) complex-valued admit.
R_s	[mΩ]	84.0	84.0
$L_{\sigma s}$	[mH]	0*	0*
L_m	[mH]	25.6	17.0
L_c	[mH]	1.67	1.27
R_c	[mΩ]	0*	0*
$L_{\sigma r1}$	[mH]	0*	0*
R_{r1}	[mΩ]	306	318
$L_{\sigma r2}$	[mH]	1.00	0.948
R_{r2}	[mΩ]	102**	87.0
L_{mt}	[mH]	14.6	–
L_{ct}	[mH]	1.12	–
L_t	[mH]	−0.850	–

* fixed in advance, ** calculated

The small-signal model proposed by Melkebeek (1983a) was also tried in the fitting. The model takes into account the saturation of magnetising inductance as a function of magnetising current. It is observed that the model fits well only in the relatively narrow frequency range of 0…6 Hz.

The performances of different analytical models and parameter estimates can be evaluated by calculating the stator current, power factor λ and electromagnetic torque, and comparing them with the results of the FEAs. In the case of the mimo admittance, only the steady-state parameters are considered. The comparison is presented in Table 4. It should be recalled that the

small-signal parameters are not intended to be used for predicting steady-state operation points. The purpose of the comparison is to adduce the differences between different parameter sets.

TABLE 4 Operation points of the 37-kW machine at the rated voltage and slip given by the FEAs and analytical models.

(a) The operation points from the time-stepping and time-harmonic FEA and the corresponding points calculated using the steady-state parameters from the impedance method and voltage impulse test (mimo admittance, only the steady-state parameters considered).

		Time-stepping FEA	Time-harmonic FEA	Impedance method	Mimo admit. (steady. param.)
I_s	[A]	69.2	68.9	68.9	65.5
λ		0.837	0.849	0.849	0.837
T_e	[Nm]	238	235	237	223

(b) The operation points calculated using the parameters obtained from fitting the complex-valued admittance for the results of two different voltage impulse tests and the torque model for the results of the angle impulse test.

		Volt. imp. (low dc) complex. adm.	Volt. imp. (aver.) complex. adm.	Angle imp. torque model
I_s	[A]	86.8	76.8	69.2
λ		0.698	0.701	0.882
T_e	[Nm]	242	216	248

The performance of the complex-valued admittance can be best evaluated by comparing the predicted current perturbations with the results of the harmonic excitation. In the harmonic excitation, a voltage perturbation $\Delta\underline{u}_s$ at a certain frequency is superimposed on the supply voltage of the time-stepping FEA and the corresponding current perturbation $\Delta\underline{i}_s$ is computed. The predicted current perturbation $\Delta\underline{i}_s^{est}$ is calculated by supplying the same voltage perturbation $\Delta\underline{u}_s$ as an input to the complex-valued admittance with the third set of parameters in Table 2. This is the model that gives the best fit for the results of the voltage impulse test. Table 5 shows the comparison between the amplitudes and arguments of the resulting current perturbations. In all the FRF points, $\Delta\underline{u}_s$ has been 10% of the operation-point voltage. Therefore, especially at low frequencies, the amplitudes of current perturbations are very high. In P2 and P4, the amplitude of $\Delta\underline{u}_s$ has been decreased at low frequencies to 0.1…1%. However, it has been noticed that the ratio of $\Delta\underline{i}_s$ and $\Delta\underline{u}_s$ is practically constant regardless of whether $\Delta\underline{u}_s$ is 0.1% or 10%.

TABLE 5 Comparison between the complex-valued admittance model and the harmonic excitation performed with the time-stepping FEA. Current perturbations given as amplitudes and arguments.

f_d [Hz]	Harmonic exc. $\lvert\Delta i_\mathrm{s}\rvert$ [A]	Complex. adm. $\lvert\Delta i_\mathrm{s}^\mathrm{est}\rvert$ [A]	Harmonic exc. arg Δi_s [deg]	Complex. adm. arg $\Delta i_\mathrm{s}^\mathrm{est}$ [deg]
100	14.9	15.1	–69.0	–68.9
75	17.9	18.0	–65.1	–66.0
50	5.85	5.45	–45.2	–45.5
20	73.0	74.5	–85.9	–85.9
10	137	137	–61.7	–62.4
5	185	184	–34.0	–35.7
0	186	186	0.0	0.0
–5	145	143	26.1	26.0
–10	107	107	41.6	40.2
–20	68.0	68.5	54.7	53.4
–50	32.8	33.2	67.3	66.0
–75	23.0	23.6	71.4	70.3
–100	17.7	18.4	69.4	73.2

In order to find explanations for the differences between the steady-state and small-signal parameters, computations have been performed with linearised FE models. This means that the effects of saturation are removed by setting the relative permeabilities of saturable materials to $\mu_\mathrm{r} = 1000$. Table 6 presents the circuit parameters obtained for the linearised FE model. Table 7 presents the calculated operation points. It can be seen that when the saturation is removed, the parameter estimates and calculated operation points are close to each other.

TABLE 6 Parameter estimates for the 37-kW machine (linearised FE model).

	Impedance method	Volt. imp. complex. adm.	Angle imp. torque model
R_s [mΩ]	83.57	83.57*	83.57*
$L_{\sigma\mathrm{s}}$ [mH]	0.783	0.579	0.724
L_m [mH]	24.32	22.00	24.16
L_c [mH]	0.564	0.650	0.419
R_c [mΩ]	15.39	15.39*	15.39*
$L_{\sigma\mathrm{r1}}$ [mH]	–0.0720	0*	0*
R_r1 [mΩ]	206	240	223
$L_{\sigma\mathrm{r2}}$ [mH]	0.7450	0.810**	0.841**
R_r2 [mΩ]	70.1	70.3	71.7

*fixed in advance, **calculated

TABLE 7 Operation points given by different methods and models for the 37-kW machine (linearised FE model).

		Time-harm. FEA	Impedance method	Time-step. FEA	Volt. imp. complex. adm.	Angle imp. torque model
I_s	[A]	68.5	68.5	69.7	69.1	67.1
λ		0.853	0.853	0.839	0.834	0.854
T_e	[Nm]	240	237	238	234	233

It should be recalled that using the double-cage model is an approximation with respect to the skin effect. When fitting the data from impulse tests, some assumptions of the dependencies between the parameters have to be made and these assumptions can cause small differences between the different parameter sets. In addition, when fitting the numerical FRF from the angle impulse test, the steady-state current components are fixed to the values given by the impedance method and, therefore, these two sets are connected. However, the fixing does not devalue the result that shows that the fit for the numerical FRF is very good. The relative differences of the real and imaginary parts of the fitted model and numerical FRF are less than 0.8% within the frequency range studied. In the case of the linearised model, it is assumed and noticed during the study that the shape of the voltage impulse has a negligible effect on the resulting FRF.

4.1.2 850-kW cage-induction machine

The 850-kW cage-induction machine with semi-closed rotor slots is mainly studied in P8. In P1, the data obtained from the voltage impulse test is fitted to a single-cage complex-valued admittance. The obtained fit is fairly good. P8 is focused on the angle impulse test. It is observed that for fitting the numerical FRF, a double-cage model is needed to obtain a good fit. It seems that the skin effect has a stronger influence on the torque response than on the current response. The assumptions concerning the parameters and current components are those explained in Section 4.1.1.

The parameters obtained from fitting the torque model are shown in Table 8. These are compared with the parameters given by the impedance method. The third set of parameters is obtained by fitting the average of the FRFs obtained from two voltage impulse tests, as in the case of the 37-kW machine. These parameters are presented in P8.

Table 9 presents the operation points calculated using the analytical models with the estimated parameters. They are compared with the operation points given by FEAs.

TABLE 8 Parameters obtained by different methods for the 850-kW machine.

		Impedance method	Volt. imp. (aver.) complex. adm.	Angle imp. torque model
R_s	[mΩ]	2.84*	2.84*	2.84*
$L_{\sigma s}$	[mH]	0.277	0.120	0.144
L_m	[mH]	5.98	3.92	6.15
L_c	[mH]	0.119	0.256	0.209
R_c	[mΩ]	0.734	0.734*	0.734*
$L_{\sigma r1}$	[mH]	–0.00713	0*	0*
R_{r1}	[mΩ]	5.91	9.35	7.55
$L_{\sigma r2}$	[mH]	0.0803	0.0689**	0.0825**
R_{r2}	[mΩ]	2.42	2.75	2.42

* fixed, ** calculated

TABLE 9 Operation points given by different FEAs and analytical models with parameter estimates, 850-kW machine.

		Time-harm. FEA	Impedance method	Time-step. FEA	Volt. imp. complex. adm.	Angle imp. torque model
I_s	[A]	831	831	834	806	829
λ		0.869	0.872	0.866	0.814	0.885
T_e	[Nm]	8173	8209	8182	7436	8317

Next, the FRFs predicting the torque perturbations are considered more closely. Visual comparison of the FRFs obtained by using different analytical models and parameter estimates gives an idea of their performance. The following results are obtained using the torque model and the torque model for a single-cage rotor.

In Figure 10, different analytical models are compared with the numerical FRF. Figure 10(a) shows the FRF obtained from the angle impulse test and the fitted torque model. They are compared with the torque model for which the parameters are obtained from fitting the complex-valued admittance using the results of the voltage impulse test (average of two FRFs). For the latter, the current components are calculated by substituting the same small-signal parameters into the double-cage circuit (Figure 1) and solving the currents at the known supply voltage. Thus, the result is independent of the parameters and quantities obtained by the other means.

Figure 10(b) shows how the steady-state parameters obtained from the impedance method perform in the case of torque models. The steady-state parameters are substituted into the torque model and torque model for a single-cage rotor. The current components are calculated from the corresponding circuit models at the known supply voltage. As in Figure 10(a), the results are compared with the numerical FRF. It can be seen that all the models except the last one with a single-cage rotor predict the range of negative damping to be within 43…50 Hz.

The single-cage torque model gives a range that is a bit wider. This could be interpreted so that the oscillation-induced rotor currents cause a skin effect in deep rotor bars and provide more positive damping by increasing the resistive losses.

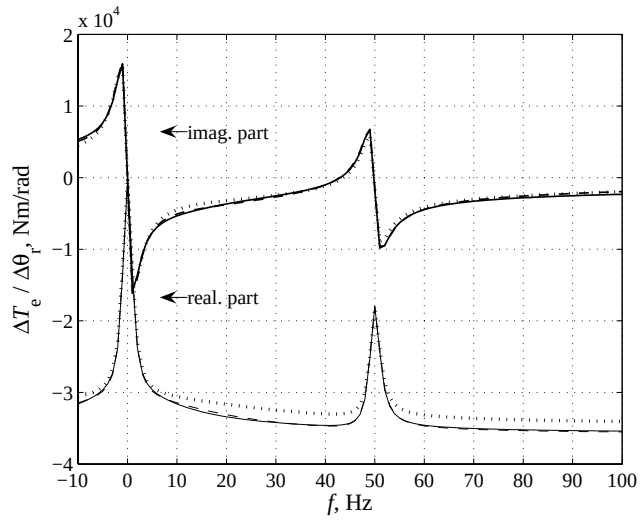

(a)

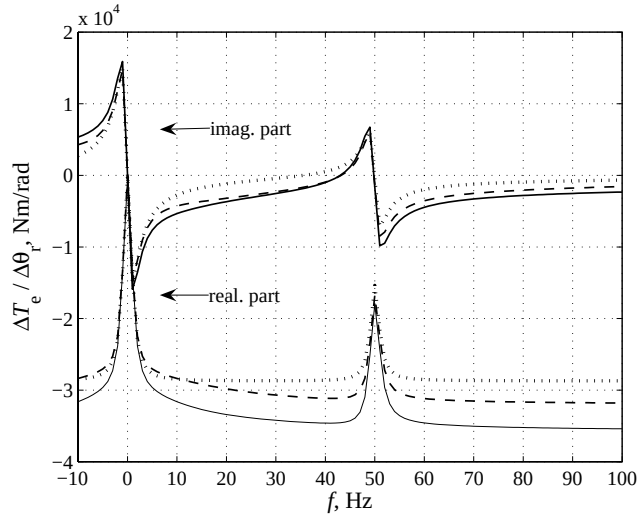

(b)

Figure 10. Comparison between the FRFs obtained by different methods for the 850-kW machine.

(a) The FRF obtained from the angle impulse test (solid line), the FRF of the torque model (dashed line), and the FRF calculated using the parameters obtained from the complex-valued admittance (dotted line).

(b) The FRF obtained from the angle impulse test (solid line) and the FRFs calculated using the steady-state parameters given by for a double-cage rotor (dashed line) and single-cage rotor (dotted line).

4.2 Measurements of torsional oscillations with two 37-kW cage-induction machines

In P8, the angle impulse tests are performed for the 850-kW and 37-kW cage-induction machines. The results of impulse tests predict negative damping of torsional oscillations within a frequency range below the supply frequency. The phenomenon is studied experimentally using two 37-kW cage-induction machines. The rotor is changed, otherwise the machines are

similar to the one in the previous publications. The new rotor is designed especially for a frequency-converter supply, and it does not have a double-cage structure or deep rotor bars. For this rotor, the angle impulse test predicts a slightly wider range of negative damping, 40…50 Hz. The torsional oscillations induce two harmonic components to the stator current on both sides of the fundamental frequency. The lower component is at $\omega_s - \omega_d$, where ω_d is the frequency of torsional oscillations. The upper component is at $\omega_s + \omega_d$, respectively. In the results, the upper component is presented.

The measurement set-up is presented in Figure 11. In the set-up, two practically identical 37-kW cage-induction machines were coupled with a flexible shaft. The shaft was designed so that the natural frequency of the system fell within the range of negative damping. The measurement set-up is depicted in detail in P8. Based on the computed FRFs, the range of negative damping was almost independent of the load. The first measurements were performed at sinusoidal supply at no load. The supply frequency was varied and the flux was kept at the rated level. In P8, the measured torsional oscillations and corresponding upper stator current harmonic are presented. The flexible shaft was connected with rigid shaft couplings with a shrunk-on-fit but no key. It is possible that some mechanical damping was present because of friction losses in the coupling.

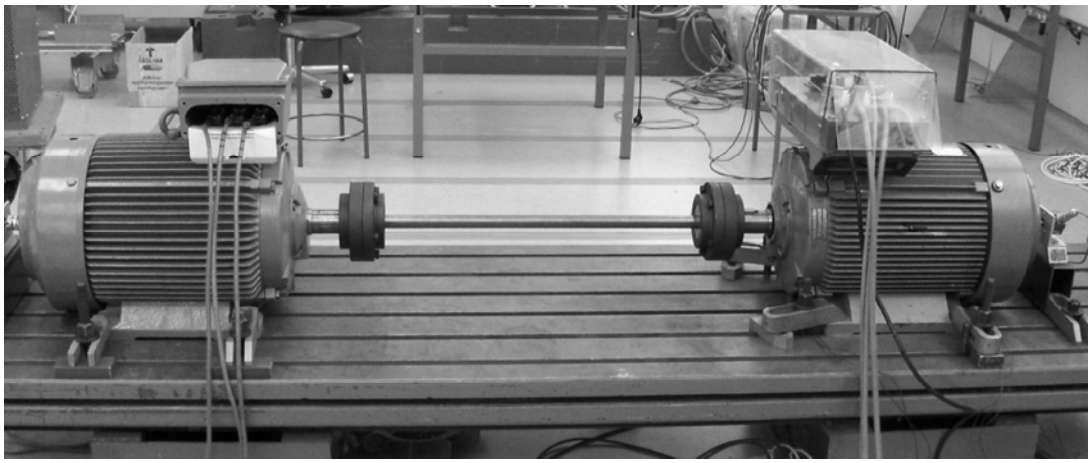

Figure 11. The measurement set-up for torsional oscillations.

The measurements have been continued from those presented in P8. Some of the results are presented here. The simple shaft was replaced by another shaft equipped with proper keyways, and the measurements were repeated. However, only the stator current components were recorded. Figure 12(a) shows the upper harmonic with respect to the no-load fundamental component of 27.5 A (rms-value). The amplitudes are more than three times the ones obtained with the simple shaft. The influence of load was also tested. The machines were supplied by frequency converters so that the first one was operating as a generator and the other one as a motor. The supply frequencies were adjusted so that the motor was operating at the rated load. In this case, the rotation frequency of the shaft in electrical degrees is 1 Hz less than the supply frequency. The upper current harmonic with respect to the rated fundamental component of 71.2 A (rms-value) is shown in Figure 12(b).

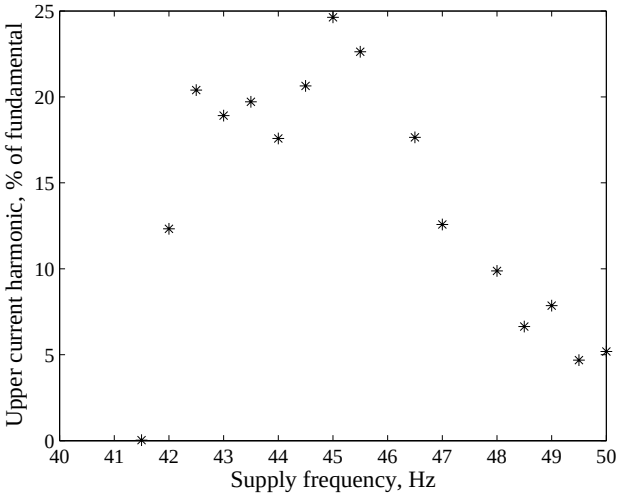

(a)

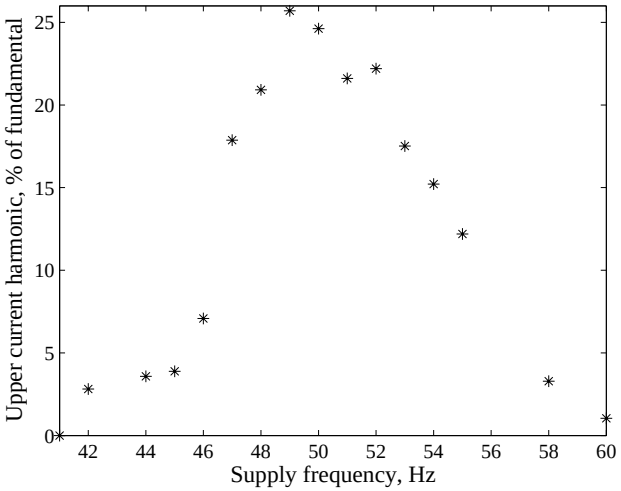

(b)

Figure 12. Upper stator current harmonic induced by torsional oscillation: (a) no load operation, (b) rated load operation.

Based on the results presented in P8, it can be concluded that the self-excited torsional oscillations occur in the frequency range for which the angle impulse test predicts negative electromagnetic damping. The results in P8 show that the amplitudes of the oscillation-induced stator current harmonics are proportional to the amplitudes of torsional oscillations. The current harmonics shown above are significantly higher than those measured in P8. The higher amplitudes are obtained by reducing friction losses, which provide positive damping.

5 Discussion

5.1 Applicability of impulse tests

The voltage impulse tests have been performed using various impulse types and sizes. It has been noticed that the amplitude of the impulse has a very small effect on the shape of the response. Consequently, the goodness of the fit and the values of parameter estimates are practically unaffected when a_{rel} is varied between 1…30%. At a_{rel} = 50…80%, the shape of FRF begins to distort compared to the lower amplitudes. Within this study, impulses of length between 1…10 ms have been tried. It is observed that, within this range, the length does not influence the shape of the resulting FRF. Similarly, the time instant or rotor position at which the impulse is applied does not seem to affect the results of voltage impulse tests.

However, in reality, the magnetic coupling between the stator and rotor depends on the position of the rotor or time. The rotation is modelled by the time-stepping FEA. In the case of voltage impulse tests, this time-dependency is practically unobservable from the FRFs. In the response of electromagnetic torque with respect to the rotor angle perturbation, the time-variance can be detected as harmonics. Yet, in the case of cage-induction machines, the harmonics related to slotting occur at 1…3 kHz frequencies and their effects at the low frequencies are very small. Within this work, the frequency ranges used for parameter estimation are below a couple of hundred hertz, which is sufficient for the analytical models adapted. In practice, the assumption of time-invariance means that the steady-state current (or flux) components needed in some models can be assumed constants in the synchronous reference frame.

In addition to impulse and harmonic excitations, some other excitation signals have also been tried. Similarly to the impulse, white-noise and PRBS signals have been superimposed on the three-phase supply voltage. A chirp signal was supplied to one phase voltage. The basic shapes of the resulting FRFs are more or less close to the one obtained using the harmonic excitation. However, they contain a fairly large ripple.

5.2 Influence of saturation

The harmonics induced by saturation are studied by several means in P4. It is noticed that for the 37-kW machine with closed rotor slots, the harmonics are clearly detectable. In the case of semi-closed rotor slots, the amplitudes of the harmonics are low. Congruent results with an FEA have been obtained by Salon et al. (1994) also. In the case of closed rotor slots, saturation-induced harmonics are clearly visible around 100 Hz, 300 Hz, 500 Hz, etc. and around –200 Hz, –400 Hz, –600 Hz, etc.

Regardless of the structure of slots, the effects of saturation can be detected from the inductance values obtained by different methods. When the complex-valued admittance is fitted to the data obtained from a voltage impulse test, the values of inductance estimates are smaller than the steady-state values obtained from the impedance method. These values are obtained when the best possible fit for the data is sought and the parameters are not fixed to the operation-point voltage and current. A similar result is obtained when any of the voltage impulses

or the harmonic excitation are applied. For the linearised FE model, on the other hand, the inductance values given by different methods are close to each other. When the different parameter sets are used to determine the operation point, the results are almost alike.

The best fit for the complex-valued admittance is obtained by using the average of two FRFs obtained from the perpendicular voltage impulses. The results are practically the same with the FRF computed with the harmonic excitation. Table 5 confirms the observation. The reason for this is that some of the saturation-induced harmonics are at the opposite phases with respect to each other, if the impulses are perpendicular. The theoretical explanation is derived in P4. A similar phenomenon is noticed for the 850-kW and 2.2-kW machines. Thus, it can be concluded that the complex-valued model depicts well the response of stator current vector to small perturbations in stator voltage. On the other hand, the same model does not depict the steady-state operation point correctly.

In P6 and P7, mimo admittance models including both the effects of magnetising and leakage-flux saturation are studied. The results of two voltage impulse tests with perpendicular impulses are used as separate inputs in the fitting. Both the steady-state and incremental inductances are estimated simultaneously. A prior knowledge of the operation point, such as stator voltage and current, is utilised in the estimation. Thus, the steady-state rotor currents of the model can also be estimated. The obtained fit is good and the steady-state parameters depict the operation point well. The incremental parameters are also physically reasonable. The negative sign of incremental mutual inductance L_t (Table 3) is also realistic since the magnetising flux decreases when the rotor current increases, if the magnetising current is assumed constant.

The estimate of magnetising inductance of the complex-valued admittance is close to the average of steady-state and incremental inductances obtained using the mimo admittance. In the small-signal dynamics, both the steady-state and incremental permeability are present. The complex-valued admittance cannot distinguish between them since it is too simple by structure. It seems as if it models them in average. Fitting the complex-valued admittance by using the knowledge of operation-point stator voltage and current has also been tried. This type of estimation is performed for a single-cage model when the estimated parameters are stator resistance and magnetising inductance. The rotor resistance and leakage inductance are calculated from the estimates and known operation-point quantities. The obtained parameters are close to the steady-state parameters obtained by fitting the mimo admittance. The fit itself, however, is rather poor. A drawback of the technique is that the double-cage rotor parameters cannot be obtained.

In the case of angle impulse tests, the effects of saturation are different from those of the voltage impulse tests. For the complex-valued torque model, the estimated magnetising inductance is close to the steady-state value. This result can be partly because of the applied assumptions concerning the steady-state current components. The torque model is always fixed to the steady-state operation point. Nevertheless, the fitted model corresponds best to the numerical FRF when compared to other models studied (Figure 10). The next best alternative is to choose the parameters obtained from the voltage impulse test and use them as circuit pa-

rameters to solve the current components required. Nevertheless, it is clear that the parameters depicting the small-signal dynamics between voltage and current vectors are able to predict the dynamics between the rotor position angle and electromagnetic torque only approximately. This result is obtained when the saturation is present.

In P6 and P7, the parameters obtained by fitting the mimo admittance are used to depict the small-signal dynamics between the rotor position angle and electromagnetic torque. The performance of these more advanced torque models is evaluated both in P6 and P7 by comparing their results with the numerical FRF obtained from the angle impulse tests. The FRFs correlate well. However, these advanced torque models have not been used for fitting the numerical FRF. A reason for this is that the fitting requires plenty of presumptions.

By using the more advanced torque models, the effect of neglecting different terms related to saturation can be studied. In the frequency range below 100 Hz, neglecting the terms originating from saturation gives results that are practically as good as with the complete model. However, at higher frequencies, the differences begin to show. Especially, neglecting the term depicting the rotor leakage saturation causes a clear difference compared to the numerical FRF.

5.3 Parameter estimates

The goodness of the steady-state parameters can be evaluated fairly easily by measurements. If they are able to predict the operation-point quantities, such as rms-valued stator current, power factor, and torque correctly, they can be considered as reasonable. The parameters given by the impedance method have been evaluated with respect to measurements at the rated operation point in P2. The circuit parameters which predict the measured stator current, power factor and torque are iterated by using the results of the impedance method as initial values. The final parameters are close to the estimated ones even though the 2D FE model neglects some features of the real machine. In addition, in P3, the torque-versus-speed curve is measured at a reduced voltage level. The measured curve correlates fairly well with the one obtained by the time-harmonic FEA. Within this work, the impedance method has been applied to estimate parameters at numerous operation points and naturally, all those points have not been measured. However, the impulse tests have been mainly performed at rated operation points.

To model the steady-state operation at a certain operation point, a single-cage circuit model is sufficient regardless of whether the machine has a single-cage or double-cage structure. At a fixed frequency, the multi-cage models can be arithmetically reduced to a single-cage model. However, as proposed in several previous works, in order to model large-signal transients more accurately, a double-cage or even a higher-order model is needed. Basically, this requirement means that the large-signal model should be able to take into account the effects of changing rotor frequency. The frequency response tests have been used to capture the behaviour related to frequency dependency. These are based on the idea of small-signal dynamics. In the case of SSFR tests (IEEE Guide, 1996), all the model parameters are estimated from the small-signal data. Only a single value for each inductance is used and there is no indica-

tion whether the value of an inductance is related to the effective permeability or incremental permeability or both. Based on the study of this dissertation, it seems that the estimates of inductances obtained using the complex-valued admittance may fall between the values of steady-state and incremental inductances. These parameters are reasonable for stability analyses since they can predict the small-signal behaviour well. However, some care should be taken when implementing these in large-signal simulations.

What is somewhat surprising, is that the results of the impulse tests are so unaffected by the size of the amplitude. When the voltage impulse test is performed at $a_{\mathrm{rel}} = 0.01$ and $a_{\mathrm{rel}} = 0.2$, the differences of the parameter estimates obtained are generally less than one percent and less than three percents at the most. The results presented in Chapter 4 are obtained using $a_{\mathrm{rel}} = 0.1$. It seems that, in the case of the impulse tests presented, the small-signal excitation can have rather large amplitude.

Verbeeck et al. (2000) performed the SSFR tests for a synchronous machine at different flux levels. As expected, it was observed that especially the estimate for the magnetising inductance depends on the flux level. Within this work, the effect of flux level, or operation point in general, has been studied mainly in the case of steady-state parameters. The voltage impulse tests have been performed mainly at the rated loads. In P5, some other operation points are also surveyed. The impulse tests are performed at the half load and reduced supply voltage. For these, the fits obtained are good and the parameter estimates reasonable. For example, the value of magnetising inductance is increased at the reduced supply voltage.

Some limitations have also been found. For an 80-kW cage-induction machine, at the supply frequencies above the base value, a reasonable estimate for magnetising inductance could not be found. The goodness of the fit seems to be almost insensitive to the value of magnetising inductance. The impulse tests have also been performed at no-load operation and for a locked rotor for several machines. For the locked rotor, a good fit and reasonable parameter estimates have been obtained. In the case of no load, the fitting of the numerical FRF is difficult. This is understandable since around the no-load point, the saturation of iron bridges closing the rotor slots varies with the slightest change in the air-gap flux. For example, the estimates of steady-state parameters in P5 vary close to the no-load operation.

In P1, parameters for the 1.7-MW slip-ring machine are estimated using the voltage impulse test. Similarly to the cage-induction machines studied, the estimate for the magnetising inductance is smaller than the steady-state value given by the impedance method. In P9, the small-signal parameters are estimated using the angle impulse test. The parameters obtained are otherwise close to the values given by other methods, but the magnetising inductance is twice the steady-state value. It is possible that there are too many free parameters to be estimated. The torque model for slip-ring machines contains both steady-state currents and coefficients relating the angle perturbations to the rotor voltage perturbations, as presented in P9. By fixing some parameter or a ratio of parameters to a physically reasonable value might assist in finding a physically correct set of parameters.

5.4 FE model

Within this work, the 2D time-stepping FEA is treated as a complete model that would depict the machine behaviour realistically enough in most of the applications. The analytical models are developed using the FEA and their performance is evaluated with respect to it. However, the used FE model is rather simple. The 3D effects of the end-rings and end-windings are taken into account only analytically by an additional impedance in the circuit equations. The iron losses are modelled by analytical expressions that give only a rough approximation. In addition, only a single-valued magnetisation curve is applied and the hysteresis is neglected. The skin effect in laminations and stator conductors is omitted.

A time-harmonic FEA including eddy currents in stator conductors is applied by Islam et al. (2007). It is noticed that the eddy current losses in the stator conductors vary between 7.8 and 41% of the total dc stator resistive losses. The losses depend strongly on the placement of the conductors in the slot. Including ferromagnetic hysteresis in the time-stepping FEA has been studied by Saitz (2001) and using a dynamic hysteresis model by Dlala (2007). A more comprehensive core-loss model would include the retarding harmonic torques to the FE model and could affect, for example, the estimated torque model. A future research aim is to perform impulse response tests with more advanced FE models and codes. An important advantage of the method is that since only the inputs and outputs of the FE code are utilised modified, the FE code does not have to be modified. Therefore, commercial codes could also be applied.

Within this work, the differences and similarities of the numerical and analytical models are brought out frequently. However, the original purpose of the study has not been to estimate parameters specifically for the models derived from the theory of electrical machines. Although models with physically meaningful structure and parameters are preferred for many occasions, the study has not been limited to those. The starting point for the study was more general – the identification of such analytical models that are able to depict the results of numerical computations performed. However, the frequency contents of the impulses applied fall between –1000…1000 Hz. Therefore, the high-frequency effects such as slot harmonics are omitted. Some low-frequency stator harmonics can be detected from the results, but developing models for them has not been found significant. Any truly unexpected dynamics have not been observed. On the contrary, the analytical models with relatively simple structure seem to perform well. For example, transfer functions of an order higher than that of the physical models do not seem to provide better fits.

5.5 Torsional oscillations

The angle impulse test predicts a range of negative damping for the 850-kW and 37-kW cage-induction machines at, for example, no-load and rated load conditions. The range appears below the supply frequency 50 Hz approximately from 40 Hz upwards. For the 1.7-MW slip-ring machine operating at the rated load, a corresponding range is observed, and, in addition, another one is observed at the frequencies between dc and the slip frequency. The range of negative damping is scanned experimentally by using two 37-kW machines. It is noticed that at no load, the self-excited torsional oscillations occur at those frequencies where the impulse

test predicts the negative damping. However, no instability occurs. A similar phenomenon has been reported, by, for example, Lipo and Krause (1969).

In P8, the behaviour of the measurement set-up is simulated by the time-stepping FEA. The oscillation amplitudes predicted by simulations are significantly higher than the measured ones. In the case of measurements reported in Section 4.2, the oscillation amplitudes are clearly higher than those in P8. Because of the different shaft, friction losses in the shaft couplings are decreased compared to the first measurements. It is proposed that the differences between the measurements and the FEA emerge partly because of the inadequate loss model of the FEA. It is believed that, with the more accurate loss models discussed in 5.4, more profound explanations for the differences can be found.

5.6 Further research

The relative motion of the slotted stator and rotor makes the electrical machine and the related time-discretised FE model time-variant. For example, the stator current and electromagnetic torque contains harmonics caused by slotting. In the case of the 37-kW cage-induction machine, a relatively high harmonic component occurs in the stator current at 930 Hz. At the rated operation, it is 3.4% of the fundamental current. However, within this work the small-signal dynamics are extracted by subtracting the results of the steady-state computation from the results of an impulse test or harmonic excitation. For example, the slotting-harmonic caused by the excitation signal at 15 Hz occurs at 965 Hz. It is 2.4% of the response at the excitation frequency. However, the slotting-harmonic at 930 Hz is only 0.7% of the response signal at 15 Hz. With respect to the fundamental component at 50 Hz, this harmonic decreases from 3.4% to 1.5%.

The steady-state electromagnetic torque contains two higher slotting-harmonics. The harmonic at 880 Hz is 3.6% and the harmonic at 1180 Hz is 1.9% of the rated torque. In contrast to the current harmonic, the torque harmonics are not affected by the subtraction. The effect of these harmonics can be seen in the numerical FRF already at frequencies below 100 Hz. By performing angle impulse tests and varying the initial time of the impulse, it is noticed that the shape of the resulting numerical FRF varies with the initial time. However, the variation is so small that the parameter estimates obtained are practically unaffected.

In the case of the 1.7-MW machine, the significant torque harmonics appear at the frequencies 336 Hz, 672 Hz, 1344 Hz and 1680 Hz. The electromagnetic torque at the rated load is presented in Figure 13. Figure 14(a) presents two FRFs computed at the rated load $s = -12\%$ and $u_\mathrm{r} = 286$ V for a linearised FE model. The linearised model is chosen to emphasise the effect of time variance. The impulses are otherwise similar but the time instants at which the impulse is applied differ by 19 ms. The difference between the time instants is chosen randomly. Figure 14(b) presents otherwise identical cases, but now $u_\mathrm{r} = 0$ V providing a stator current five times the rated one. This operation point is not realistic for continuous operation but it is chosen to emphasize the effect of harmonics.

For cage-induction machines, a similar phenomenon may occur when the machine is operating at standstill or slip values close to one. In addition, in the case of permanent magnet ma-

chines, the so-called cogging torque may cause this effect. In all these cases, the time-variation of the ‘noise’ source is periodic. If a small-signal model for the electrical machine is to be estimated using an impulse test, the effects of time-variance need to be either filtered or included in the estimation procedure. In the latter case, the identification of a time-variant noise model may be needed. This could be a highly interesting subject for further studies.

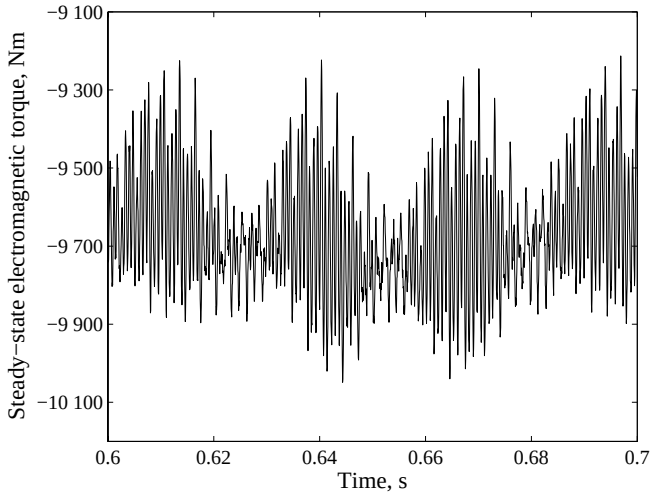

Figure 13. The steady-state torque for the 1.7-MW slip-ring machine at the rated load.

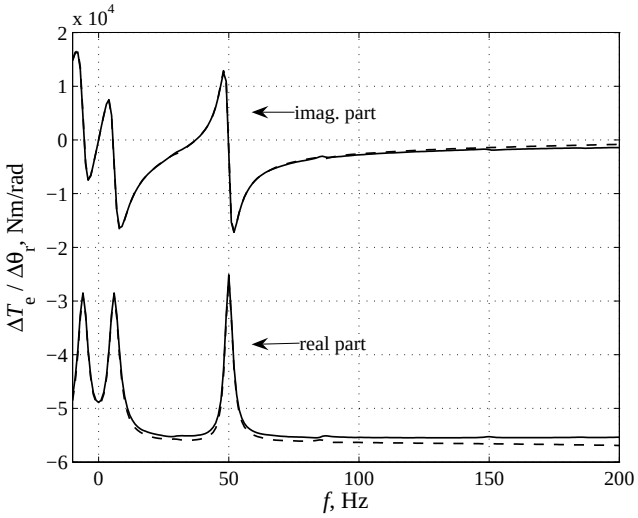

(a)

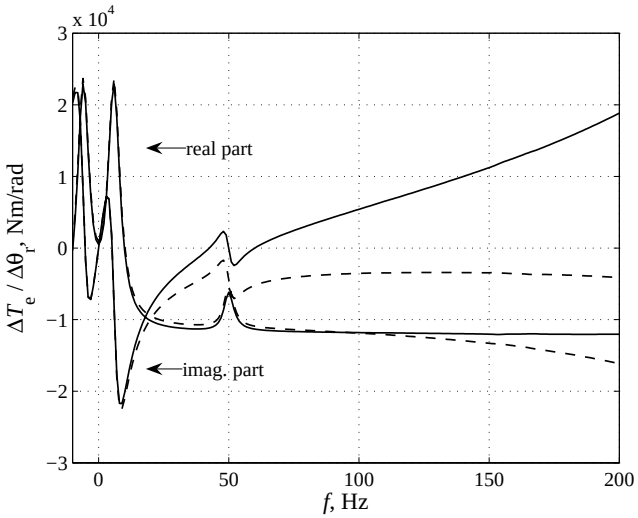

(b)

Figure 14. FRFs obtained from the angle impulse test for the 1.7-MW slip-ring machine (linearised FE model). (a) The rated load, (b) the rated slip, $u_r = 0$ V. Solid line: impulse applied at the time instant $t = 0.544$ s. Dashed line: impulse applied at the time instant $t = 0.563$ s.

6 Summary

Within this study, two new applications for numerical impulse response tests have been presented. The focus is centred on cage-induction machines and particularly the effects of closed rotor slots and deep rotor bars. The voltage impulse test is specifically applied to estimate parameters of small-signal models. The angle impulse test is applied both to estimate the parameters and to depict the torsional dynamics of induction machines.

Particular attention is given to the parameter estimation for small-signal models. However, for comparison, and as an independent subject of interest, as well, the parameter estimation for steady-state circuit models also constitutes an important part of the study. Within this work, the time-harmonic FEA and the impedance method are implemented to estimate steady-state or large-signal parameters for circuit models with multiple rotor branches. The method is also applied to study variation of circuit parameters as a function of different operation-point quantities.

The applicability of the impulse tests is based on the assumption of a linear, time-invariant behaviour of the output variables in the neighbourhood of an operation point. The assumption is studied by numerous computations. It is concluded that the assumption holds well for cage-induction machines at their rated operation points. However, the saturation is always present, especially in the case of closed rotor slots. The effect of saturation as a function of magnetising and rotor currents can be included in the small-signal model. When this is done, the parameter estimates receive a clear physical interpretation. The effect of time-dependence can be detected from the results of angle impulse tests. However, in practice, the variation is so insignificant that the estimation results are not affected.

At slip values close to one and in the case of slip-ring machines, the time variation may have a greater influence. Therefore, the effect of time-variance on the results of numerical impulse response tests is proposed as a subject for further studies. However, the studies performed refer to the fact that, under usual operation, the slip-ring machines can also be modelled fairly well by time-invariant analytical models.

It is concluded that the numerical impulse response test can be used to estimate parameters of analytical small-signal models. The impulse excitation detects the effects of saturation; this has to be kept in mind when interpreting and implementing the results. In addition, the skin effect in rotor bars has a great influence on the results. This work can be seen as a possible basis for further studies, in which the method used in this work could be developed further, perhaps with a view to discovering new applications.

References

Alonge, F., D'Ippolito, F., Ferrante, G., Raimondi, F.M. 1998. Parameter identification of induction motor model using genetic algorithms. *IEE Proceedings – Control Theory Applications*, Vol. 145, No. 6, November 1998, pp. 587–593.

Amaya, M., Costa, A., Palacios, J., Cadavid, W. 2003. Identification of the synchronous machine parameters by the simulation of time domain tests using finite-elements method. *IEMDC'03, IEEE International Conference on Electric Machines and Drives*, Volume 1, 1–4 June 2003, Madison, Wisconsin, USA, pp. 456–460.

Arjona L., M.A. 2004. Parameter calculation of a turbogenerator during an open-circuit transient excitation. *IEEE Transactions on Energy Conversion*, Vol. 19, No. 1, March 2004.

Arkkio, A. 1987. Analysis of induction motors based on the numerical solution of the magnetic field and circuit equations. *Acta Polytechnica Scandinavica*, *Electrical Engineering Series, No. 59,* Helsinki 1987, 97 p. Available at: http.//lib.tkk.fi/Diss/198X/isbn951226076X/.

Arkkio, A., Antila, M., Pokki, K., Simon, A., Lantto, E. 2000. Electromagnetic force on a whirling cage rotor. *IEE Proceedings – Electric Power Applications*, Vol. 147, No. 5, pp. 353–360.

Bae, D., Kim, D., Jung, H., Hahn, S., Koh, C.S. 1997. Determination of induction motor parameters by using neural network based on FEM results. *IEEE Transactions on Magnetics*, Vol. 33, No. 2, March 1997, pp. 1924–1927.

Benn, L.C., Burton, B., Harley, R.G. 2003. Online converter fed induction motor impulse response identification and parameter extraction using pseudorandom modified PWM. *SDEMPED Symposium on Diagnostics for Electric Machines, Power Electronics and Drives*, 24–26 August 2003, Georgia, USA, pp. 70–75.

Bianchi, N., Bolognani, S., Comelato, G. 1999. Finite element analysis of three-phase induction motors, comparison of two different approaches. *IEEE Transactions on Energy Conversion*, Vol. 14, No. 4, December 1999, pp. 1523–1528.

Boldea, I., Nasar, S.A. 1988. A general equivalent circuit (GEC) of electric machines including crosscouplings saturation and frequency effects. *IEEE Transactions on Energy Conversion*, Vol. 3, No. 3, September 1988, pp. 689–696.

Boldea, I., Nasar, S.A. 1986. Upon unitary treatment of magnetic saturation in orthogonal axis models of electric machines. *Proceedings in International Conference in Electrical Machines*, Part I, September 1986, pp. 172–175.

Briz, F., Degner, M.W., Guerrero, J.M., Diez, A.B. Temperature estimation in inverter fed machines using high frequency carrier signal injection. *Proceedings – IEEE-IAS Industry Applications Society Annual Meeting,* New Orleans, Louisiana, USA, September 2007, pp. 2030–2037.

Brown, J.E., Kovacs, K.P., Vas, P. 1983. A method of including the effects of main flux path saturation in the generalised equations of AC machines. *IEEE Transactions on Power Apparatus and Systems*, Vol. 102, No. 1, January 1983, pp. 96–103.

Burakov, A. 2007. Modelling the unbalanced magnetic pull in eccentric-rotor electrical machines with parallel windings. Doctoral Thesis, *TKK Dissertations*, No. 93, Espoo 2007, 154 p. 2007. Available at. http.//lib.tkk.fi/Diss/2007/isbn9789512290062/

Chari, M.V.K., Silvester, P. 1971. Analysis of turboalternator magnetic fields by finite elements. *IEEE Transactions on Power Apparatus and Systems*, Vol. 90, No. 2, March/April 1971, pp. 454–464.

Chari, M.V.K., Minnich, S.H., Tandon, S.C., Csendes, Z.J., Berkery, J. 1981. Load characteristics of synchronous generators by the finite-element method. *IEEE Transactions on Power Apparatus and Systems*, Vol. 100, No. 1, January 1981, pp. 1–13.

Chaudhry, S.R., Ahmed-Zaid, S., Demerdash, N.A. 1995. An artificial-neural-network method for the identification of saturated turbogenerator parameters based on a coupled finite-element/state-space computational algorithm. *IEEE Transactions on Energy Conversion*, Vol. 10, No. 4, December 1995, pp. 625–633.

Cirrincione, M., Pucci, M., Cirrincione, G., Capolino, G.-A. 2003 (a). Constrained least squares method for the estimation of the electrical parameters of an induction motor. *COMPEL. The international Journal for Computation and Mathematics in Electrical and Electronic Engineering*, Vol. 22, No. 4, 2003, pp. 1089–1101.

Cirrincione, M., Pucci, M., Cirrincione, G., Capolino, G.-A., 2003 (b). A new experimental application of least-squares techniques for the estimation of the induction motor parameters. *IEEE Transactions on Industry Applications*, Vol. 39, No. 5, September/October 2003, pp. 1247–1256.

Cirrincione, M., Pucci, M., Cirrincione, G., Capolino, G.-A. 2005. Constrained minimization for parameter estimation of induction motors in saturated and unsaturated conditions. *IEEE Transactions on Industrial Electronics*, Vol. 52, No. 5, October 2005, pp. 1391–1402.

Concordia, C. 1952. Induction motor damping and synchronizing torques. *AIEE Transactions on Power Apparatus and Systems*, Vol. 71, January 1952, pp. 364–366.

Concordia, C., Kron, G. 1945. Damping and synchronizing torques of power selsyns, *AIEE Transactions*, Vol. 64, 1945, pp. 366–271.

Concordia, C., Crary, S.B., Kron, G. 1942. The doubly fed machine. *Electrical Engineering*, Vol. 61, May 1942, pp. 286–289.

Concordia, C. 1950. Synchronous machine damping torque at low speeds. *AIEE Transactions*, Vol. 69, 1950, pp. 1550–1553.

Conte, R.N., Pereira, L.F.A., Haffner, J.F., Scharlau, C.C., Campestrini, L., Fehlberg, R.P. 2003. Parameter identification of induction machines based on frequency response and opti-

mization techniques. *IECON '03 The 29th Annual Conference of the Industrial Electronics Society*, 2–6 November 2003, Roanoke, Virginia, USA, pp. 596–599.

Corcoles, F., Pedra, J., Salichs, M., Saintz, L. 2002. Analysis of induction machine parameter identification. *IEEE Transactions on Energy Conversion*, Vol. 17, No. 2, June 2002, pp. 183–190.

De Doncker, R.W. 1992. Field-oriented controllers with rotor deep bar compensation. *IEEE Transactions on Industry Applications*, Vol. 28, Nol 5, September/October 1992, pp. 1062–1071.

Dlala E., Belahcen A., Arkkio A. 2007. Magnetodynamic vector hysteresis model for ferromagnetic steel laminations. *Physica B*. In press.

Doherty, R.E., Nickle, C.A., 1928. Synchronous machines, Part IV, *AIEE Quarterly Transactions*, Vol. 47, April 1928, pp. 457–470.

Dolinar, D., De Weerdt, R., Freeman, E.M., 1997. Calculation of two-axis induction machine model parameters using finite elements. *IEEE Transactions on Energy Conversion*, Vol. 12, No. 2, June 1997, pp. 133–142.

Dolinar, D., Ljusev, P., Stumberger, G., 2003. Input-output linearising tracking control of an induction motor including magnetic saturation effects. *IEE Proceedings – Electric Power Applications*, Vol. 150, No. 6, November 2003, pp. 703–711.

Escarela-Perez, R., Niewierowicz, T., Campero-Littlewood, E. 2001. Synchronous machine parameters from frequency-response finite-element simulations and genetic algorithms. *IEEE Transactions on Energy Conversion*, Vol. 16, No. 2, June 2001.

Ewins, D.J. Modal testing. theory, practice and application. 2nd edition, Research studies press Ltd., Hertforshire, England, 2000.

Fang, C.-H., Lin, S.-K., Wang, S.-J., 2005. On-line parameter estimator of an induction motor at standstill. *Control Engineering Practice* 13, Elsevier 2005, pp. 535–540.

Hannalla, A.Y., MacDonald, D.C., 1977. The calculation of machine transient performance. *IEEE Transactions on Magnetics*, Vol. 13, No. 5, September 1977, pp. 1134–1136.

He, Y-K., Lipo, T.A., 1984. Computer simulation of an induction machine with spatially dependent saturation. *IEEE Transactions on Power Apparatus and Systems*, Vol. PAS-103, No. 4, April 1984.

Healey, R.C., Williamson, S., Smith, S.C., 1995. Improved cage rotor models for vector controlled iInduction motors. *IEEE Transactions on Industry Applications*, Vol. 31, No. 4, July/August 1995, pp. 812–822.

Hinkkanen, M., Repo, A.-K., Luomi, J., 2006. Influence of magnetic saturation on induction motor model selection. *Proceedings in International Conference in Electrical Machines*, Crete, Greece, 2006, on CD No. 203.

Holliday, D., Green, T.C., Williams, B.W., 1994. On-line measurement of induction machine stator and rotor winding parameters. *Fifth International Conference on Power Electronics and Variable-Speed Drives*, 1994 London, United Kingdom, pp. 465–469.

Holopainen, T.P., 2004. Electromechanical interaction in rotordynamics of cage induction motors. Doctoral Thesis, *VTT Publications* 543, Espoo 2004, 64 p. Available at: http.//lib.tkk.fi/Diss/2004/isbn9513864057/.

Holtz, J., 2006. Sensorless control of induction machines – with or without signal injection? *IEEE Transactions on Industrial Electronics*, Vol. 53, No. 1, February 2006, pp. 7–30.

Huang, K.S., Kent, W., Wu, Q.H., Turner, D.R. 2001. Parameter identification for FOC induction motors using genetic algorithms with improved mathematical model. *Electric Power Components and Systems* 29, Taylor & Francis 2001, pp. 247–258.

IEEE Committee Report, 1977. First benchmark model for computer simulations of subsynchronous resonance. *IEEE Transactions on Power Apparatus and Systems*, Vol. PAS-96, September/October 1977, pp. 1565–1570.

IEEE Guide, 1996. Test procedures for synchronous machines. *IEEE Standard* 115-1995, 1996.

Islam, M.J., Pippuri, J., Perho, J., Arkkio, A. 2007. Time-harmonic finite-element analysis of eddy currents in the form-wound stator winding of a cage induction motor. *IET Electric Power Applications*, Vol. 1, No. 5, September 2007, pp. 839–846.

Jang, J.-H., Ha, J.-I., Ohto, M., Ide, K., Sul, S.-K. 2004. Analysis of permanent-magnet machine for sensorless control based on high-frequency signal injection. *IEEE Transactions on Industry Applications*, Vol. 40, No. 6, November/December 2004, pp. 1595–1604.

Jansen, P.L., Lorenz, R.D. 1995. Transducerless position and velocity estimation in induction and salient AC machines. *IEEE Transactions on Industry Applications*, Vol. 31, No., 2, March/April 1995, pp. 240–247.

Joswig, F., Kulig, S. 2001. Perceptions about new kinds of subsynchronous resonances. *Proceedings of International Conference Power Systems Transients IPST*, June 24–28, Rio de Janeiro Brasil, paper 240, http.//www.ipst.org/IPST01Papers.htm.

Kanerva, S., Seman, S., Arkkio, A. 2005. Inductance model for coupling finite element analysis with circuit simulator. *IEEE on Transactions on Magnetics*, Vol. 41, No. 5, May 2005, pp. 1620–1623.

Kanerva, S., Arkkio, A. 2006. Extraction of circuit parameters from time stepping FEM computation for coupled field-circuit simulation. *COMPEL. The International Journal for Computation and Mathematics in Electrical and Electronic Engineering*, Vol. 25, No. 2, pp. 334–343.

Kerkman, R.J. 1985. Steady-state and transient analyses of an induction machine with saturation of the magnetizing branch. *IEEE Transactions on Industry Applications*, Vol. IA-21, No. 1, January/February 1985, pp. 226–234.

Kovacs, K.P. 1984. On the theory of cylindrical rotor a.c. machines, including main flux saturation. *IEEE Transactions on Power Apparatus and Systems*, Vol. 103, No. 4, April 1984, pp. 754–761.

Kwon, C., Sudhoff, S.D. 2006. Genetic algorithm-based induction machine characterization procedure with application to maximum torque per amp control. *IEEE Transactions on Energy Conversion*, Vol. 21, No. 2, June 2006, pp. 405–415.

Kron, G. 1942. Equivalent circuits for the hunting of electrical machinery. *Electrical Engineering*, vol. 61, May 1942, pp. 290–296.

Lee, Y.-S., Hsu, K.-C. 1995. Shaft torsional oscillation of induction machine including saturation and hysteresis of magnetising branch with an inertia load. *IEEE catalogue* No. 95^{TH} 8130, IEEE 1995, pp. 134–139.

Lemaire-Semail, B., Bouillault, F., Razek, A. 1991. Modelling of vector-controlled cage induction motor with FEM. *IEE Proceedings-B*, Vol. 138, No. 6, November 1991, pp. 297–302.

Levi, E.C. 1959. Complex-curve fitting. *IRE Transactions* on *Automatic Control*, Vol. AC-4, 1959, pp. 37–44.

Levi, E., 1996. Main flux saturation modelling in double-cage and deep-bar induction machines. *IEEE Transactions on Energy Conversion*, Vol. 11, No. 2, June 1996, pp. 305–311.

Levi, E. 1995. A unified approach to main flux saturation modelling in d-q axis models of induction machines. *IEEE Transactions on Energy Conversion*, Vol. 10, No. 3, September 1995, pp. 455–461.

Levi, E. 1997. Impact of cross-saturation on accuracy of saturated induction machine models. *IEEE Transactions on Energy Conversion*, Vol. 12, No. 3, September 1997, pp. 211–216.

Levy, W., Landy, C.F., McCulloch, M.D. 1990. Improved models for the simulation of deep bar motors. *IEEE Transactions on Energy Conversion*, Vol. 5, No. 2, June 1990, pp. 393–400.

Lindenmeyer, D., Dommel, H.W., Moshref, A., Kundur, P. 2001. An induction motor parameter estimation. *Electrical Power and Energy Systems*, Vol. 23, Elsevier 2001. pp. 251–262.

Lima, A.M.N., Jacobina, C.B., Filho, E.B.S. 1997. Nonlinear parameter estimation of steady-state induction machine models. *IEEE Transactions on Industrial Electronics*, Vol. 44, No. 3, June 1997, pp. 390–397.

Lipo, T.A., Krause, P.C. 1969. Stability analysis of a rectifier-inverter induction motor drive. *IEEE Transactions on Power Apparatus and Systems*, Vol. 88, No. 1, January 1969, pp. 55–66.

Luomi, J., Niemenmaa, A., Arkkio, A. 1986. On the use of effective reluctivities in magnetic field analysis of induction motors fed from a sinusoidal voltage source. *Proceedings International Conference on Electrical Machines*, 1986, Munich, Germany, pp. 706–709.

Macdonald, D.C., Reece, A.B.J., Turner, P.J. 1985. Turbine-generator steady-state reactances. *IEE Proceedings*, Vol. 132, Pt. C, No. 3, May 1985, pp. 101–108.

Melkebeek, J.A.A., Novotny, D.W. 1983 (a). The influence of saturation on induction machine drive dynamics. *IEEE Transactions on Industry Applications*, Vol. 19, No. 5, September/October 1983, pp. 671–681.

Melkebeek, J.A.A. 1983 (b). Magnetizing field saturation and dynamic behavior of induction machines. Part I. An improved calculation method for induction machine dynamics. *IEE Proceedings – Electric Power Applications*, Vol. 130, pt. B, No. 1, 1983, pp.1–9.

Moraes, R.M., Ribeiro, L.A.S., Jacobina, C.B., Lima, A.M.N. 2003. Parameter estimation of induction machines by using its steady-state model and transfer function. *IEMDC'03, IEEE International Conference on Electric Machines and Drives*, Vol. 3, 1–4 June, Madison, Wisconsin USA, pp. 1965–1971.

Moreira, J.C., Lipo, T.A. 1992. Modeling of saturated ac machines including air gap flux harmonic components. *IEEE Transactions on Industry Applications*, Vol. 28, No. 2, March/April 1992, pp. 343–349.

Nangsue, P., Pillay, P., Conry, S.E. 1999. Evolutionary algorithms for induction motor parameter determination. *IEEE Transactions on Energy Conversion*, Vol. 14, No. 3, September 1999, pp. 447–453.

Nelles, O. 2001. Nonlinear system identification. Springer-Verlag, Berlin Heidelberg 2001, ISBN 3-540-67369-5, p. 785.

Nelson, R.H., Lipo, T.A., Krause, P.C. 1969. Stability analysis of a symmetrical induction machine. *IEEE Transactions on Power Apparatus and Systems*, Vol. 88, No. 11, November 1969, pp. 1710–1717.

Nickle, C.A., Pierce, C.A. 1930. Stability of synchronous machines – Effect of armature circuit resistance. *AIEE Transactions*, Vol. 49, January 1930, pp. 338–350.

Ojo, J.O., Consoli, A., Lipo, T.A. 1990. An improved model of saturated induction machines. *IEEE Transactions on Industry Applications*, Vol. 26, No. 2, March/April 1990, pp. 212–220.

Orlowska-Kowalska, T., Lis, J., Szabat, K. 2006. Identification of the induction motor parameters at standstill using soft computing methods. *COMPEL. The International Journal for Computation and Mathematics in Electrical and Electronic Engineering*, Vol. 25, No. 1, Emerald 2006, pp. 181–194.

Palko, S. 1996. Structural optimisation of an induction motor using a genetic algorithm and a finite element method. Doctoral Thesis, *Acta Polytechnica Scandnavica, Electrical Engineering Series*, No. 84, Espoo 1996, p. 99. Available at: http.//lib.tkk.fi/Diss/199X/isbn951225588X/.

Papazacharopoulos, Z.K., Tatis, K.V., Kladas, A.G., Manias, S.N. 2004. Dynamic model for harmonic induction motor analysis determined by finite elements. *IEEE Transactions on Energy Conversion*, Vol. 19, No. 1, March 2004, pp. 102–108.

Park, R.H. 1929. Two-reaction theory of synchronous machines, generalized method of analysis – Part I, *AIEE Transactions*, Vol. 49, July 1929, pp. 716–727.

Park, R.H. 1933. Two-reaction theory of synchronous machines – Part II, *AIEE Transactions*, Vol. 52, June 1933, pp. 352–354.

Price, K.V., Storn, R.M., Lampinen, J.A. 2005. Differential evolution. A practical approach to global optimization. Springer Berlin 2005.

Proca, A.B., Keyhani, A. 2002. Identification of variable frequency induction motor models from operating data. *IEEE Transactions on Energy Conversion*, Vol. 17, No. 1, March 2002, pp. 24–31.

Retiere, N., Ivanes, M. 1999. An introduction to electric machine modeling by systems of non integer order. *IEEE Transactions on Energy Conversion*, Vol. 14, No. 4, December 1999, pp. 1026–1032.

Ribeiro, L.A.S., Jacobina, C.B., Lima, A.M.N. 1999. Linear parameter estimation for induction machines considering the operating conditions. *IEEE Transactions on Power Electronics*, Vol, 14, No. 1, January 1999, pp. 62–73.

Ribeiro, L.A.S., Jacobina, C.B., Lima, A.M.N., Oliveira, A.C. 2000. Real-time estimation of the electric parameters of an induction machine using sinusoidal PWM voltage waveforms. *IEEE Transactions on Industry Applications*, Vol. 36, No. 3, May/June 2000, pp. 743–754.

Riu, D., Retiere, N., Ivanes, M. 2002. Diffusion phenomenon modeling by half-order systems. Application to squirrel-cage induction machine. *Journal of Magnetism and Magnetic Materials*, 242-245, Elsevier, pp. 1243–1245.

Riu, D.M., Retiere, N.M., Ivanes, M.S. 2003. Induced currents modeling by half-order systems application to hydro- and turbo-alternators. *IEEE Transactions on Energy Conversion*, Vol. 18, No. 1, March 2003, pp. 94–99.

Riu, D., Retiere, N., Ivanes, M. 2000. Electric machine modeling by half order systems. *Proceedings of International Conference on Electrical Machines* 2000, Espoo, Finland, Vol. 3, pp. 1646–1650.

Rogers, G.J. 1965. Linearised analysis of induction-motor transients. *Proceedings IEE*, Vol. 112, No. 10, October 1965, pp. 1917–1925 (1932).

Saitz, J. 2001. Magnetic field analysis of electric machines taking ferromagnetic hysteresis into account. *Acta Polytechnica Scandinavica, Electrical Engineering series*, Espoo 2001, pp. 123. Available at: http.//lib.tkk.fi/Diss/2001/isbn9512256908/.

Salon, S., Burow, D., DeBortoli, M., Slavik, C. 1994. Effects of slot closure and magnetic saturation on induction machine behaviour. *IEEE Transactions on Magnetics*, Vol. 30, No. 5, September 1994, pp. 3697–3700.

Smith, A.C., Healey, R.C., Williamson, S. 1996. A transient induction motor model including saturation and deep bar effect. *IEEE Transactions on Energy Conversion*, Vol. 11, No. 1, March 1996, pp. 8–15.

Shadley, J.R., Wilson, B.L., Dorney, M.S. 1992. Unstable self-excitation of torsional vibration in AC induction motor driven rotational systems. *Journal of Vibration and Acoustics*, Vol. 114, April 1992, pp. 226–231.

Seman, S., Saitz, J., Arkkio, A. 2003. Dynamic model of cage induction motor considering saturation and skin effect. *ICEMS 2003 6th International Conference on Electrical Machines and Systems*, Vol. 2, November 2003, pp. 710–713.

Shaltout, A.A, Abu Al-Feilat, E.A. 1992. Damping and synchronizing torque computation in multimachine power systems. *IEEE Transactions on Power Systems*, Vol. 7, No. 1, February 1992, pp. 280–286.

Shaltout, A.A. 1994. Analysis of torsional torques in starting of large squirrel cage induction motors. *IEEE Transactions on Energy Conversion*, Vol. 9, No. 1, March 1994, pp. 135–141.

Sheppard, D.J. 1988. Torsional vibration resulting from adjustable-frequency AC drives. *IEEE Transactions on Industry Applications*, Vol. 24, No. 5, September/October 1988, pp. 812–817.

Smith, K.S., Ran, L. 1994. Investigation of starting dynamics of electrical submersible pumps with soft starting. *Proceedings of Fifth International Conference on Power Electronics and Variable-Speed Drives*, October 26–28, London, United Kingdom, No 399, 1994.

Strangas, E.G., Theis, K.R. 1985. Shaded pole motor design and evaluation using coupled field and circuit equations. *IEEE Transactions on Magnetics*, Vol. 21, No. 5, pp. 1880–1882.

Sudhoff, S.D., Aliprantis, D.C., Kuhn, B.T., Chapman, P.L. 2002. An induction machine model for predicting inverter-machine interaction. *IEEE Transactions on Energy Conversion*, Vol. 17, No. 2, June 2002, pp. 203–210.

Sudhoff, S.D., Kuhn, B.T., Aliprantis, D.C., Chapman, P.L. 2001. An advanced induction machine model for predicting inverter-machine interaction. *PESC 32nd Annual Power Electronics Specialists Conference*, June 17–21 2001, Vancouver, Canada, pp. 2043–2052.

Sudhoff, S.D., Aliprantis, D.C., Kuhn, B.T., Chapman, P.L. 2003. Experimental characterization procedure for use with an induction machine model. *IEEE Transactions on Energy Conversion*, Vol. 18, No. 1, March 2003, pp. 203–210.

Sullivan, C.R., Sanders, S.R. 1995. Models for induction machines with magnetic saturation of the main flux path. *IEEE Transactions on Industry Applications*, Vol. 31, No. 4, July/August 1995, pp. 907–917.

Suontausta, A. 1988. Influence of saturation and skin effect on the slot impedance of cage-induction motor. Licenciate Thesis (in Finnish), Helsinki University of Technology, Espoo 1988, p. 85.

Tabesh, A., Iravani, R. 2004. Frequency-response analysis of torsional dynamics. *IEEE Transactions on Power Systems*, Vol. 19, No. 3, August 2004, pp. 1430–1437.

Tabesh, A., Iravani, R. 2005. On the application of the complex-torque coefficients method to the analysis of torsional dynamics. *IEEE Transactions on Energy Conversion*, Vol. 20, No. 2, June 2005, pp. 268–275.

Tenhunen, A. 2003. Electromagnetic forces acting between the stator and eccentric cage rotor. Doctoral Thesis, Report / Helsinki University of Technology, Department of Electrical and Communications Engineering, Laboratory of Electromechanics, Report 69, Espoo 2003, 40 p. Available at: http.//lib.tkk.fi/Diss/2003/isbn9512266830/

Thiringer, T. 1996. Measurements and modelling of low-frequency disturbances in induction machines. Doctoral Thesis, Chalmers University of Technology, 1996, 130 p.

Turner, P.J., MacDonald, D.C. 1982. Electromagnetic simulation of the flux decay test for determining turbine-generator parameters. *International Conference on Electrical Machines, Design and Applications*, 13–15 July, London, United Kingdom, pp. 90–93.

Ueda, R., Sonoda, T., Koga, K., Ichikawa, M. 1992. Stability analysis in induction motor driven by V/f controlled general-purpose inverter. *IEEE Transactions on Industry Applications*, Vol. 28, No. 2, March/April 1992, pp. 472–480.

Ursem, R.K., Vadstrup, P. 2003. Parameter identification of induction motors using differential Evolution. *Proceedings CEC 2003 The 2003 Congress on Evolutionary Computation*, Vol. 2, Canberra, Australia, pp. 790–796.

Vas, P., Brown, J.E., Hallenius, K.E. 1984. Cross-saturation effects in smooth-air-gap electrical machines, *Proceedings of International Conference in Electrical Machines* 1984, Lausanne, Switzerland, 1984, pp. 261–264.

Vas, P. 1992. Electrical machines and drives, a space-vector approach. Oxford. Clarendon Press, 1992.

Velez-Reyes, M., Minami, K., Verghese, G.C. 1989. Recursive speed and parameter estimation for induction machines. *Proceedings in Industry Applications Society Annual Meeting*, 1989, San Diego, USA, pp. 607–611.

Verbeeck, J., Pintelon, R., Lataire, P. 1999. Identification of synchronous machine parameters using a multiple input multiple output approach. *IEEE Transactions on Energy Conversion*, Vol. 14, No. 4, December 1999, pp. 909–917.

Verbeeck, J., Pintelon, R., Lataire, P. 2000. Influence of saturation on estimated synchronous machine parameters in standstill frequency response tests. *IEEE Transactions on Energy Conversion*, Vol. 15, No. 3, September 2000, pp. 277–283.

Wagner, C.F. 1930. Effect of armature resistance upon hunting of synchronous machines. *AIEE Transactions*, Vol. 49, January 1930, pp.1011–1026.

Wang, Y.-N., Gu, J.-C., Chen, C.-M. 2001. Real-time tracking of the torsional vibration of an induction motor supplied by distorted voltage sources. *Electric Power Systems Research*, Elsevier 2001, Vol. 57, pp. 205–215.

Widdle Jr., R.D., Krousgrill Jr., C.M., Sudhoff, S.D. 2006. An induction motor model for high-frequency torsional vibration analysis. *Journal of Sound and Vibration*, Vol. 290, pp. 865–881.

Williamson, S., Begg, M.C. 1985. Analysis of cage induction motors – A combined fields and circuits approach. *IEEE Transactions on Magnetics*, Vol. 21, No. 6, November 1985, pp. 2396–2399.

Williamson, S., Lim, L.H., Robinson, M.J. 1990. Finite-element models for cage induction motor analysis. *IEEE Transactions on Industry Applications*, Vol. 26, No. 6, November 1990, pp. 1007–1017.

Williamson, S., Robinson, M.J. 1991. Calculation of cage induction motor equivalent circuit parameters using finite elements. *IEE Proceedings-B*, Vol. 138, No. 5, September 1991, pp. 264–276.

Williamson, S., Gersh, D.R. 1996. Finite element calculation of double-cage equivalent circuit parameters. *IEEE Transactions on Energy Conversion*, Vol. 11, No. 1, March 1996, pp. 41–48.

Williamson, S., Healey, R.C. 1996. Space vector representation of advanced motor models for vector controlled induction motors. *IEE Proceedings – Electrical Power Applications*, Vol. 143, No. 1, January 1996, pp. 69–77.

Willis, J.R., Brock, G.J., Edmonds, J.S. 1989. Derivation of induction motor model from standstill frequency response tests. *IEEE Transactions on Energy Conversion*, Vol. 4, No. 4, December 1989, pp. 608–615.

Yahiaoui, A., Bouillault, F. 1994. 2D and 3D numerical computation of electrical parameters of an induction motor. *IEEE Transactions on Magnetics*, Vol. 30, No. 5, September 1994, pp. 3690–3694.

Yahiaoui, A., Bouillault, F. 1995. Saturation effect on the electromagnetic behaviour of an induction machine. *IEEE Transactions on Magnetics*, Vol. 31, No. 3, May 1995, pp. 2036–2039.

Appendix A

Main dimensions and rating of the 37-kw cage-induction motor

Table A1. Dimensions [mm] and rating.

Dimensions	
Length of the laminated core	249
Outer diameter of the stator core (d_{se})	310
Inner diameter of the stator core (d_s)	200
Number of slots in the stator	48
Outer diameter of the rotor core (d_r)	198.4
Inner diameter of the rotor core (d_{ri})	70.0
Number of slots in the rotor	40
Stator slot	
h_s	23.9
h_{s1}	1.0
h_{s2}	17.5
b_{s1}	3.5
b_{s2}	6.5
b_{s3}	8.8
Rotor slot	
h_{r1}	0.7
h_{r2}	16.1
h_{r3}	17.8
b_{r1}	6.0
b_{r2}	2.5
b_{r3}	5.85
Stator winding	
Number of poles	4
Number of phases	3
Number of parallel paths	2
Number of turns in a slot	12
Coil span	12
Resistance of stator phase at 80 °C	0.079 Ω
Rated power, [kW]	37
Rated voltage, [V]	380
Rated current, [A]	73
Rated frequency, [Hz]	50
Rated slip, [%]	2

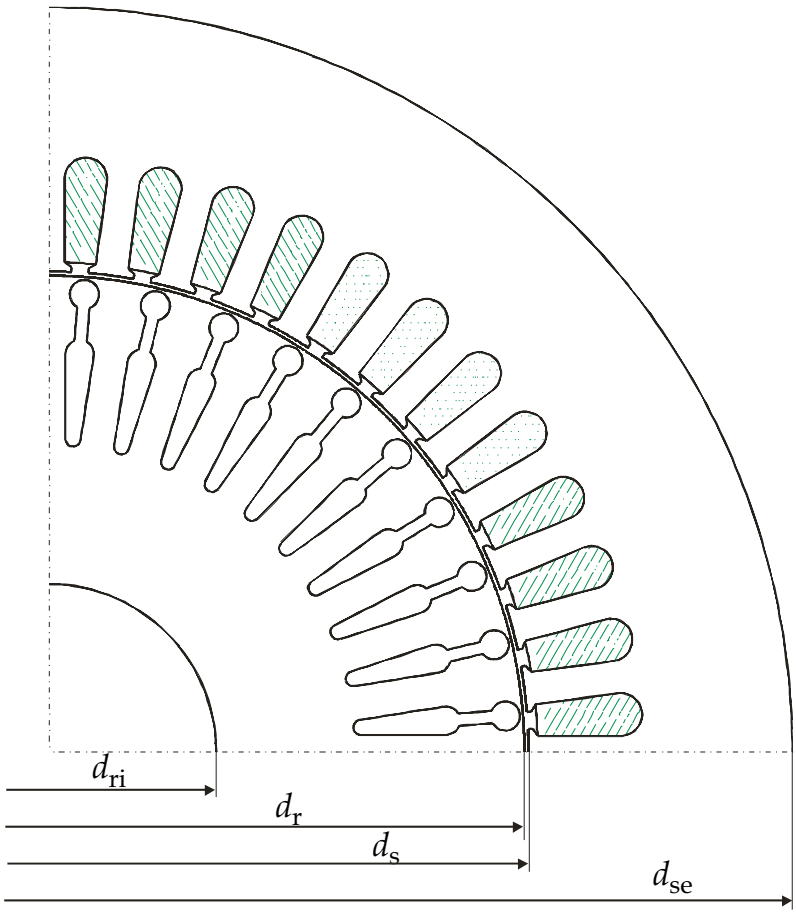

Figure A1. Basic construction and main diameters.

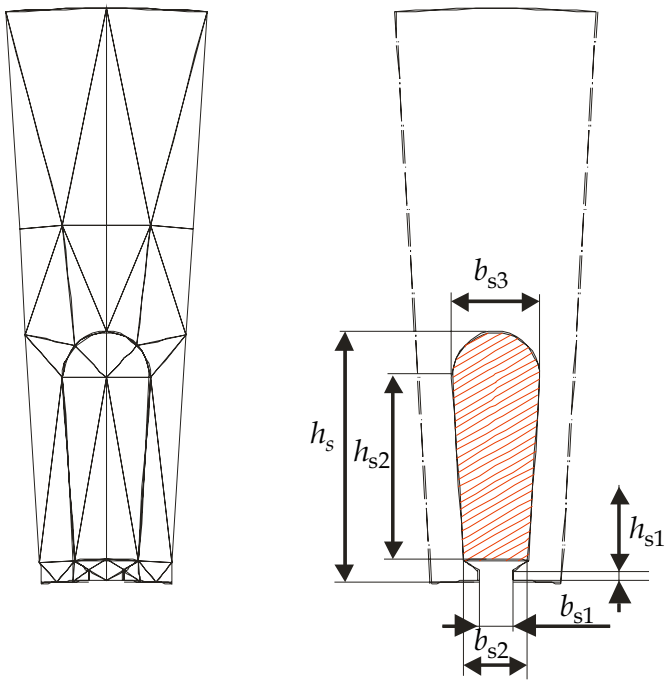

Figure A2. Stator slot shape.

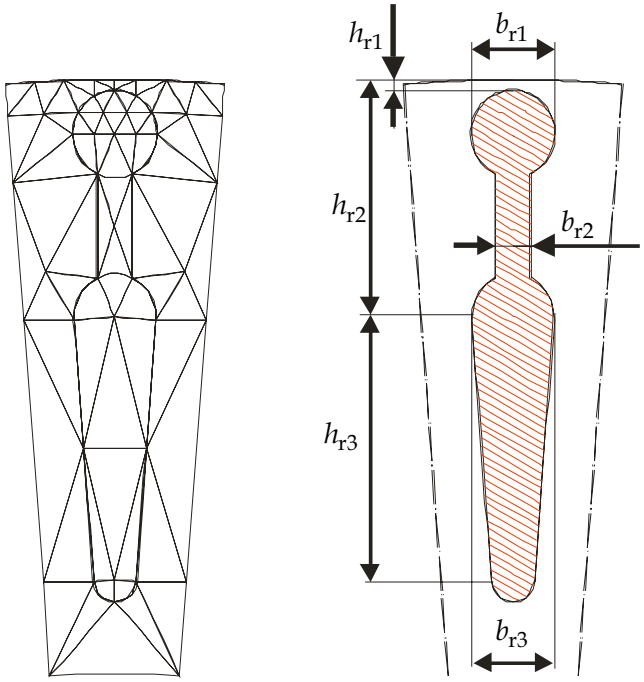

Figure A3. Rotor slot shape.

ISBN 978-951-22-9274-5
ISBN 978-951-22-9275-2 (PDF)
ISSN 1795-2239
ISSN 1795-4584 (PDF)